OPTICAL, ELECTROMAGNETIC, AND THERMAL MODELING OF NEAR-FIELD RADIATIVE ENERGY TRANSFER FROM PLASMONIC NANOANTENNAS TO A MAGNETIC RECORDING MEDIUM

by

SEYDİ EREN ÜNLÜ

Submitted to the Graduate School of Engineering and Natural Sciences
in partial fulfillment of
the requirements for the degree of
Master of Science

Sabancı University

Spring 2012

OPTICAL, ELECTROMAGNETIC, AND THERMAL MODELING OF NEAR-FIELD RADIATIVE ENERGY TRANSFER FROM PLASMONIC NANOANTENNAS TO A MAGNETIC RECORDING MEDIUM

APPROVED BY:

Associate Prof. Dr. İbrahim Kürşat Şendur …….

Associate Prof. Dr. Mahmut Faruk Akşit ……

Associate Prof. Dr. Ali Koşar …….

Assistant Prof. Dr. Güllü Kızıltaş Şendur …….

Assistant Prof. Dr. Burç Mısırlıoğlu ……

DATE OF APPROVAL:

Optical, electromagnetic, and thermal modeling of near-field radiative energy transfer from plasmonicnanoantennas to a magnetic recording medium

Seydi Eren Ünlü

ME, MSc. Thesis, 2012

Thesis Supervisor: Assoc. Prof. İbrahim KürşatŞendur

Keywords: Plasmonics, nano antenna, optical, electromagnetic, thermal modeling, near-field radiative energy transfer, temperature control

ABSTRACT

Developments in nanotechnology have brought new challenges in heat transfer and temperature control in nanoscale devices. In this thesis, the electromagnetic and thermal behavior of plasmonicnanoantennas are investigated when they are illuminated with a focused beam of light and placed in the vicinity of thin film magnetic layer structures. To investigate this problem, optical, electromagnetic, and thermal models are developed and integrated. An optical modeling tool is developed to define a tightly focused beam of light by utilizing Richards-Wolf theory, which is primarily based on ray-tracing of optical beams. An electromagnetic modeling tool is used to analyze nano antennas and thin-film magnetic layers in terms of electric field and dissipated power distribution profiles. A thermal modeling tool is developed to control the temperature distribution on nanoantennas and thin film magnetic layer structures.

Optical, electromagnetic and heat transfer modeling tools are integrated and simulations are conducted by generating script files using MATLAB codes. Electromagnetic and heat transfer analysis are conducted for dipole, bowtie and arrow shaped nanoantennas. The conditions to obtain single optical and hot spots on the thin film magnetic layer are presented. A novel nanoantenna type is proposed to improve thermal performance. It has been demonstrated that dipole, bowtie and a newly proposed arrow-shaped nano antennas show similar electromagnetic behaviors while the arrow-shaped nano antenna shows significant improvement in terms of temperature control which yields low antenna temperatures.

Plasmonik nanoantenlerden manyetik kayıt ortamına yakın alan radyasyon enerji transferinin optik, elektromanyetik ve termal modellenmesi

Seydi Eren Ünlü

ME, Yüksek Lisans Tezi, 2012

Tez Danışmanı: Assoc. Prof. İbrahim Kürşat Şendur

Anahtar kelimeler: Plasmonik, nano anten, optik, elektromanyetik, termal modelleme, yakın alan radyasyon enerji transferi, sıcaklık kontrolü

ÖZET

Nanoteknolojideki gelişmeler, nano düzeydeki cihazların ısı transferi ve sıcaklık kontrolüne yeni zorluklar getirdi. Bu tezde, odaklanmış ışık demeti ile aydınlatılan ve ince film manyetik tabaka yapısının yakınına yerleştirilen plasmoniknano antenlerin elektromanyetik ve termal davranışları incelenmiştir. Bu problemi inceleyebilmek için, optik, elektromanyetik ve termal modeller geliştirilmiş ve birbirleriyle entegre edilmiştir. Sıkıca odaklanmış ışık demetini tanımlamak için optik ışın demetlerinin takibine dayanan Richards-Wolf teorisi kullanılarak optik model aracı geliştirilmiştir. Nano antenlerin ve ince film manyetik tabakaların elektrik alan ve dağılmış güç profillerini analiz edebilmek için elektromanyetik modelleme aracı kullanılmıştır. Nano antenlerin ve ince film manyetik tabaka yapılarının üzerindeki sıcaklık dağılımının kontrolü için termal model geliştirilmiştir.

Optik, elektromanyetik ve ısı transferi modelleri entegre edilmiş ve simülasyonlar MATLAB kodu aracılığıyla hazırlanan komut dosyalarıyla gerçekleştirilmiştir. Elektromanyetik ve ısı transferi analizleri dipol, fiyonk ve ok şeklindeki nano antenler için gerçekleştirilmiştir. İnce film manyetik tabaka üzerinde tek optik ve ısı beneği elde edilen durumlar sunulmuştur. Termal performansı artırmak için yeni nano anten türü önerilmiştir. Dipol, fiyonk ve yeni önerilen ok şeklindeki nano antenlerin benzer elektromanyetik dağılım özellikleri gösterirken, daha düşük anten sıcaklığı sağlayan, yeni önerilen ok şeklindeki nano antenin sıcaklık kontrolü açısından ciddi ilerleme sağladığı gösterilmiştir.

To my family & those who believe in me

ACKNOWLEDGEMENTS

First, and foremost, I want to express my deepest gratitude to my advisor, Associate Prof. Dr. İ. Kürşat Şendur for his endless patience and help during my master and thesis work.

I also would like to express my gratitude to all of the professors of the Mechatronics Engineering program in Sabancı University, especially, Assist. Prof. Dr. Güllü Kızıltaş Şendur, Assoc. Prof. Dr. Mahmut Faruk Akşit, Assoc. Prof. Dr. Ali Koşar and Assist. Prof. Dr. Burç Mısırlıoğlu for joining my thesis jury and their support during my study.

Last but not least, I would like to express my deepest gratitude and special thanks to my family and to my friends who supported me all the time during my master studies.

TABLE OF CONTENTS

Page

TABLE OF FIGURES

Page

LIST OF TABLES

TABLE OF SYMBOLS

d	Diameter
D	Distance between nano antennas and thin film magnetic layer
$\mathbf{E}^t(\mathbf{r})$	The total electric field
$\mathbf{E}^i(\mathbf{r})$	The incident electric field component
$\mathbf{E}^s(\mathbf{r})$	The scattered electric field component
G	Gap between nanoantennas
k	Wavevector
L	Antenna length
n	Refractive index of the medium
$\hat{n}_1$	The normal directions to the surface,S_1
$\hat{n}_2$	The normal directions to the surface,S_2
$\mathbf{r}_p$	The observation point
S_1	The curved hemispherical surface
S_2	The planar surface
T	Antenna thickness
V_1	Semispherical Volume
W	Antenna width
W_1	Width of the bowtie nano antenna short edge
W_2	Width of the bowtie nano antenna long edge
x,y,z	Coordinates in space frame
λ	Wavelength
θ	Angle of incident beam
α	Half angle of the beam
$\mathbf{a}(\theta,\phi)$	The weighting vector for a plane wave
P_z	z- component of Poynting vector
σ	Conductance

LIST OF ABBREVATIONS

FEM	Finite element method
NA	Numerical Aperture
PV	Photovoltaic
SIL	Solid Immersion Lens
2D	Two Dimensional
3D	Three Dimensional

1. INTRODUCTION

Developments in nanotechnology have brought new challenges on the heat transfer and temperature control on nanoscale devices. The examples of this problem can be found in different fields such as plasmonic nanostructures [1-3], thermophotovoltaic energy devices [4-7], thermal microscopes [8-9] and heat-assisted magnetic recording [10-12]. The theoretical and experimental aspects of the near-field radiative heat transfer have been recently drawn a lot of research interests to overcome nanoscale heat transfer and temperature control problems on nanoscale devices. It has been shown that radiative heat transfer between bodies separated by distances smaller than the dominant wavelength of thermal radiation can exceed the values predicted by the Planck blackbody distribution due to tunneling of the evanescent waves for the system of two semi-infinite absorbing bodies with arbitrary dielectric properties at slightly different temperatures separated by a vacuum gap [13]. Due to this dramatic increase in radiative heat flux rate in near field, study of near-field radiative heat transfer is significant for nanoscale applications. Besides understanding the heat transfer dynamics in nanoscale, the ability to obtain point-like heat sources, which opens up a variety of promising applications in different fields such as medicine, microfluidics, magnetism, photonics and nanoscale catalysis, makes near-field radiative heat transfer studies significant. The aims of this thesis are to investigate the radiative energy transfer and near-field radiative heat transfer from near-field emitter to magnetic layer which is placed in close vicinity of near-field emitter, to understand the heat generation and control of temperature on nanostructures and to determine the case that creates single optical and hot spot on the magnetic layer by using nano-antennas which are excited by tightly focused beam of light.

1.1.Problem Definition

In this thesis, to investigate the near-field radiative heat transfer between nano-antennas and the magnetic thin-film structure, the problem illustrated in Figure 1.1(a) and in Figure 1.1(b) is analyzed. The oblique view of the system is illustrated in Figure 1.1(a) and the cross-view of the system studied is illustrated in Figure 1.1(b). The system consists of the nano-antenna structure, the magnetic layer thin-film structure, insulator layer, heat sink and the substrate. The nano-antennas are separated from each other by a gap, G and the nano-antennas are separated from magnetic thin-film layer with distance, D. The magnetic thin-film layer, insulator layer and the heat sink have same lengths in x and y directions and they are parallel both within themselves and with nano-antenna structure.

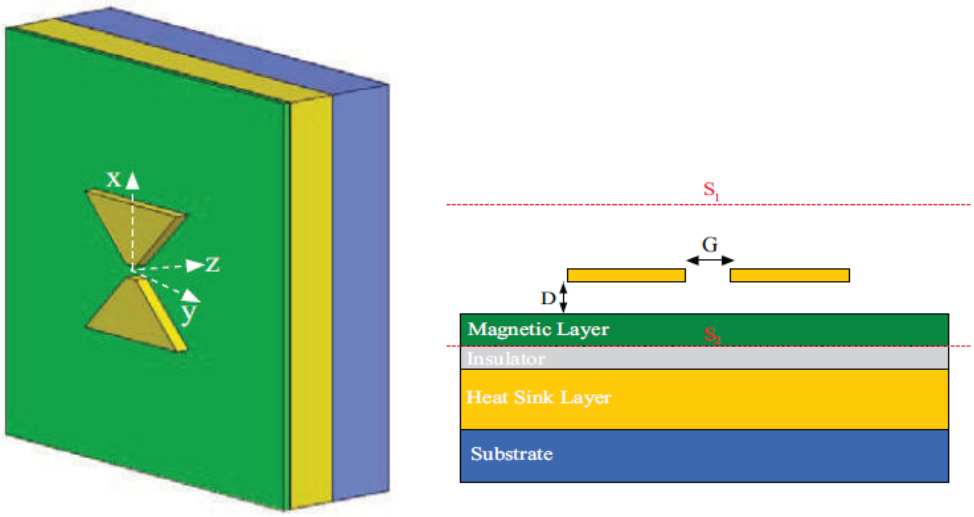

Figure 1.1(a) An oblique view of the problem geometry involving a bow-tie antenna and a magnetic thin-film stack. (b) A cross-section view that shows the details of the magnetic thin-film and the antenna's geometry.

The optical nano-antennas can be utilized as a near-field emitter for radiative energy transfer to an object placed in the close vicinity. To couple incident electromagnetic energy with small scale electronic devices, antennas have been utilized. The antennasachieve this coupling by localizing the incident radiation to dimensions smaller

than the wavelength. The coupling mechanism between small scale electronic devices and antennas at radio and microwave frequencies has been well understood. A similar coupling mechanism is applicable between nano-antennas operating at optical frequencies and objects with feature dimensions below the diffraction limit.

At optical frequencies, nanoscale metallic antennas can be utilized to couple incident optical beams to length scales much smaller than the diffraction limit. In the problem studied, three types of nano-antennas, dipole nano-antenna, bow-tie nano-antenna and the arrow shaped nanoantennas, are studied. An antenna is composed of metallic parts. Figure 1.2(a) illustrates the dipole nano-antenna structure which is composed of two metallic rods with the physical parameters of antenna length (L), antenna width (W), antenna thickness (T) and gap between two nano-antennas (G). Figure 1.2(b) illustrates the bow-tie nano-antenna which is composed of two triangular metallic structures with the physical parameters of length of the antenna (L), widths of the antenna edges (W_1, W_2), thickness of the antenna (T) and gap between two antennas (G).

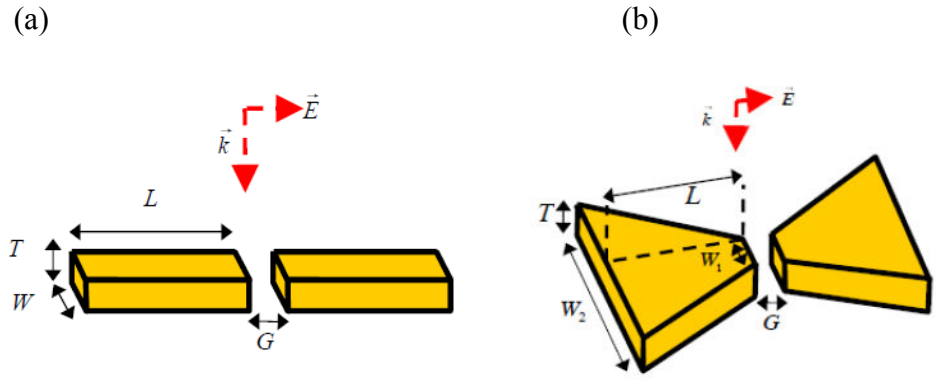

Fig. 1.2. (a) A schematic illustration of dipole nano-antenna. (b) A schematic illustration of bow-tie nano-antenna

Metallic nano-antennas which are shown in Figure 1.2, primarily utilize evanescent waves to couple electromagnetic energy to a sample in the near-field. The direction of the polarization of the incident radiation and the antenna geometry play an important role in this process. If the incident polarization is along the long-axis of the antenna as shown in Figure 1.2., then the incident electromagnetic radiation creates induced currents along this axis in the antenna. These induced currents are the source of charge accumulation at the ends of the antenna. The charges created across the gap separating the metallic parts of the antenna have opposite polarity. The oscillation of the charges with opposite polarity is the source of localized near-field electromagnetic radiation. This localized near-field radiation is composed of propagating and evanescent components. If a structure is brought into the near-field of this gap, then the electromagnetic fields radiating due to this charge oscillation interact with the structure. The evanescent component of the electromagnetic field is particularly important in achieving high power transmissionfrom the antenna.

In the problem studied in this thesis, the dipole, bowtie and arrow shaped nano-antennas are utilized to enhance the localized near-field radiative energy transfer to the magnetic thin film structure. Near-field optical power transmission is significant to utilize the nano-antennas in the nanoscaleplasmonic applications. The power transmission efficiency of the nano-antennas is determined by the ratio of power transmitted to the sample over the optical power input to the system. Since the power transmission is significant measurement for nano-antennas, such as in the data transfer rate of storage devices and the scan times of near-field optical microscopes applications, a nano-antenna with low power transmission is not practical to use. There are different possibilities to increase the power transmission efficiency of the nano-antennas. One method is to increase the input power; however, it is limited by the power of the laser diodes. In addition, high input power usually results in power dissipation in the metallic parts, which can cause significant heating and structural deformation of the nano-optical transducers. Therefore, a nano-antenna with high transmission efficiency is more feasible to increase the transmitted output power in practical applications. One possible method of further improving the transmitted power to the sample is to utilize a tightly focused beam of incident light onto the antenna. As the incident electromagnetic radiation becomes more tightly focused, the spot size of the diffraction limited radiation

incident onto the nano-antenna reduces. Reducing the spot size of the incident radiation increases the magnitude of the incident electric field illuminating the nano-antenna. Since the incident electric field illuminating the nano-antenna increases, the near-field radiation from the nano-antenna also increases. Therefore, a tightly focused beam of incident light exciting the antenna is used to further improve the near-field optical power transmission in the system studied in this thesis. The aplanatic lens system is used to obtain a tightly focused beam of incident light. A tightly focused incident optical beam with a wide angular spectrum is formulated using Richards-Wolf vector field equations which will be discussed in Optical Modeling tool section of this thesis.

The total electric field is obtained by using the Maxwell equations. In this thesis, the total electric field distribution on the center of the dipole and bow-tie antennas are analyzed for the case of a single plane wave with incident electric field 1 V/m and for the case of a tightly focused optical beam. The effects of the antenna physical parameters which are length, width, thickness of nano-antenna, gap between two nano-antennas, wavelength of the incident beam and numerical aperture of optical system is analyzed to determine their effects on the electric field distribution. The total electric field intensity distribution on the magnetic thin-film layer is also studied and the effects of antenna physical parameters, wavelength of the incident beam and the effects of the distance between nano-antennas and magnetic layer are studied. The cases in which the single optical spot is obtained on the center of the magnetic thin-film layer are determined and the effects of the parameters are analyzed.

In addition, calculation of the electric field intensity distribution on nano-antennas and magnetic thin-film structure, the dissipated power on the nano-antennas and magnetic thin-film structure are determined. The dissipated power distribution on the nano-antennas and the magnetic thin-film structure is used as heat generation rates for the thermal radiation calculations. The analysis of the heat transfer in the near-field is conducted by assigning the electromagnetic power output as a heat generation input with the same geometrical parameters as in the electrodynamics part. The heat transfer analysis gives the temperature profiles of the nano-antenna structure and the magnetic thin-film structure as a function of distance and as a time. The effects of the physical parameters of the nano-antennas and the wavelength on the temperature profiles on both nano-antennas and corresponding magnetic thin-film structure are determined. The time

dependence of temperature is important to see the nature of the near-field radiative heat transfer and to find the possible solutions to lower the antenna temperature while increasing temperature of the magnetic thin-film structure. Therefore, heat transfer contribution is important part of this thesis to control temperature and to determine the contribution of near-field effects on the near-field radiative heat transfer. The thermal analysis results are analyzed according to time-dependence and space dependence.

The assumptions made through the analysis in this thesis are presented here. First, all bodies considered in the problem are continuous, homogeneous and isotropic. The assigned material properties are homogeneous. The incident power assigned in the electromagnetic analysis is assumed to be 1V/m plane wave. The bodies are assigned radiation boundary condition in the outer surfaces with only radiating fields which is assumed to be perfectly radiating bodies in the electromagnetic analysis. In the heat transfer analysis, bodies are assigned zero celcius degree as an initial temperature. The meshes in the electromagnetic analysis are made automatically in HFSS 12 simulation program based on length which adjusts maximum length between nodes. In the heat transfer analysis, triangular meshes are assigned to the bodies in ANSYS Multiphysics 12 program.

1.2. Literature Survey

Near-field radiative heat transfer has been drawing a lot of research interests both theoretically and experimentally for last decades. When the spacing between the bodies are smaller than the dominant wavelength of thermal radiation, radiative heat transfer increases strongly due to evanescent electromagnetic fields which exists close to the surface of the bodies. This phenomenon was studied by Polder and van Hove between two identical semi-infinite macroscopic bodies with arbitrary dispersive and absorptive dielectric properties [13]. In their study, the formula for the heat flux at an arbitrary point due to radiation is derived by using fluctuation-dissipation theorem and electromagnetic theory. Their study showed the difference between the radiative heat transfer rates between closely spaced bodies and large spacing distances and concluded that this difference is caused by two reasons; firstly, when the spacing between bodies are smaller than the dominant wavelength, interference effects in the waves reflected

between the two surfaces and secondly, the evanescent waves can reach to the other surface when the distance is small enough which is the strongest effect between two reasons. After, Polder and van Hove's work, Loomis and Maris [14] studied the radiative energy flow between two half-spaces with using same method used by Lifshitz [15] in his derivation of the van der Waals force between two dielectric slabs using electromagnetic fluctuations theory developed by Rytov [16]. They calculate the radiative heat transfer between two macroscopic half-spaces with different temperatures which separated by a gap by adding extraneous fluctuating inductions which are random variables to the Maxwell's equations. With the help of Fourier transform and solution of Maxwell's equations by using fluctuation-dissipation theorem, they obtained the power density between two bodies which shows the contribution of propagating and evanescent waves separately. In their study, they showed the effect of the conductivity and gap distance on the heat flow and showed that the smaller gap distances, the radiative heat flux can exceed the Planck's blackbody radiation limit.

Since initial studies on the subject determined general near field radiative heat and energy transfer, later studies broaden the perspective and start to focus on the other aspects of the near field radiative heat transfer such as surface phonon contributions. Muletet. al [17] studied the radiative heat transfer between two semi-infinite bodies at nanoscale and they investigate the effects of evanescent waves on radiative heat transfer and surface phonon-polaritons contribution to the radiative heat transfer. Rytov [16], Polder and van Hove [13] ,and Loomis and Maris [14] have calculated the radiative heat transfer based on electrodynamics theory for only metal surfaces. Muletet. al have broaden the problem towards the case of dielectrics to show the effects of the surface phonon-polaritons which are electromagnetic modes of the interfaces. It has been shown in theirstudy that the radiative heat flux can be increased by several orders of magnitude when the materials support surface-phonon polaritons and determined the heat transfer coefficients for SiC and glass materials between the separation distances of 10^{-8} to10^{-4} meters.

Besides the studies about the near field radiative heat transfer for semi infinite and infinite bodies, later studies focused on the near field radiative heat transfer for different geometries, which are close to more practical applications. Muletet. al [18] studied the radiative heat transfer between a small particle which acts like a point-like dipole, and a

bulk placed in the close vicinity of the particle. The contribution of the tunneling waves to the radiative heat transfer is investigated and it has been shown that the order of transfer is increased by several orders of magnitude when the surface or the particle supports the resonant surface waves. The distribution of power inside the bulk material is studied when the particle is illuminated and energy is radiated from the particle towards the bulk and relation between the distance of bulk-particle and deposited power per unit volume is illustrated. Domingues et al. [19] has introduced the thermal conductance with the help of fluctuation-dissipation theorem between two nano-particles which are separated by a few nanometers. Their investigation's aim is to understand how the heat transfer between a tip and a sample is exchanged before they touch. The molecular dynamics simulation and model based on a Coulumb interaction between fluctuating dipoles are used to determine the heat conductance for nanoparticles with different radius and with different separation distances.

Besides the abovementioned studies in the literature, other studies which focus on the other aspects of the near field radiative energy transfer such as material property effects and surface waves contributions are studied. Firstly, Francoeur et al. [20] studied the near-field radiative heat transfer between a nanometric thin SiC film emitter which is submerged in vacuum or coated on a dielectric bulk and bulk SiC. Since SiC supports the surface phonon polaritons, narrow spectral band enhancement of the radiative heat transfer is investigated in this study and it is shown that the total radiative heat flux increases in a very narrow spectral range which could be exploited in near-field thermophotovoltaic power generation devices. Basu and Francoeur [21] studied the radiative heat transfer between two thin films which are perfectly smooth, parallel, homogeneous, isotropic, nonmagnetic and identical. In their study, optimum values for real and imaginary parts of dielectric functions are determined for different thicknesses of the vacuum gap between thin films. Their research determined the optimum real and imaginary parts of the dielectric function for a given gap distance which maximizes the radiative heat transfer between two thin-films. Francoeur and Mengüç [22] also studied the thin-films in terms of the control of the near-field radiative heat transfer via surface phonon-polariton coupling. Silicon carbide is used as a material that the films are made of, which supports the surface phonon-polaritons in the infrared spectrum. The local density of electromagnetic states for nanometric gap distances between two SiC films and radiative heat flux are calculated. Their research contributes to the determination of

the maximum radiative heat flux by finding the optimal film thickness and separation distance.

Francoeur et al. [23] has demonstrated the underlying physics behind the coexistence of multiple regimes for near-field radiative heat transfer between two layers supporting the surface phonon polaritons. In their study, the analysis of near-field radiative heat flux is conducted for different layer thicknesses in which thin-films have same thickness, different gap lengths and asymptotic layer thicknesses in which thin-films do not have same thicknesses. An analytical expression of near-field radiative heat transfer coefficient for the two films is derived and analyzed for different cases. The different near-field thermal regimes, which are d^{-2}, d^{-3}, d^{-4} regimes that show the radiative heat transfer variation as a function of distance, are proved that they exist. The reasons why these different thermal regimes exist are that near-field radiative heat transfer is a function of the penetration depth of dominant surface phonon polaritons which is a function of the gap thickness.

Also the effects of near field radiative heat transfer on the thermophotovoltaic applications are studied in the literature. Since near field radiative heat transfer is significant for efficiency and reliability of the photovoltaic systems, it attracts a lot of research interests. Narayanaswamy and Chen [24] has studied the thermal radiative energy transfer for near-field thermophotovoltaics system which consists of polar material layer, that supports surface phonon polaritons such as SiC, cubic boron nitride (cBN) or hexagonal boron nitride (hBN), vacuum gap and PV material layer. The analysis is conducted by using Green's functions method and fluctuation-dissipation theorem where polar material layer acts as a thermal source. Their research demonstrates that the surface waves enhance the radiative heat flux and show the narrowband characteristics which can be exploited to improve the power density and efficiency of the low temperature thermophotovoltaic power generators.

Since the near-field radiative heat transfer problems between two layers discussed in the abovementioned studies are based on the fluctuation-dissipation theorem, Francoeur and Mengüç [25] discussed the role of fluctuational electrodynamics in the near-field radiative heat transfer problems for generalized problems in detail in their research. Their research demonstrated the theoretical background on the fluctuation-dissipation

theorem used in the radiative heat transfer problems and illustrates the subject clearly. After the theoretical information provided in their study, the application of theorem was provided via solving the radiative heat flux between two semi-infinite layers spaced by a vacuum gap. The results were obtained for the heat flux between bodies and the propagating and the evanescent contributions of the radiative heat transfer are provided as an equation. The case for two semi-infinite layers which have temperatures of 800 K and 200 K is solved and the contribution of the evanescent waves are illustrated for different vacuum gap distances in which for lower than 10^{-7} m gap distances, the evanescent waves contribute 90% of the total radiative heat flux.

Based on the Francoeur and Mengüç'sabovementioned study [25] for the one-dimensional layered media which uses dyadic Green's functions and the scattering matrix method, they provided the solution algorithm for the near-field thermal radiation problem [26]. The general equations for the near-field thermal radiation problem are defined and the algorithm to solve this kind of layered media radiative heat transfer problems is proposed. The simulations for the two bulks of cubic boron nitride (cBN) are conducted and the corresponding dielectric function of cBN and monochromatic evanescent component of the radiative heat flux per unit dielectric constant was illustrated with the evanescent and propagating components of the radiative heat flux for certain frequency interval. The results showed that the near-field radiative heat flux for a bulk emitter is recovered for an emitting film of thickness above 1μm. And it was also shown that the presence of a body in close vicinity to an emitter can modify the near-field spectrum emitted due to a perturbation of the dispersion relation of surface phonon-polaritons which has important applications in the nanoscale gap thermophotovoltaics power generators.

Besides the near field radiative energy transfer studies in the literature, the heat generation in the plasmonic nanostructures is also studied in various researches. Quidant et al. [27] studied the effects of the object's morphology at the constant metal volume on the heat generation on the plasmonic nanostructures. Since, the metal nano-particles could be used as nano heat sources; the heat generation rates and the heating efficiency problems are addressed in the literature. In the study of Quidant et al. [27], two types of homogeneous gold nanostructures, which are colloidal nano-particles (spheres and nanorods), placed in water and planar nanostructures on glass, are studied to determine the morphology effects on the heat generation. The Green's dyadic method

is used to map spatial distribution of the heat power density inside the nano-particles which makes possible to understand the origin of heat generation as a function of morphology and wavelength. Their study demonstrated that the small gaps between adjacent particles do not increase the heating efficiency however; small, flat, elongated, or sharp nano-particles are much more efficient heaters than the massive plasmonic nanostructures. The reason of this result is that the incoming electric field penetrates more easily inside the thin nanostructures by making all gold volume contribute to heating. The morphology effects are seen on the calculated spectra of the heat generated through the colloidal gold nano-particles of the same volume. As the rods are elongated and becoming thinner, the heat power generated increases and the wavelength in which the peak heat power occurs shifted towards the right of the spectrum [27]. Quidant et al. [28] have studied the physics of the photo-induced heat generation on the nanoscaleplasmonic nanostructures with the help of the thermal microscopy technique based on molecular fluorescence polarization anisotropy. In this study, it is shown that the temperature distribution profiles through the plasmonic nanostructures are uniform due to fast thermal diffusion caused by the low length scale; the heat source density is more concentrated. In this study, it was shown that the thermal hot spots where the heat origin exists usually do not match with the optical spots of the plasmon mode. The reason of this contrary is that the optical hot spots come from tip effect and charge accumulation at the metal interfaces while, the heat generation comes from the points where charges can freely flow.

The temperature effects related to near field radiative heat transfer exchange in nanostructures are also studied in the literature. Quidant et al. [29] introduced a numerical method to investigate the temperature distribution in complex plasmonic nanostructures which are illuminated by external optical beam sources. Thermal capacitance constants and curves are determined for the different plasmonic nanostructures such as ellipsoids, rods, disks and rings. The electromagnetic and thermodynamic calculations are done for the different geometries. Maxwell's equations are solved for electromagnetic calculations and Poisson's equation is solved for the temperature distribution profiles by using the common boundary element method approach. The temperature distributions for the gold single spheres, sphere dimmers, and sphere chains are presented for different wavelengths and angle of light incidence for fixed gap distances between identical structures.

Near-field radiative heat transfer has been studied experimentally by different research groups recently. Rousseau et al. [30] have demonstrated an experimental setup to measure radiative conductance between a sphere and a heating element for different gap distances ranging from 30nm to 2.5 μm. It is shown that the data gathered from the experiments agree with the theoretical results and the radiative heat flux can be enhanced by several orders of magnitude in near-field. Shen et al. [31] has demonstrated experimentally the surface phonon polaritons can enhance the near-field radiative heat transfer between two surfaces at smaller gaps with calculation of the radiative heat flux between nano-sphere and a flat surface down to 30nm gap distance. Their study showed that the three orders of magnitude high radiative heat flux than Planck's blackbody radiative heat flux can be achieved between polar dielectrics materials which supports the surface phonon polaritons. Ottens et al. [32] have studied experimentally the near-field radiative heat transfer between two macroscopic sapphire planar surfaces. The experiments were done at 300 K and the heat transfer was calculated for a gap distance varying from mm to μm and for a temperature differences between 2.5 and 30 K. The experiments showed that the evanescent waves are dominant in the near-field heat transfer applications. Kittel et al. [33] have measured the near-field radiative heat transfer between the tip of a thermal profiler and planar material surfaces experimentally under the ultrahigh vacuum conditions. For the tip-sample distances below the 10^{-8} m, the results deviates from the results obtained theoretically by using fluctuation-dissipation theorem. The reason of the deviation is that the existence of a material-dependent small length scale below the macroscopic dielectric properties fails and the heuristic model agrees with the experimental data.

Besides the near-field radiative heat transfer problems addressed in the literature, the localized radiative heat transfer with the help of the plasmonic bow-tie nano-antennas to a magnetic thin-film structure is studied in the literature by Sendur et al. [34]. In their investigation, the bow-tie nano-antennas which were illuminated by a tightly focused beam of light were investigated in terms of radiative energy transfer between near-field emitter and the magnetic thin-film structure. The theory of the tightly focused beam and the power calculations was presented in the study and the dissipated optical power density on the cobalt magnetic thin-film layer is presented as a function of the gap distance between nano-antennas and the magnetic thin-film layer and results showed

that the increasing gap distance significantly reduces the power density. This result proved that the evanescent component of the near-field radiative energy transfer is significant within the total radiative energy flux.

1.3. Contributions

This thesis focus on the optical, electromagnetic and heat transfer analysis of the plasmonic nanostructure which consists of nanoantennas that are utilized to overcome the diffraction limit and to obtain single optical and hot spots on the thin film magnetic layer in the close vicinity of those nanoantennas. Analyses are conducted for different nanoantenna types with different geometrical parameters to assess the efficiency of nanoantennas, electromagnetic and heat transfer behaviours under specified conditions. The main contributions of this thesis are presented below.

- Optical, electromagnetic and heat transfer analysis modeling tools based on algorithm are developed.
- They are coded in MATLAB for each modeling tool and scripts are generated by MATLAB codes for ANSOFT HFSS for electromagnetic analysis and ANSYS Multiphysics for heat transfer analysis.
- Developed optical modeling tool is integrated to the electromagnetic and heat transfer models.
- Performances of dipole and bowtie nanoantennas in terms of electromagnetic absorption efficiency, single spot creation and heat transfer efficiency are assessed.
- Electromagnetic behavior of bowtie nanoantennas and the corresponding thin film magnetic layer for different nanoantenna lengths and for different wavelengths are assessed.
- The most efficient conditions to obtain single optical and hot spots on the thin film magnetic layer are determined.
- The heat transfer analysis for different nanoantenna lengths and different wavelengths is conducted and temperature distributions for each cases are determined.

- Electromagnetic analysis of dipole and bowtie nanoantennas shows similar behaviors for two types of nanoantennas while thermal performance of bowtie nanoantenna is better than that of dipole nanoantenna.
- New arrow shaped antenna type is introduced andelectromagnetic and heat transfer performance is investigated and compared with dipole and bowtie nanoantennas and it is seen that electromagnetic behavior does not show significant differences compared to those of dipole and bowtie nanoantennas however, the thermal efficiency of arrow shaped nanoantennas is the best compared to those of the dipole and bowtie nanoantennas.
- The effects of nanoantenna temperature on the thin film magnetic layer temperature are investigated.

1.4. Outline of thesis

This thesis consists of five main sections. Section 1 is the introduction section which has problem definition in Section 1.1, literature survey in Section 1.2 and contribution of this thesis in Section 1.3. Section 2 explains modeling tools used in this thesis. In section 2.1, optical modeling tool is explained, in section 2.2, electromagnetic modeling tool is explained and in section 2.3 heat transfer modeling tool is explained which are used throughout the analysis to obtain results in this thesis. Section 3 is the electromagnetic and heat transfer results comparison section for different types of nano antennas. In section 3.1, comparison of the dipole and the bowtie nanoantennas are presented in terms of electromagnetic and heat transfer performances. After that, in section 3.2, the nanoantennas spectral responses and the corresponding thin film magnetic layer's electromagnetic absorption responsed and heat transfer results are discussed. In section 4,new antenna type is proposed and described. In section 4.1, electromagnetic and thermal analyses of new arrow shaped nano antenna are presented. In section 4.2, new arrow shaped nano antenna is compared with dipole and bowtie nano antenna structures to assess thermal performance of different antenna types. In section 4.3, the effects of the nanoantenna temperature on the thin film magnetic layer's temperature is investigated and results are presented. In section 5, conclusions of this thesis are presented.

2. MODELING TOOLS

In this thesis, the problem defined in the preceding chapter is studied to obtain optical, electromagnetic and heat transfer performances for different parameters. Therefore, it requires three different modeling tools, optical system, electromagnetic and heat transfer tools to obtain solutions for electromagnetic and heat transfer analysis. Each of three different areasis clarified further in the following sections starting from optical modeling tool and continues with electromagnetic modeling tool and heat transfer modeling tools.

2.1 Optical Modeling Tool

In the optical system modeling part, a tightly focused beam of light which is obtained by aplanatic lens system is used throughout the analysis of the problem in this thesis. A tightly focused beam of light is significant for many practical nanoscale applications ranging from optical levitation towards the optical storage [34]. Therefore, a thorough understanding of the interaction of focused beam of light with metallic nanostructures is essential to understand the underlying physical mechanism. Most of the studies related to the surface plasmon resonances on nano-particles in the literature use the plane wave or Gaussian beam representations to deal with these problems [34]. However, even a Gaussian beam is a more accurate representation of a highly focused beam compared to a plane wave representation; a Gaussian beam is still an inadequate model of a highly focused beam.

An accurate prediction of three-dimensional distributions of various polarizations requires proper analysis of the vector nature of the incident electromagnetic fields. Richards and Wolf developed a method for calculating the electric field semi-

analytically near the focus of an aplanatic lens [35, 36]. Using Richards-Wolf method, we can obtain both transverse and longitudinal components near the focus. Richards and Wolf method can be used to obtain the electric field components for different polarizations. A highly focused beam with a linear polarization has a stronger transverse component than a longitudinal component. Linearly polarized focused beams interact differently with the particles that are placed around the focal region.

In this thesis, the dipole, bow-tie and arrow shapednano-antennas are used to overcome the diffraction limit which will be explained below and the nanoantennas are excited using a focused beam of light from aplanatic lens system.

There is a maximum limit to the resolution of any optical system, microscopes, telescopes, etc., due to the diffraction limit. Diffraction limit is defined by Ernst Abbe in 1873. It is stated that the light with wavelength, λ, traveling in a medium with refractive index n and converging to a spot with angleθ makes a spot with diameter, d;

$$d = \frac{\lambda}{2n \sin \theta} \tag{1}$$

wheren $\sin \theta$ equals to numerical aperture (NA) which can reach about 1.4 in modern optics.

Due to diffraction limit, further developments in nanoscaleplasmonic applications are required to overcome the diffraction limit. Therefore, it attracts a lot of research interests lately.

However, there are techniques to obtain higher resolution than diffraction limited optics. One possible solution to overcome diffraction limit is utilization of a nanoscale metallic antenna at optical frequencies. The nanoscale metallic antennas are used to couple an incident optical beam to length scales much smaller than the diffraction limit. Since this thesis is focused on the localized radiative energy transfer to the magnetic thin-film layer, the nano-antennas are utilized.

.

The total electric field in the vicinity of the focus is defined by

$$\mathbf{E}(\mathbf{r}_p) = -\frac{i}{\lambda}\int_0^{\alpha} d\theta \sin\theta \int_0^{2\pi} d\phi\, \mathbf{a}(\theta,\phi)\exp\left(-i\mathbf{k}.\mathbf{r}_p\right) \quad (2)$$

whereα is the half angle of the beam, $\mathbf{r}_p$ is the observation point

$$\mathbf{r}_p = x_p\hat{x} + y_p\hat{y} + z_p\hat{z} = r_p\cos\phi_p\hat{x} + r_p\sin\phi_p\hat{y} + z_p\hat{z} \quad (3)$$

and

$$\mathbf{k} = \frac{2\pi}{\lambda}\left(\sin\theta\cos\phi_p\hat{x} + \sin\theta\sin\phi_p\hat{y} - \cos\theta\hat{z}\right) \quad (4)$$

In Eqn. (3) and Eqn. (4),λ is the wavelength of the beam, $r_p = \sqrt{x_p^2 + y_p^2}$, and ϕ_p = arctan(y_p/x_p). In Eqn. (2), $\mathbf{a}(\theta,\phi)$ is the weighting vector for a plane wave incident from the (θ,ϕ) direction and given by

$$\mathbf{a}(\theta,\phi) = \begin{bmatrix} \cos\theta\cos^2\phi + \sin^2\phi \\ \cos\theta\cos\phi\sin\phi - \cos\phi\sin\phi \\ \sin\theta\cos\phi \end{bmatrix}\sqrt{\cos\theta} \quad (5)$$

In Eqn. (5), the $\sqrt{\cos\theta}$ factor is applied to the incident beam for energy conservation in a solid immersion lens (SIL), but no other apodization is applied.

The total electric field $\mathbf{E}^t(\mathbf{r})$ is composed of two components,

$$\mathbf{E}^t(\mathbf{r}) = \mathbf{E}^i(\mathbf{r}) + \mathbf{E}^s(\mathbf{r}) \quad (6)$$

where$\mathbf{E}^i(\mathbf{r})$ and $\mathbf{E}^s(\mathbf{r})$ are the incident and scattered electric field components, respectively. The incident electric field can be defined as the electric field propagating in space in the absence of the scattering object. In this problem, the incident field is the optical beam generated by the lens system in the absence of the nano-antenna and sample. In other words, the incident field can be considered as the focusedbeam

propagating in free space. The scattered electric field $\mathbf{E}^s(\mathbf{r})$in Eqn. (6) represents the fields resulting from the interaction of the incident field$\mathbf{E}^i(\mathbf{r})$ with the scattering objects, which in our case, are composed of the nano-antenna and sample. As shown in Eqn. (6), the total field is the summation of the incident and scattered field components.

Figure 2.1 illustrates the focused incident $|E^i|^2$ distributions onto the dipole nano-antennas. The fields are plottedat the focal plane *x–y* for various half-beam angles. For small half beam angle values, the field distribution is similar to that of a plane wave. Ashalf beam angleincreases, the beam becomes more tightly focused. Therefore, to obtain the tightly focused beam, higher beam angles should be utilized. As also seen from Figure 2.1, the optical spots have diameters of 400 nm. To obtain the more tightly focused optical spots beyond the diffraction limit, the nanoantennas must be utilized.

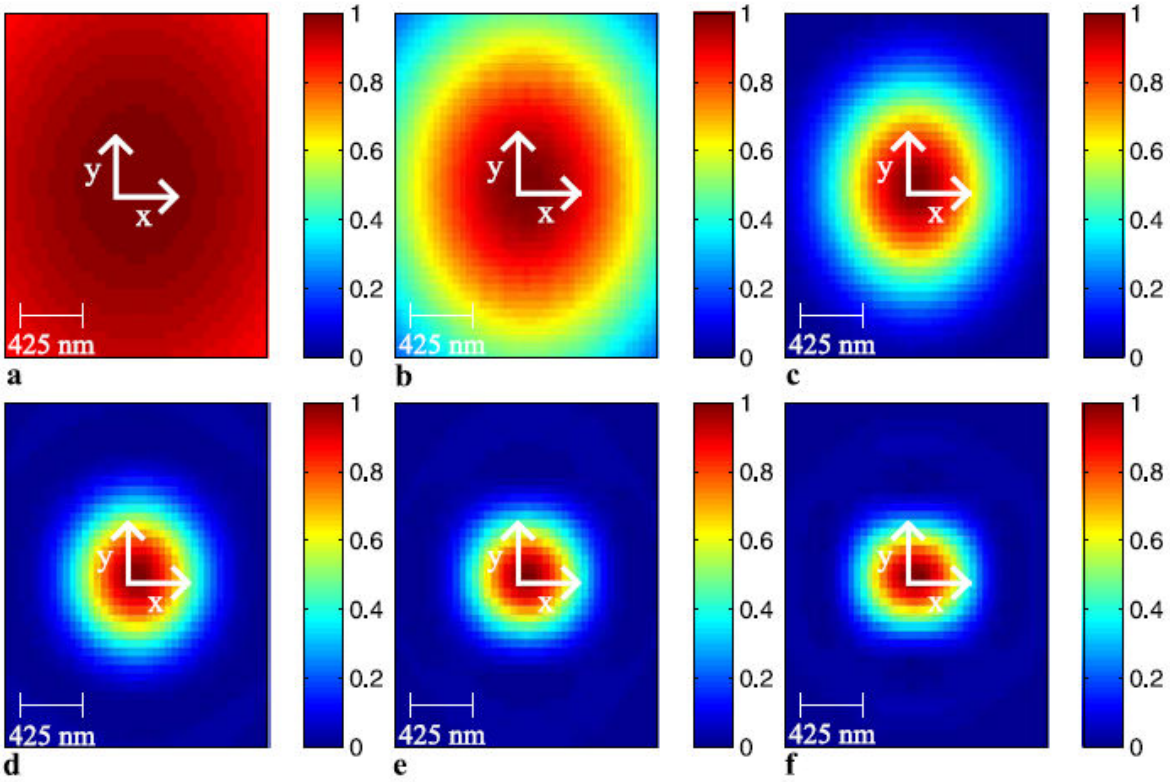

Figure 2.1. Incident $|E|^2$ distribution in the absence of the nanoantennasfor different half beam angles α of the incident beam (a) $\alpha=5^0$(b)$\alpha=15^0$(c) $\alpha=30^0$(d)$\alpha=45^0$(e) $\alpha=60^0$(f) $\alpha=75^0$

As mentioned already, in this thesis, the nanoantenna is illuminated with a focused beam of light that is obtained using a lens system. In Figure 2.2, the aplanatic lens system used to obtain the tightly focused beam of light is illustrated.V_1 is a semispherical volume that will be utilized in the power calculations. V_1 can either be a vacuum or a high-index transparent material. If a far field excitation is utilized, then V_1 is represented as a vacuum. To further increase the incident electric field, a solid immersion lens can be utilized on top of a nano-antenna. In this case V_1 is composed of a high-index transparent dielectric. In Figure2.2,S_1 represents the curved hemispherical surface, and S_2 represents the planar surfacethat forms the bottom surface of volume V_1. As shown in Figure 2.2,$\hat{n}_1$ and $\hat{n}_2$ represent the normal directions to the surfaces S_1 and S_2, respectively.

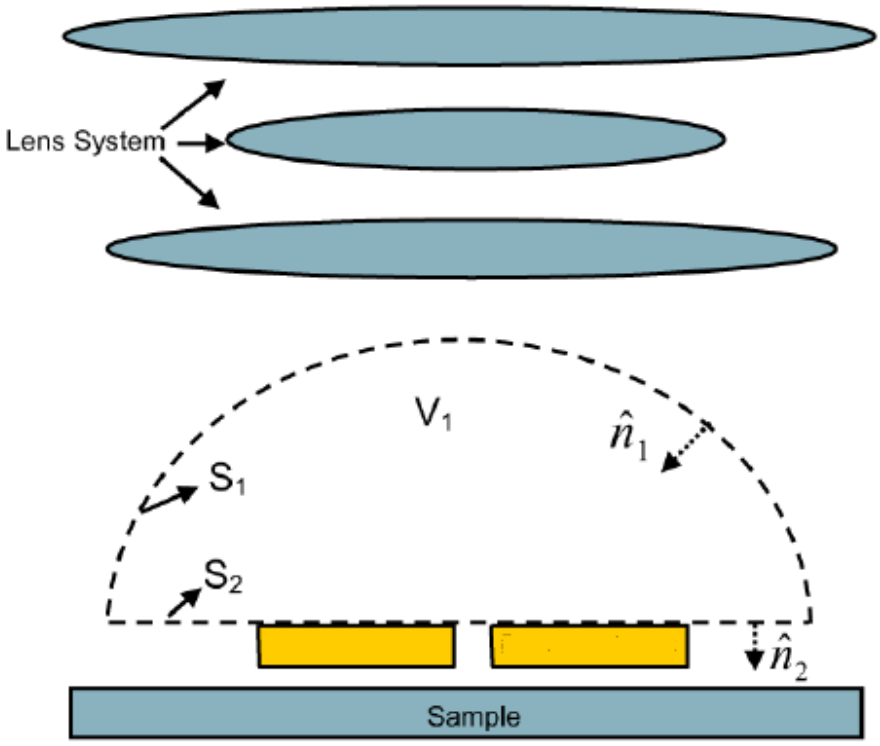

Figure 2.2. A schematic illustration of nano-antenna and sample object illuminated with a focused beam of incident light from a lens system. The sample object is in the near-field of the nano-antenna. V_1 is an semi-spherical volume that will be utilized in the power calculations.

Lastly, since the dissipated power on the nano antennas and the thin film magnetic layer is utilized for heat transfer analysis, the electromagnetic power calculations are necessary. For the power conversion, scaling factors will be based on the incident fields. These scaling factors will later be utilized to adjust the electric field magnitudes of scattered and total electric field quantities. The power of the incident beam propagating in the $\hat{z}$ direction is given by the Poynting's vector

$$P_z = Re\left[\iint_{S_1}\left(\frac{1}{2}\boldsymbol{E^i}(\boldsymbol{r}) \times \boldsymbol{H^{i*}}(\boldsymbol{r})\right).\hat{n}_1 dS\right] - \iiint_{V_1}\sigma\left|\boldsymbol{E^i}(\boldsymbol{r})\right|^2 (7)$$

The incident field geometry is already illustrated in Figure 2.2. In Eqn. (7), $\mathbf{E}^{i}(\mathbf{r})$ is the electric field defined by Eqn. (2) for vacuum and the second term of equation is zero since σ =0 for vacuum.

2.2. Electromagnetic Modeling Tool

In this thesis, the second part of the problem deals with the electromagnetic analysis of the nano-antenna and the magnetic-thin film layer. As discussed in the last part of the optical modeling tool section, the power of the incident beam is calculated through Poynting's vector. The electromagnetic problem consists of not only incident electric field but also scattered field due to presence of the nano-antennas. To obtain this scattered field, $\mathbf{E}^{s}(\mathbf{r})$, a 3-D finite element method (FEM) based full-wave solution of Maxwell's equations [37]. To represent the scattering geometries accurately, tetrahedral elements are used to discretize the computational domain. Radiation boundary conditions are used in FEM simulations. On the tetrahedral elements, edge basis functions, and second-order interpolation functions are used to expand the functions. Adaptive mesh refinement is used to improve the coarse solution regions with high field intensities and large field gradients. Adaptive mesh refinement helps to obtain accurate results for different types of geometries. Once the scattered field is solved via the FEM, the total field can be obtained using Eqn. (6).

Finally, to convert the $\mathbf{E}^t(\mathbf{r})$to the correct power quantities, the fields should be multiplied by

$$\sqrt{\frac{\text{Actual Input Optical Power}}{P_z}} \tag{8}$$

This power conversion will be utilized in the results to adjust the power quantities to express the actual input power entered into the system. Once this power conversion is performed, the dissipated power within the magnetic thin-film layer due to the near-field electromagnetic radiation can be obtained by utilizing Poynting's theorem

$$\iiint_{V_M} \sigma\,|\mathbf{E}(\mathbf{r})|^2 dV = \iint_{S_1} \left(\frac{1}{2}\mathbf{E}(\mathbf{r}) \times \mathbf{H}^*(\mathbf{r})\right).\hat{n}_1 dS - \iint_{S_2} \left(\frac{1}{2}\mathbf{E}(\mathbf{r}) \times \mathbf{H}^*(\mathbf{r})\right).\hat{n}_2 dS - \iiint_{V_A} \sigma\,|\mathbf{E}(\mathbf{r})|^2 dV - 2i\omega \iiint_V \left(\frac{1}{4}\epsilon|\mathbf{E}(\mathbf{r})|^2 + \frac{1}{4}\mu|\mathbf{H}(\mathbf{r})|^2\right) dV \tag{9}$$

where V_M represents the magnetic layer, V_A represents the nano-antenna particles, and S_1 and S_2 are the surfaces perpendicular to the direction of propagation shown in Figure 2.2. The term on the left-hand side of the equation represents the optical power dissipated over the magnetic film. The first and second terms on the right hand side of the equation represents the optical power entering and exiting the structures from surfaces S_1 and S_2, respectively. The third term represents the optical power dissipated over antenna particles and the last term represents the complex reactive energy stored in the volume between S_1 and S_2. Eqn. (9) along with Eqn. (2) and Eqn. (6) will be utilized to obtain the optical dissipated power profiles over the magnetic film. To obtain the results for Poynting's equation and the dissipated power calculations, firstly, the Maxwell's equations need to be solved to obtain the electric and magnetic fields which have extraneous fluctuating currents.

Electromagnetic calculations and simulations are done via using the commercially available software ANSYS HFSS 12 which is the industry-standard simulation tool for 3-D full-wave electromagnetic field simulation. The simulations are conducted by scripts of ANSYS HFSS 12 software. All script generator codes for ANSYS HFSS 12 are prepared in MATLAB. The simulation process starts with the geometry drawing. The nano-antennas and layers in 3-D are created by using HFSS 12 drawing tools. After

the geometry is created, the material properties are assigned to the each geometry accordingly. All of the optical material properties are taken from Palik's Handbook of Optical Constants of Solids [38]. Nano-antennas are placed in a vacuum box. Nano-antennas are assigned gold material. The magnetic thin-film layer is assigned cobalt material. The insulator thin-film layer is assigned SiO_2. The heat sink is assigned gold material. After these steps, the boundary conditions are assigned to the geometry. In ANSYS HFSS 12, the outside of the all system is assigned radiation boundary condition. After that step, a tightly focused beam equations are calculated by MATLAB for each wavelength, $\theta$and ϕ values. The calculations are done for k_x, k_y, k_z, E_x, E_y, E_z values and assigned as an input plane wave array to the system studied. Then, the analysis setup is created. In analysis setup, calculation frequency, maximum electric field error, maximum and minimum calculation passes, minimum convergence passes, percent refinement, basis order, and target value of wavelength are determined for analysis. The analysis is started for determined parameters and solution is done. When solution is completed, the complex magnitude of electric field at the center of nano-antennas and complex magnitude of electric field at the center of the magnetic thin-film layer's top surface are calculated. In addition to those, the dissipated power on the nano-antennas and magnetic thin-film layer are calculated and saved as a WordPad document to be used as an input to the ANSYS Multiphysics software program for heat transfer calculations. The dissipated power is calculated layer by layer in z-direction for all over the x-y plane. The layers consist all of the nano-antennas and magnetic layer volumes.

The simulations are conducted for each different dipole and bow-tie antenna lengths for each wavelength which are from 400 nm to 1900 nm. After the simulations are conducted, the MATLAB code is used to scale the power outputs to the power input used in this thesis which is 100 mW. When power scaling is done, the dissipated power of nano-antennas and the magnetic layer are converted to the format that ANSYS uses as heat generation rate input. This format preparation is done via using MATLAB code.

As presented above, for electromagnetic analysis that uses the optical system's output as an input are conducted in ANSYS HFSS 12 electromagnetic FEM analysis software program. The outputs of this modeling tool are electric field values and dissipated power on the nano-antennas and the magnetic thin-film layer which is used as an input

to the ANSYS 12.1 program for near-field heat transfer analysis of which the details will be presented in Section 2.3.

2.3. Heat Transfer Modeling Tool

In this thesis, the last part of analysis is the heat transfer analysis to determine the near-field radiative heat transfer calculations in the system studied. The heat transfer is linked to the electromagnetic results with the help of the thermal radiation term in the Maxwell equations. However, the thermal radiation should be considered from the electrodynamics point of view to link this with electromagnetic waves [16, 17].

In the heat transfer analysis, the dissipated power on the nano-antennas and the magnetic thin-film layer with the Poynting's theorem are used which are obtained by the tightly focused beam of light approximation. The general equations are presented in the Section 2.2. Electromagnetic Modeling Tool. The electric and magnetic field terms which are used in the abovementioned equations will be presented in this section.

The dissipated power on the nano antennas and the thin film magnetic layer is calculated by utilizing Equation 10:

$$\iiint_{V_A} \sigma \, |\mathbf{E}(\mathbf{r})|^2 dV \tag{10}$$

The dissipated power equals to conductance of material multiplied by the square of electric field.

The propagating and evanescent electromagnetic waves are emitted in the near field due to accumulated charge at the tip of the antenna with opposite signs via the oscillations of charges of opposite signs.In the analysis conducted in this thesis, the heat transfer analysis is conducted for the nanoantenna structures and the corresponding thin film

magnetic layer. Since the decreased gap distances increases the effects of the evanescent waves contribution to the radiative heat transfer, contributions of propagating and evanescent waves are both assessed.

In this thesis, the dissipated power on the nano-antennas and the magnetic thin-film layer is obtained from ANSOFT HFSS 12 electromagnetic simulation software as discussed in Section 2.2. These power profiles are input for ANSYS Multiphysics 12.1 Finite Element Method (FEM) software. The input of the heat transfer analysis is heat generation rates which are applied as body loads to represent heat generated within an element. The heat generation rate has units of W/m^3.

In the ANSYS Multiphysics 12.1, the temperature profiles of the nano-antennas and the magnetic thin-film layer are obtained. The heat transfer problem is solved via following steps.As a first step, the geometry of the problem is created by using drawing tools of ANSYS Multiphysics 12.1. After geometry creation, the density, heat conduction coefficient and heat capacity properties of materials are assigned to the each of the layers and the nano-antennas. After material assigning, the heat generation rates are assigned to the nano-antennas and the magnetic thin-film layer, respectively for each heat transfer problems. As a fourth step, the mesh of the geometries is defined and mesh operation is done. Then, the analysis setup is specified and simulation is run. When the solution is completed, the post processor tool is used to obtain the temperature profiles over the selected bodies or surfaces as a function of distance or time are saved. The results of the heat transfer analysis are transient temperatures to determine the temperature change within a small scale of time in the nano-seconds.

By utilizing the abovementioned process, the temperatures of the nanoantennas and the thin film magnetic layer are obtained which takes into account the propagating waves effects. In this analysis, the dissipated power profiles for nanoantennas and the thin film magnetic layer are used. After that, to determine the effects of thenano-antennas temperature on the magnetic thin-film layer, the analysis are conducted by only utilizing the dissipated power input for nanoantennas. This input is generated from the incident focused beam of light which results in the dissipated power on the nanoantennas. This dissipated power is used as an input to the heat transfer analysis. Therefore the temperature of the nanoantennas and the temperature of the thin film magnetic layer

which is caused by the temperature of the nanoantennas are obtained. Since the gap distance between the nanoantennas and the thin film magnetic layer in this analysis is 20 nm, the temperature contribution of the nanoantennas to the temperature of the thin film magnetic layer is important to analyze.

To sum up, the heat transfer analysis for the nanoantennas and the corresponding thin film magnetic layer are conducted for given electromagnetic input. The results are presented in the following chapters. This thesis not only shows the temperature profiles of the nanoantennas and the corresponding thin film magnetic layers, but also proposes methods to decrease temperature of the nanoantennas while keeping the thin film magnetic layer temperature at the desired level which will be discussed further in the subsequent chapters.

3. ELECTROMAGNETIC AND THERMAL PERFORMANCE RESULTS OF NANOANTENNAS

In this chapter of the thesis, the results obtained by utilizing optical, electromagnetic and heat transfer modeling tools are presented. In the first part, dipole and bowtie nanoantennas performances are compared in terms of electromagnetic and heat transfer results. In the second part, the electromagnetic and heat transfer analysis are conducted for bowtie nanoantennas with different lengths. The results of electromagnetic dissipated power profiles on nanoantennas and thin film magnetic layer structure and temperature profiles on the bowtie nanoantennas and on the thin film magnetic layer are presented. In the third section, new nanoantenna type, arrow shaped, is proposed and investigated in terms of electromagnetic and heat transfer analysis.

3.1. Comparison of dipole and bowtie nanoantennas electromagnetic and heat transfer performances

In this section of this thesis, the optical, electromagnetic and heat transfer analysis are conducted for the system shown in Figure 3.1.1.

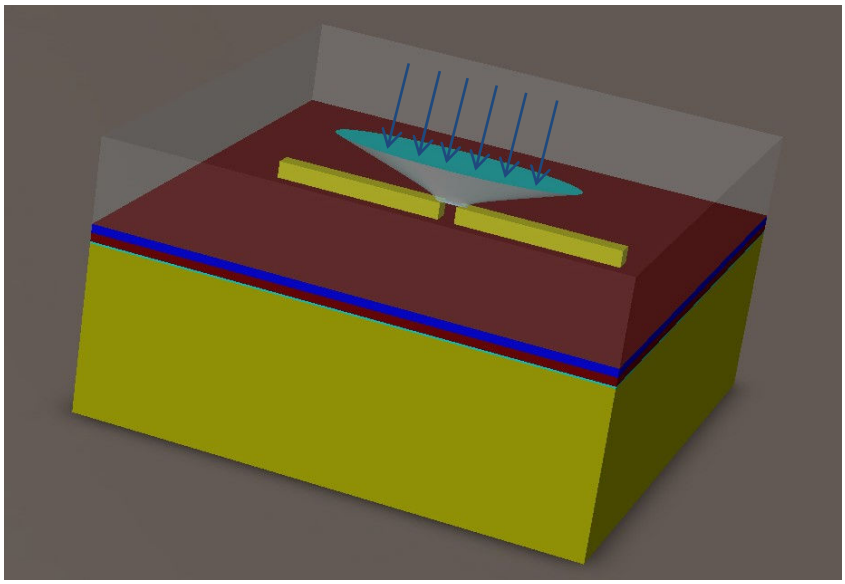

Figure 3.1.1.Geometry studied in the analysis. From top layer to bottom layer: Vacuum 100nm, Air (blue) 10nm, magnetic layer (dark red) 10nm, insulator(green) 2nm, heat sink (yellow) 200nm height and all geometries are 600 nm long through x and y directions

In this part, two types of nano antennas are analyzed for electromagnetic energy transfer and heat transfer. These dipole and bowtie nano antennas are investigated for 10 mW power input and absorption efficiency of nanoantennas, nano antenna temperature and the thin film magnetic layer temperatures with electromagnetic absorption distribution are obtained.

	Wavelength	Antenna type	Antenna Parameters	Optical spot diameter	Input power	Absorption efficiency	Antenna Temp. (Celcius)	Magnetic layer Temp (Celcius)
1.	750nm	Dipole	Length:100nm, Width:20nm, Thickness: 20nm	10nm	10mW	%3.1	87	26.5
2.	1150nm	Dipole	Length:150nm, Width:20nm, Thickness: 20nm	10nm	10mW	%19.6	1236	63
3.	1400nm	Dipole	Length:175nm, Width:20nm, Thickness: 20nm	15 nm	10mW	%17	1771	62.7
4.	1550nm	Dipole	Length:200nm, Width:20nm, Thickness: 20nm	20nm	10mW	%16.9	752	20.3
5.	700nm	Bowtie	Length:175nm, Width:20nm, Thickness: 20nm	5nm	10mW	%1.29	32	39.3
6.	1000nm	Bowtie	Length:175nm, Width:20nm, Thickness: 20nm	20nm	10mW	%3.74	138	52.1
7.	1100nm	Bowtie	Length:175nm, Width:20nm, Thickness: 20nm	40nm	10mW	%6.55	265	163
8.	1400nm	Bowtie	Length:175nm, Width:20nm, Thickness: 20nm	40nm	10mW	%0.88	39	66.1

Table 3.1.Absorption efficiency, antenna temperature and the thin film magnetic layer temperature results for different antenna types and parameters

In Table 3.1, absorbed electromagnetic power distributions for eight cases are given. The optical spots diameters, types of nano antennas and absorption efficiency are illustrated.

In the Figure 3.1.2, the case 1 in the table is illustrated as an example of magnetic layer absorption. By utilizing 100 nm dipole antenna, the single optical spot is obtained on the thin film magnetic layer with 10nm diameter. Absorption efficieny for 900 nm wavelength is 19% however, the single optical spot could not obtained for that wavelength.

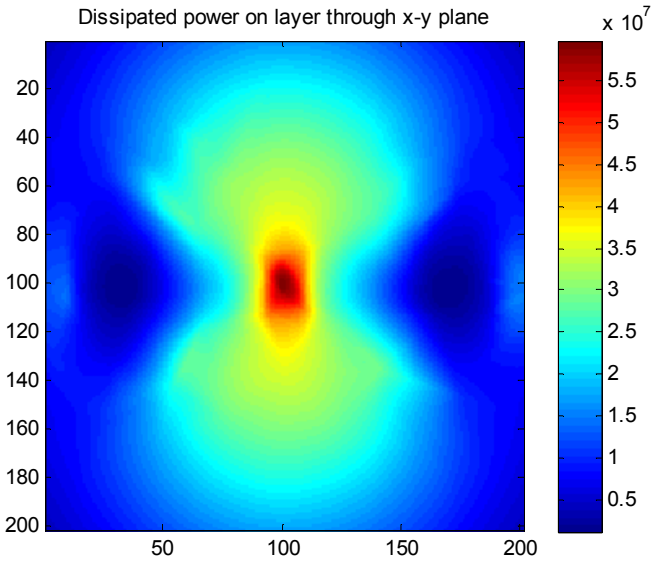

Figure 3.1.2. Electromagnetic absorption on the thin film magnetic layer of 100nm long dipole nano antenna for 750 nm wavelength

As seen from Table 3.1, the dipole antennas are more efficient to obtain high absorption efficiency which is ratio of absorbed power on the thin film magnetic layer to the input power. However, the dipole antennas experience higher temperatures due to low material volume compared to bowtie nano antennas. Therefore, for practical applications in which control of nano antenna temperature is important, usage of the bowtie nano antennas are more efficient.

When the temperature distribution profiles are investigated for dipole and bowtie nano antennas, it is seen that 175 nm dipole nano antennas reach 1700 celcius degree in Figure 3.1.3. Temperatures are calculated for the effective power applied for 0.7 nano seconds and distribution is observed until 1.7 nanoseconds which is shown in Figure 3.1.3. Compared to the 175 nm bowtie nano antennas for different wavelengths, it is seen that the bowtie nano antennas have significantly lower temperatures compared to the dipole nano antennas. Therefore, it is efficient to use bowtie nano antennas in the practical applications to prevent malfunctions due to excessive temperature increase.

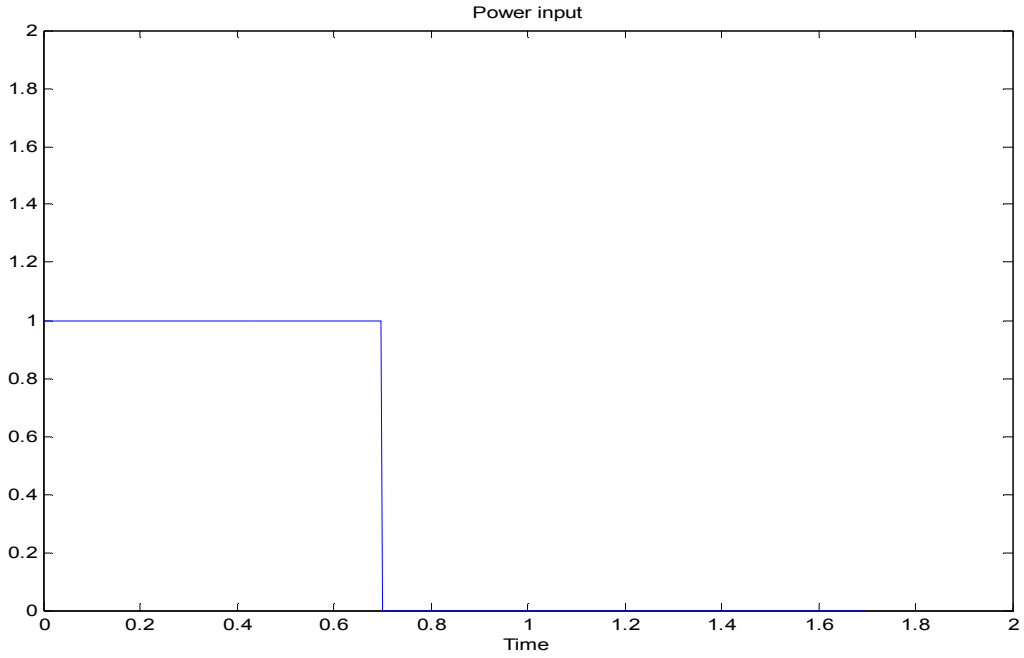

Figure 3.1.3. Input power to the system which is given only 0.7 nanoseconds and then cut off.

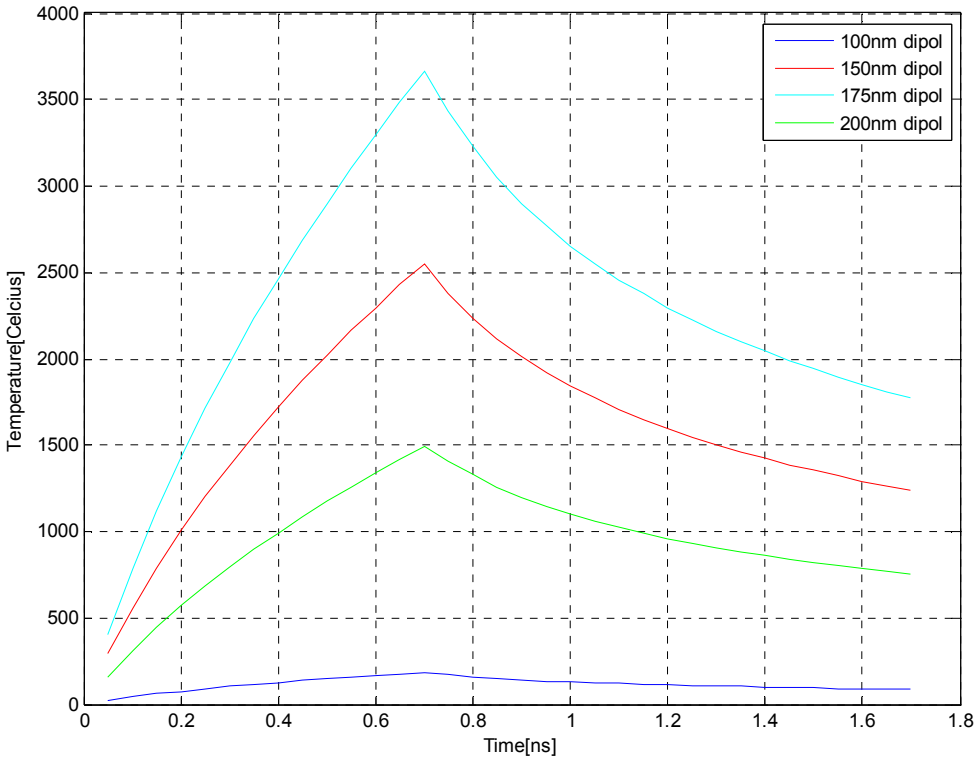

Figure 3.1.4.Temperature profile on the dipole nano antennas for power input for 0.7 nano seconds

The 175 nm long bowtie nano antenna experiences highest temperature for 1100 nm wavelength because, there are two optical spots on that wavelength.

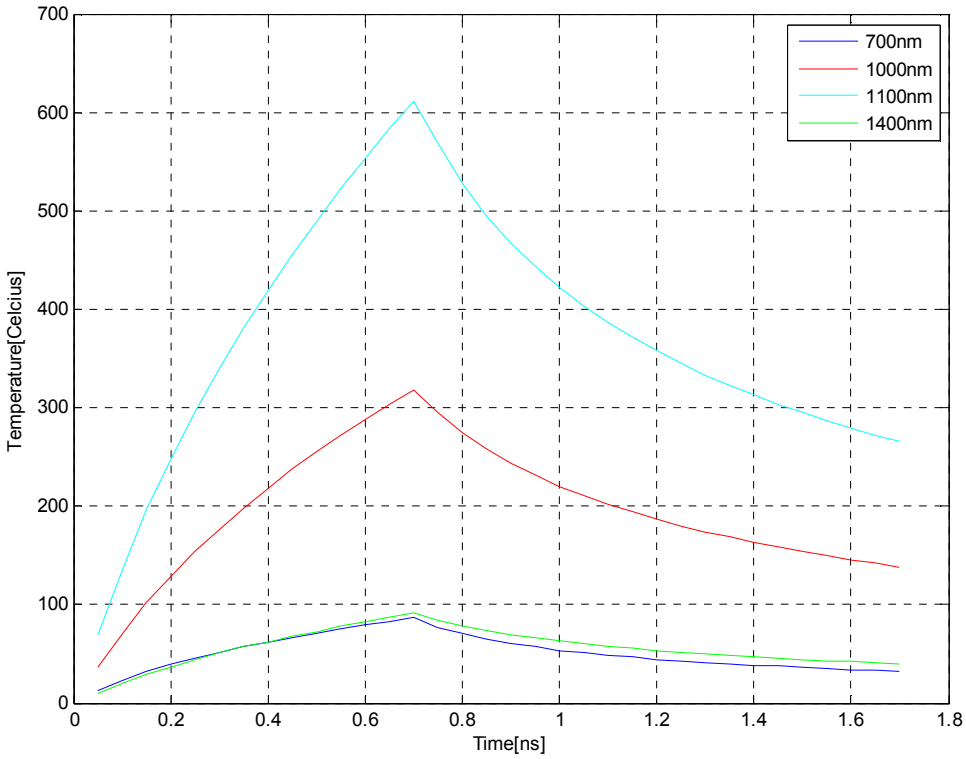

Figure 3.1.5. Temperature profile on the bowtie nano antennas for power input for 0.7 nano seconds

At last the corresponding thin film magnetic layers temperature distribution profiles are investigated. It is observed that around 0.7 nanoseconds the temperature of the thin film magnetic layer reaches steady state values. The interesting point is that 1400 nm bowtie nanoantenna has the lowest nano antenna temperature however, corresponding magnetic layer has second highest temperature profile. The reason is that the optical spots occur at the center of the nano antennas instead of on the nano antennas therefore, while the nano antenna temperature remains lower, the magnetic layer has higher values.

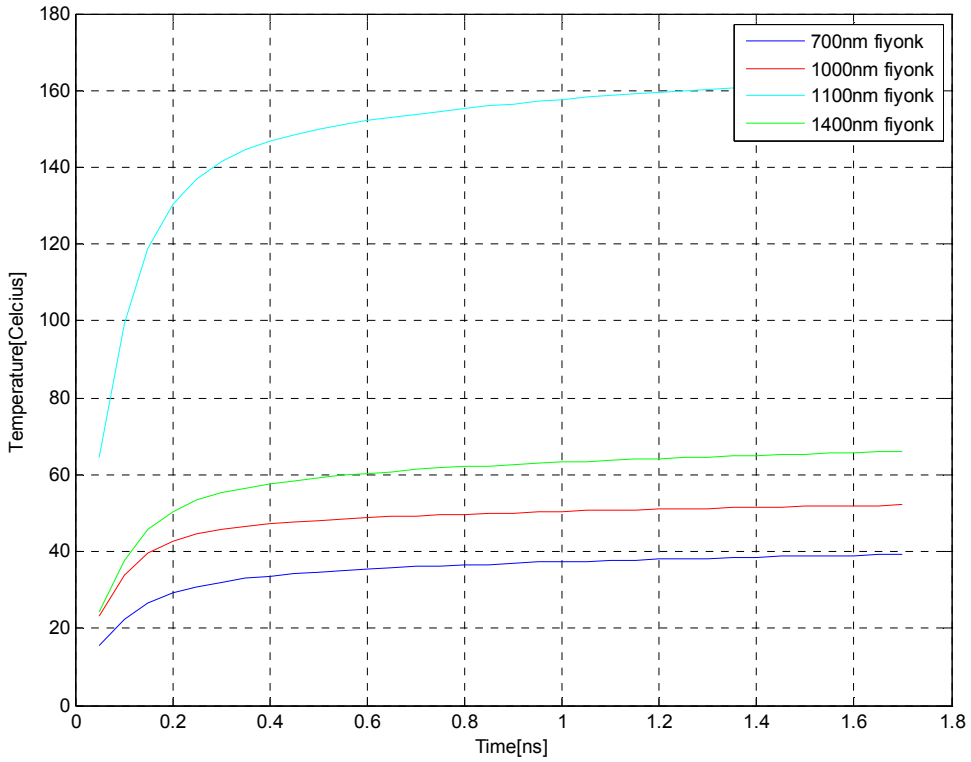

Figure 3.1.6. Temperature profile on the magnetic layer for bowtie nano antennas for power input for 1.7 nano seconds

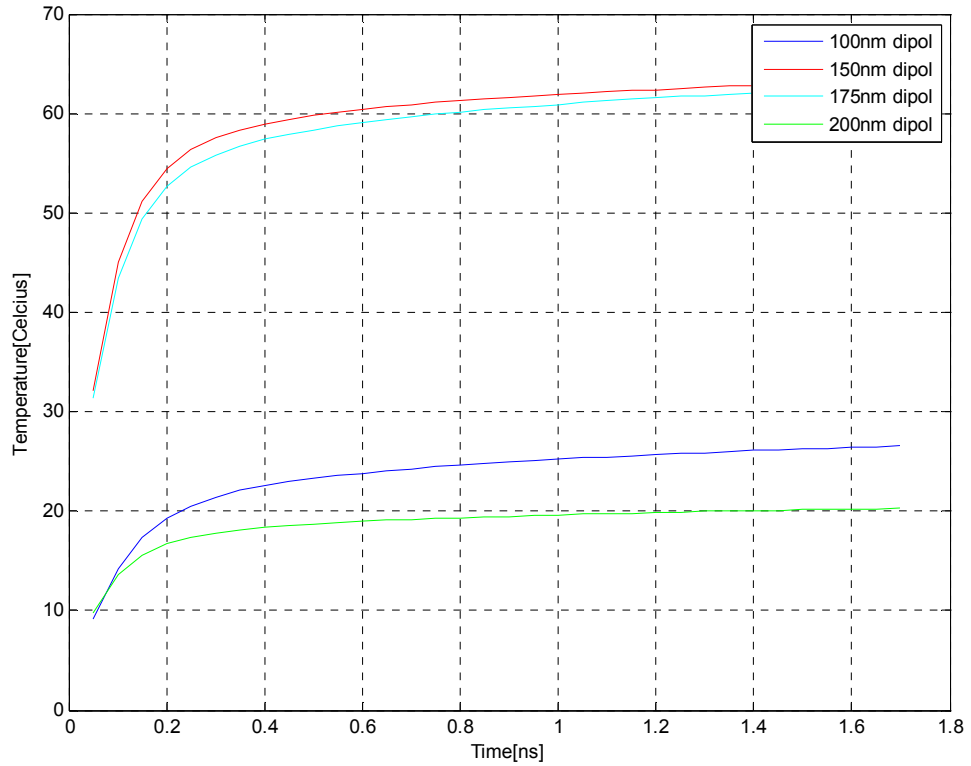

Figure 3.1.7. Temperature profile on the magnetic layer for dipole nano antennas for power input for 1.7 nano seconds

Lastly, the dipole antenna's thin film magnetic layers are investigated for temperature profiles and it is seen that 150 and 175 nm long dipole antennas reach higher values. The magnetic layers reach steady state quickly as in the upper case. The reason of quick steady state is that the magnetic layer material is cobalt and the magnetic layer has very large surface area compared to that of nano antennas.

To compare methodology, the literature benchmark is conduted. The study of Mulet et al. [18] is considered and means power radiated from the bulk gold material to the small dielectric particle, considered as a point-like dipole is studied.

The power radiated from gold bulk material to the small particle for different separation distances are analyzed and presented in the study of Mulet et al. [18]

To compare results similar analysis with same parameters are compared and the similar results are obtained. To further challenge the methodology used in the thesis, the 100 nm dipole nanoantenna and the thin film magnetic layer system studied through this thesis is analyzed in terms of power transfer from nanoantennas to the thin film magnetic layer between distances 10-8 m to 10-5 m. The results are presented in Figure 3.1.8. As seen from the figure as separation distance between dipole nanoantennas and the thin film magnetic layer increases, the power decreases and converges to the far field values.

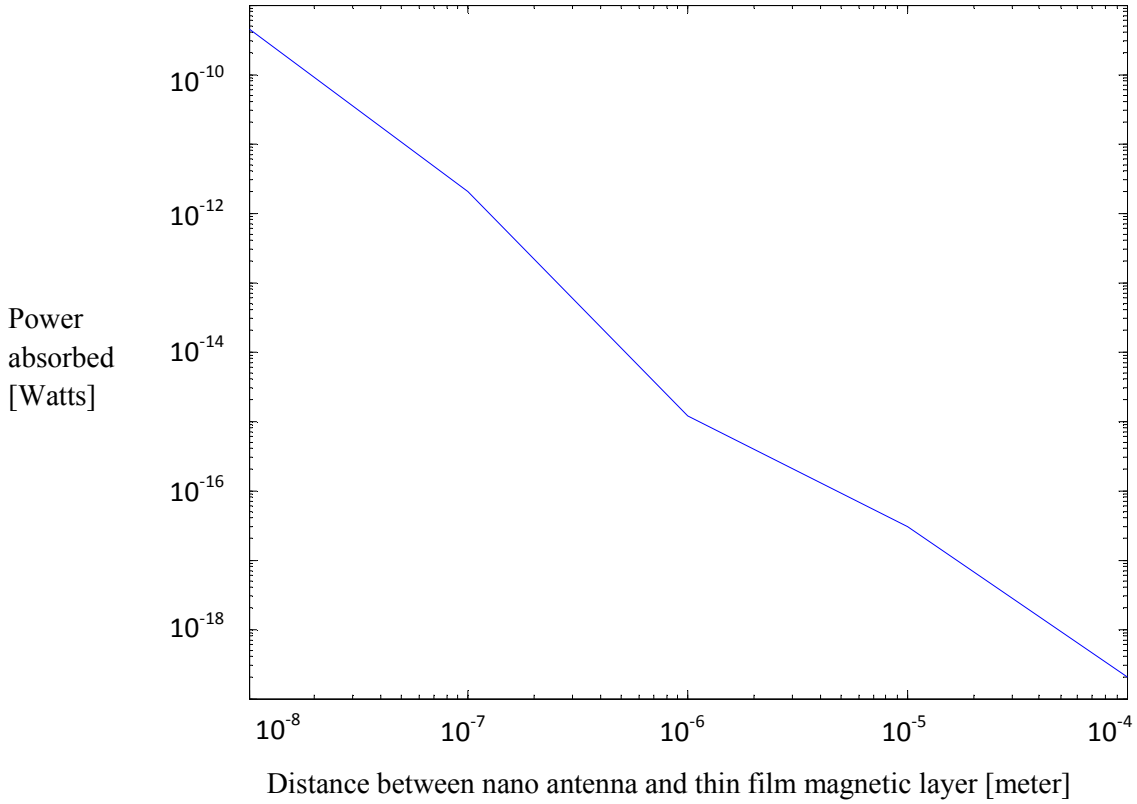

Figure 3.1.8. Power absorbed by thin film magnetic layer versus separation distance between dipole nano antenna and thin film magnetic layer

3.2.Nano antenna spectral responses & thin film magnetic layer absorption response comparisons

3.2.1.Electromagnetic results

In this thesis, the electromagnetic behaviours of the dipole, bowtie and arrow shapednano antennas are studied within the system described which consists of vacuum, thin-film magnetic layer, insulator layer and heat sink. The electromagnetic analysis is conducted in this system to find out the electromagnetic behaviour of nano antennas and the thin-film magnetic layer under specified focused beam. In this thesis, the focused beam of light is used to illuminate the nano antennas. The total description of the focused beam of light is given in the section 2.1, Optical Modeling Tool section. This focused beam of light is described with power in terms of miliwatt(mW), wavelength in terms of nanometers(nm), half angle of the beam defined as α, the numerical aperture as NA and observation point defined as r_p. The electromagnetic results are derived for nano antennas and for the magnetic layer as complex magnitude of electric field to see electric field behaviour on the center point of the nano antennas and on the thin-film magnetic layer surface. Secondly, absorbed power by nano-antennas and the thin-film magnetic layer is derived from the electromagnetic simulations. The absorbed power profiles are significant since they are used as an input to the heat transfer analysis problem part. The absorbed power profiles show the total dissipated power on the nano antennas and on the thin-film magnetic layer. All of the electromagnetic analyzesare conducted via commercially available electromagnetic simulation tool, ANSOFT HFSS 12.1 program.

In the electromagnetic simulations conducted for this thesis, the total power of the focused beam is taken as 100mW as default for all types of analysis. The wavelength range is defined between 400 to 1900nm which lies in the visible region of the electromagnetic spectrum. The half angle of the beam is taken as 60^0 for all of the electromagnetic analysis. The numerical aperture which defines an optical system is a dimensionless number that characterizes the range of angles over which the system can

accept or emit light. By incorporating index of refraction in its definition, NA has the property that it is constant for a beam as it goes from one material to another provided there is no optical power at the interface. The exact definition of the term varies slightly between different areas of optics. Numerical aperture is commonly used in microscopy to describe the acceptance cone of an objective (and hence its light-gathering ability and resolution), and in fiber optics, in which it describes the cone of light accepted into the fiber or exiting it. In this thesis, numerical aperture is taken as 0.86 for all of the electromagnetic analysis.

The electromagnetic analysis conducted in this section used different nano antenna geometries to determine the impacts of geometry itself and the parameters of the nano antennas. Two types of nano antennas are used, dipole and the bowtie nano antennas which are ilustrated in the introduction section. The nano antennas are characterized by their lengths, widths and thickness with the gap distance between two nano antennas. In electromagnetic analysis conducted in this section, the dipole nano antenna's lengths are between 100nm to 200nm, the thickness of them are 20 nm, the width of the dipole nano antennas are 20 nm and the gap distance between the nano antennas are 20 nm. The bowtie nano antennas' lengths vary between 100nm and 250nm, the thickness of them are 20 nm, the narrower width is 20 nm in the gap region between nanoantennas and the thickest width is calculated from the smaller width plus tangent 30^0 multiplied by 2 times of the length of the nano antennas and the gap separating the nano antennas is 20 nm long.

The nano antennas are made of gold and material properties are assigned those properties of gold. The nano antennas are placed in the vacuum which has 2000 nm long in x and y directions and 100 nm long in the z direction which is the same direction with the thickness of the nano antennas. There is an air gap between nano antennas and the magnetic layer which has thickness of 10 nm. The thin-film magnetic layer which has a thickness of 10 nm lies under the air gap. After the thin-film magnetic layer, there is an insulater layer which has 2 nm thickness. At the bottom of the system studied there is an heat sink which has thickness of 200 nm. The thin-film magnetic layer is made of

cobalt. The insulator is silicone dioxide (SiO_2) and the the heat sink is made of gold. All of the layers in the system has 2000 nm long in the x and y directions.

Firstly, the different antenna length effects are investigated for bowtie nano antennas with lengths 100nm, 175nm, 200nm and 250 nm. The electric field distribution on the center of bowtie nano antennas are illustrated in Figure 3.2.1.

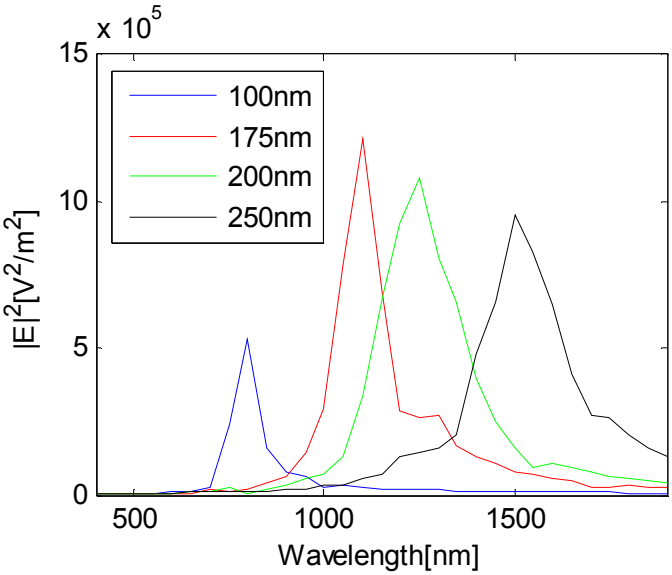

Figure 3.2.1. Electric field intensity values on the center of bowtie nano antennas

The electric field intensity on the center of the bowtie nano antennas is highly dependent on the length of the bowtienano antenna. The values are calculated for 100 nm, 175 nm, 200 nm and 250 nmlong bowtie nano antennas between 400 nm and 1900 nm wavelength range with 50 nm incrementation value.

The first observation is that increasing length of the bowtie nano antenna shifts the peak value to higher wavelength values. While 100 nm bowtie nano antenna experiences peak value at 800 nm wavelength, 175 nm bowtie nano antenna has peak value at 1100 nm wavelength. The reason of this shift is the dependence of the electric field to the

length of the nano antenna length. Varying length nano antennas focus the light beam in the different wavelengths. The peak values are also different for each case. The highest possible electric field intensity is observed when nano antenna has 175 nm length. The optimum nano antenna, which the peak electric field intensity is obtained,is 175 nm long bowtie antenna.

The electric field intensity values are obtained for the thin film magnetic layer structure. Since this thesis aims to determine the cases in which the single focused optical spot on the thin film magnetic layer structure, it is significant to assess the behaviour of the electric field intensity on the thin film magnetic layer. The electric field distribution on the thin film magnetic thin film layer for100 nm, 175 nm, 200 nm, and 250 nm long bowtie nano antennas between 400 nm and 1900 nm wavelength range with 50 nm incrementation value is shown in Figure 3.2.2.

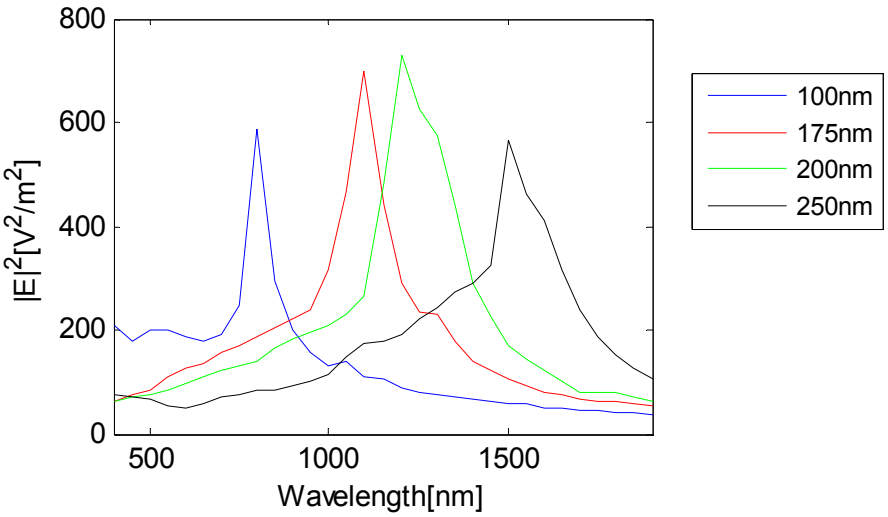

Figure 3.2.2. Electric field intensity values on the center of corresponding thin film magnetic layer for different length of bowtie nano antennas

The electric field intensity values on the center of the layer in terms of different wavelengths show same behaviour as for the case of bowtie nano antennas. However,

the main difference between nano antennas and the thin film magnetic layer is that the electric field intensity on the layer shows fluctuating behaviour for the values other than peak values. Peak values occur at the same wavelength for both nano antennas and the corresponding thin film magnetic layer structures.

The other major difference is that the 200 nm bowtie nano antenna's corresponding thin film magnetic layer has the highest peak value contrary to nano antenna electric field intensity in which 175nm has the highest value. It indicates that 200 nm bowtie nano antenna has the highest focusing ability than other nano antennas which are compared in this thesis.

After the analysis of electric field intensity for different length and wavelengths, the dissipated power distribution which is important to differentiate where single optical spot is obtained, is studied. Firstly, general look for maximum values and the center values on the thin film magnetic layer is analyzed. The dissipated power is calculated by multiplication of conductance and the complex magnitude of the electric field of the thin film magnetic layer structure. Therefore, it is expected to obtain maximum values at the center of the layer at the same wavelengths as the electric field intensity distribution. The maximum dissipated power all over the top surface of the thin film magnetic layer is shown in Figure 3.2.3. The maximum dissipated power is obtained for 100 nm bowtie nano antenna however, the important part here is to the values on the center of the thin-film magnetic layer structure. Therefore, in Figure 3.2.4, the dissipated power on the center of the thin film magnetic layer is illustrated.

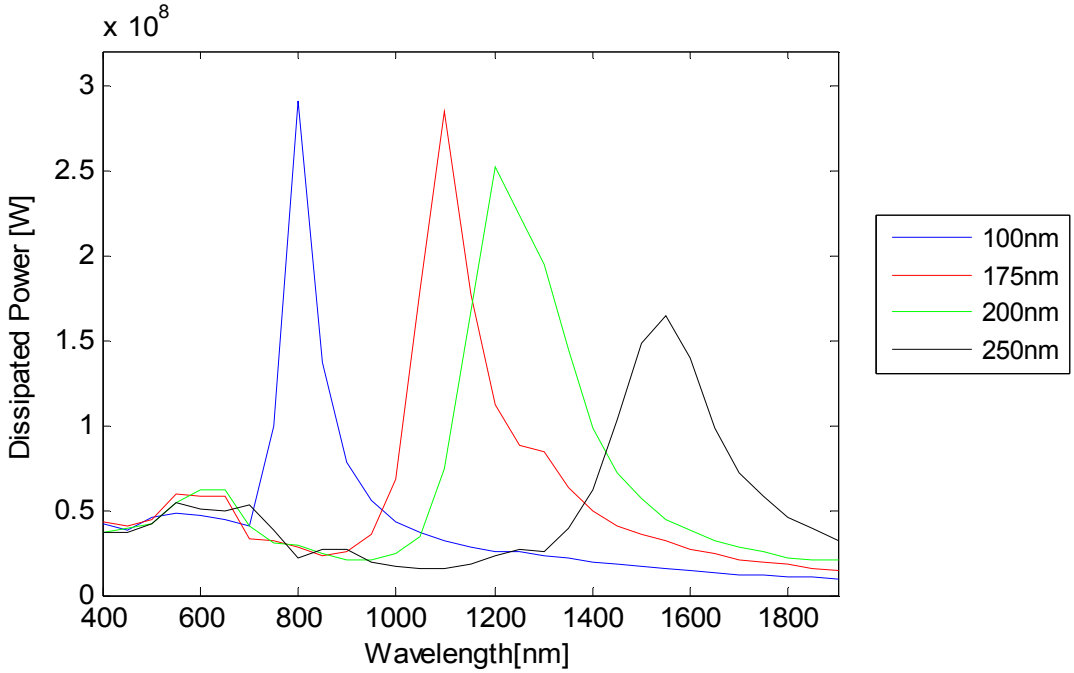

Figure 3.2.3. Maximum dissipated power values on the thin film magnetic layer between 400nm and 1900 nm wavelength

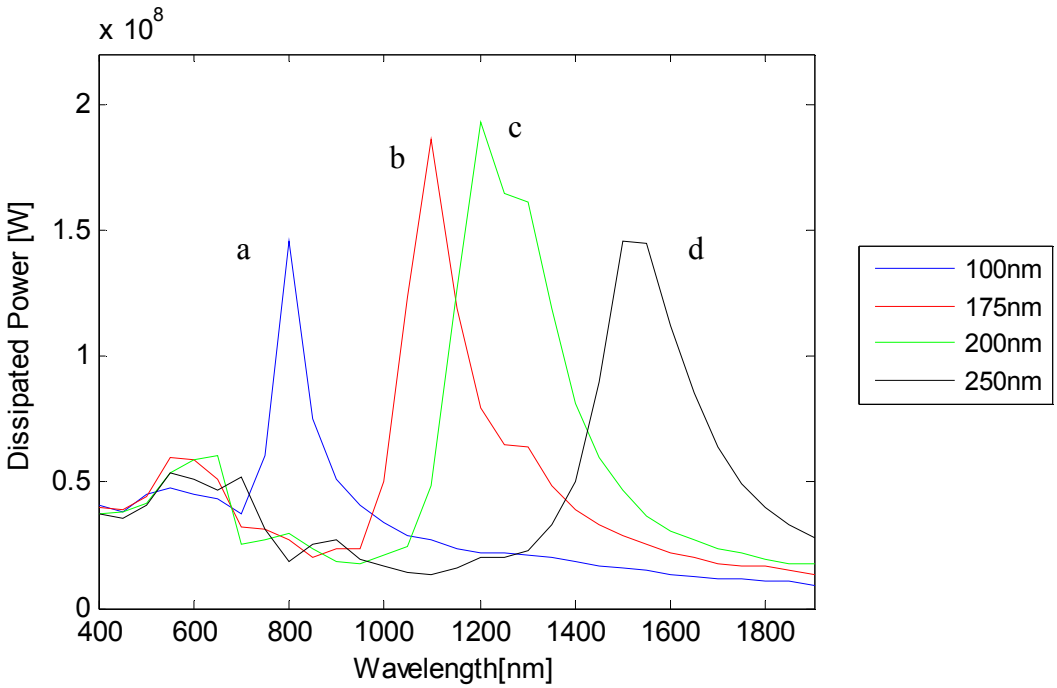

Figure 3.2.4. The dissipated power on the center of the thin film magnetic layer structure

The distribution of the dissipated power on the center of the thin film magnetic layer structure shows same behaviour as electric field intensity illustrated in Figure 3.2.2 as expected. The dissipated power values on the thin film magnetic layer structure shows different peak values for different lengths of nanoantennas. The distribution profile of dissipated power for peak values are illustrated in Figure 3.2.5 (a-d) for 100 nm, 175 nm, 200 nm and 250 nm long bowtie nanoantennas respectively. It is seen that for analyzed bowtie nanoantennas, peak values does not correspond to the single spots. The most important part is dissipated power on the center of the magnetic layer since this thesis aims to point the cases where the single optical spots obtained on the layer.

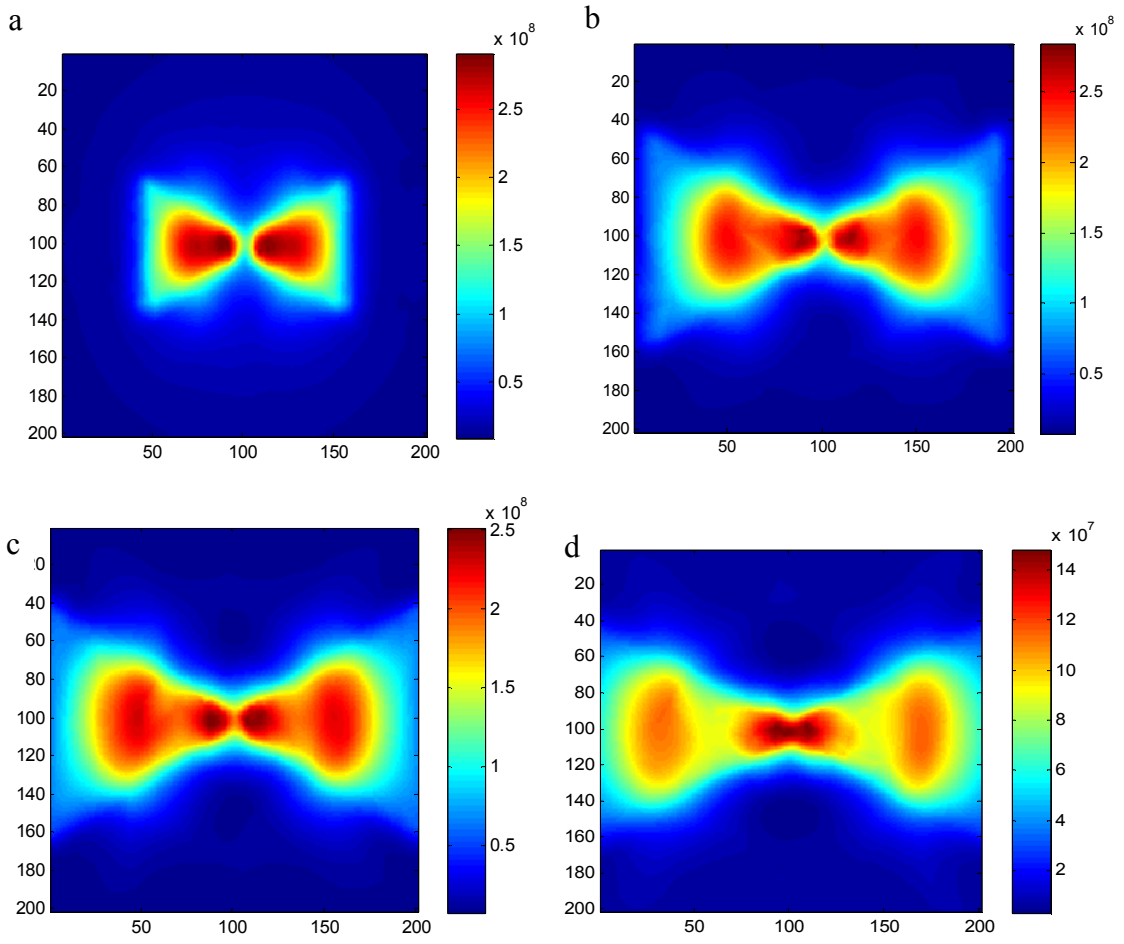

Figure 3.2.5. The dissipated power distribution profiles for peak dissipated power values of (a) 100 nm long, (b) 175 nm long, (c) 200 nm long and (d) 250 nm long bowtie nanoantennas.

To further analyze and find the ideal cases, individual figures for each of different antenna lengths for maximum and the center values of dissipated power on the thin film magnetic layer structures are drawn in Figures 3.2.6-3.2.9. The cases where the maximum value and the center value of the dissipated power coincide are the cases where the single optical spots are obtained.

In Figure 3.2.6, the electric field intensity on the center of nano antennas, maximum and center values of dissipated power for magnetic layer are illustrated. The points where maximum (red line) and the center values (green line) of dissipated power coincides shows the wavelengths in which single optical spot occurs. For 100 nm bowtie antenna the single optical spots are obtained between 400 and 700nm wavelengths. The dissipated power distribution on the surface of the thin film magnetic layer structure for 700 nm wavelength is shown in Figure 3.2.7. As seen from the figure, the single optical spot is obtained for 100 nm long bowtie nano antenna.

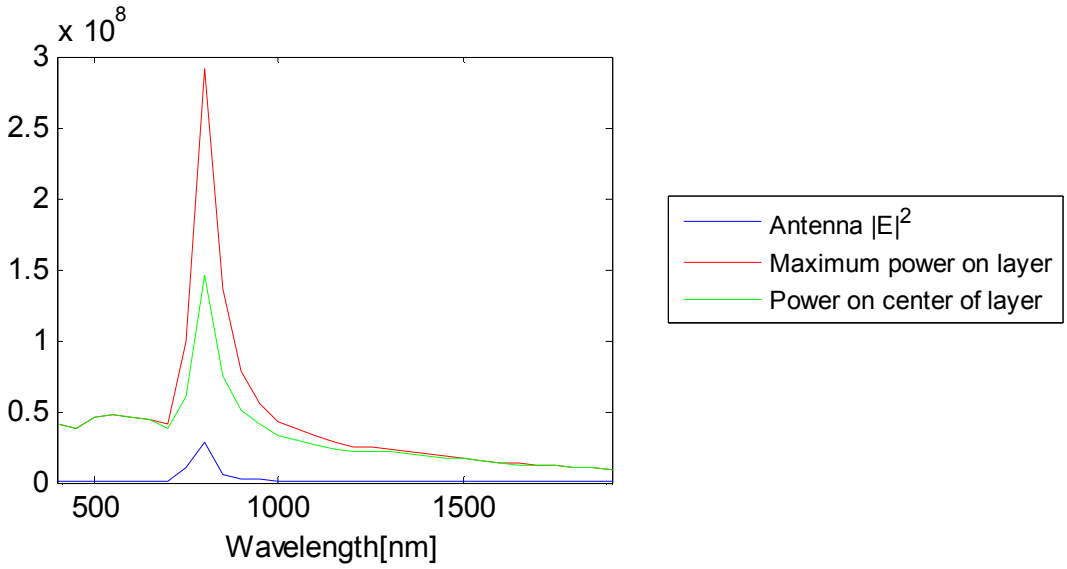

Figure 3.2.6. The electric field intensity on the center of nano antennas, dissipated power maximum and center value on the thin film magnetic layer for 100 nm bowtie nano antenna.

A similar analysis are conducted for 175 nm, 200 nm and, 250 nm long bowtie nano antennas and they are illustrated in the following figures. As expected the single optical spots are obtained in each case with shifting wavelengths. They occur on the different wavelengths. However, the highest dissipated power values do not create the single spot in every case. The reason is that the focusing ability depend on the length of the nano antennas and the wavelength, however the dissipated power values depend on the electric field intensity and conductance values. Therefore, they do not match and the single spots occur relatively low dissipated power values. The effects of them will be discussed mostly on the heat transfer analysis part of the thesis.

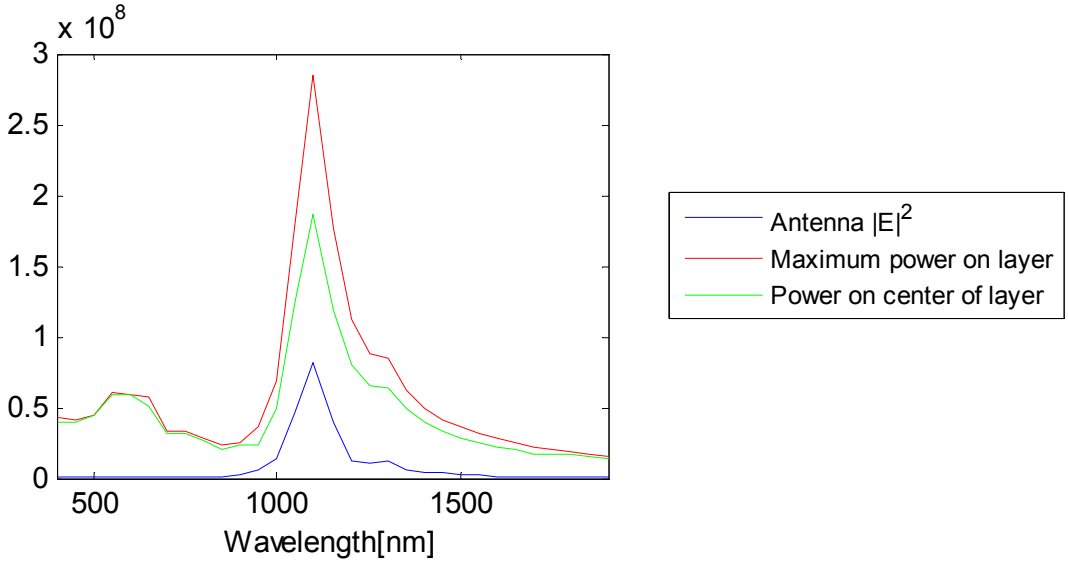

Figure 3.2.7. The electric field intensity on the center of nano antennas, dissipated power maximum and center value on the thin film magnetic layer for 175 nm bowtie nano antenna.

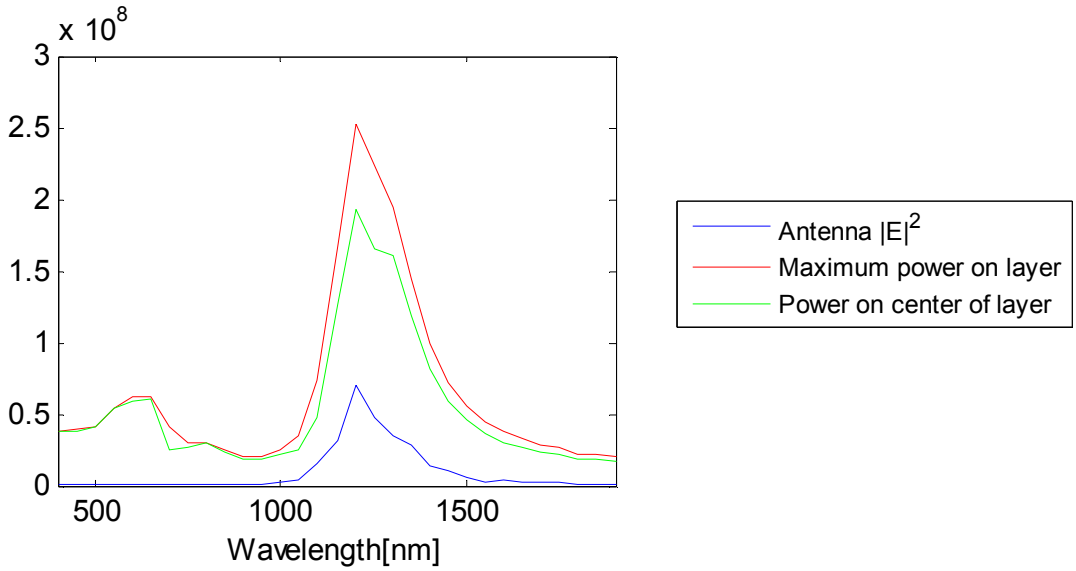

Figure 3.2.8. The electric field intensity on the center of nano antennas, dissipated power maximum and center value on the thin film magnetic layer for 200 nm bowtie nano antenna.

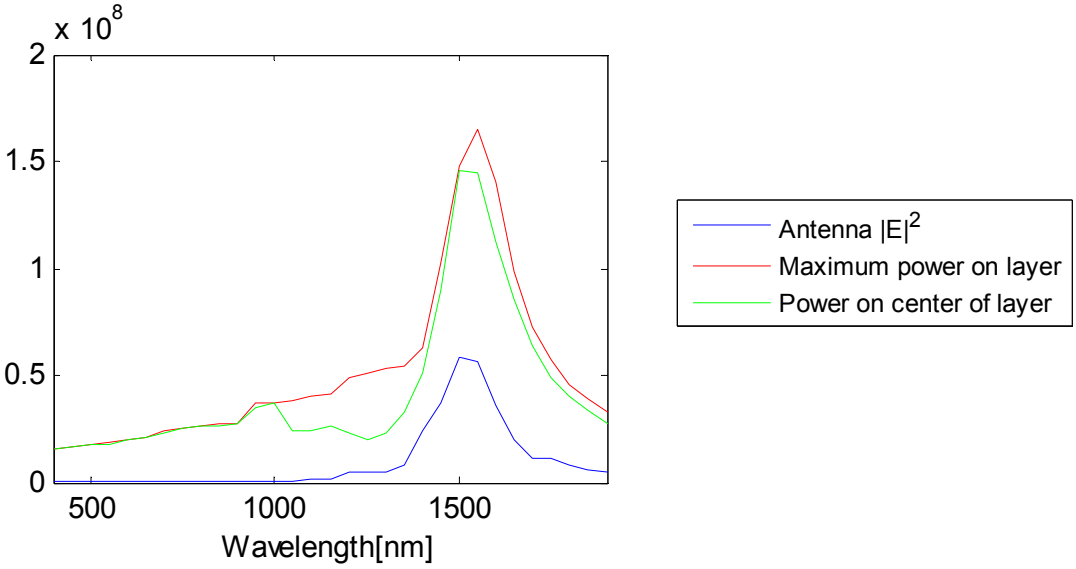

Figure 3.2.9. The electric field intensity on the center of nano antennas, dissipated power maximum and center value on the thin film magnetic layer for 250 nm bowtie nano antenna.

The single optical spots obtained for each case are shown in Figure 3.2.10. The distribution show differences around the optical spots however, the single spots are obtained for each case. Selection of the optimum nano antenna length is mostly dependent on the specification of the work and the wavelength in which it operates. The optical spots are beyond the diffraction limit which is beaten by utilizing nano antennas. The diameters of the optical spots are below 30 nm which has potential practical applications such as heat assisted magnetic recording.

The electric field intensity for nano antennas and the thin film magnetic layer structure and the maximum and center values of the dissipated power on the thin film magnetic layer structure is given in Table 3.1 in Appendix A.

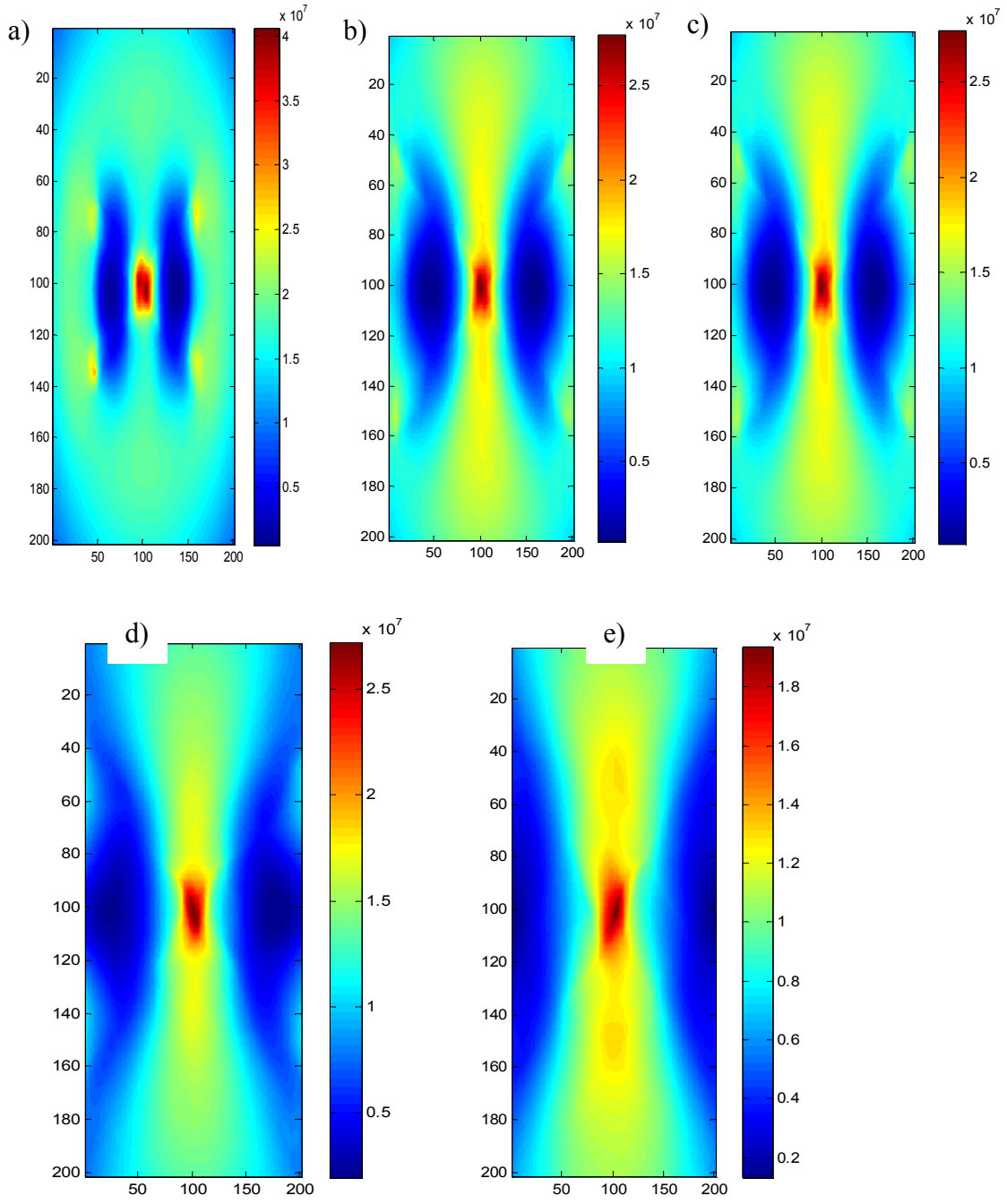

Figure 3.2.10. a)100 nm bowtie nano antenna's corresponding magnetic layer dissipated power distribution for 700 nm wavelength,b) 175 nm bowtie nano antenna's corresponding magnetic layer dissipated power distribution for 800 nm wavelength, c) 200 nm bowtie nano antenna's corresponding magnetic layer dissipated power distribution for 800 nm wavelength, d) 250 nm bowtie nano antenna's corresponding magnetic layer dissipated power distribution for 900 nm wavelength and e)350 nm bowtie nano antenna's corresponding magnetic layer dissipated power distribution for 1150 nm wavelength

After the electromagnetic analysis of bowtie nano antennas, dipole nano antennas electromagnetic behaviors are also investigated to compare the electromagnetic performances of dipole and bowtie nano antennas. In Figure 3.2.11, the square of the electric field at the center point of the dipole nano antennas for 100 nm, 150 nm and 200 nm is presented. This analysis is similar that in Figure 3.2.1.

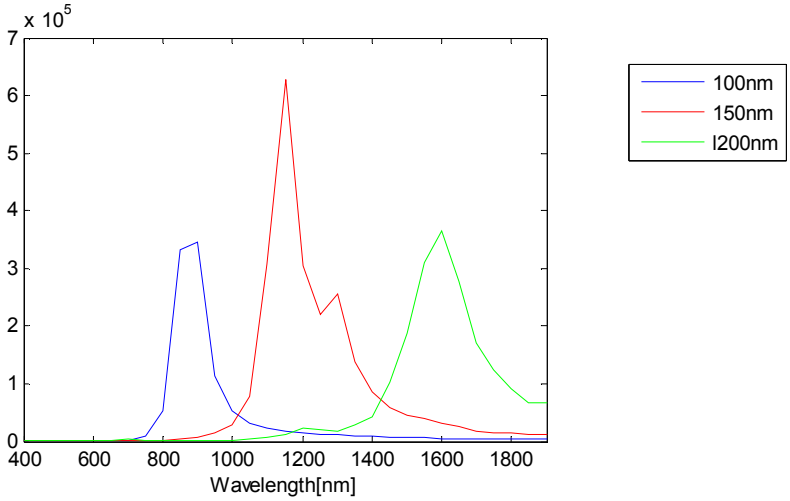

Figure 3.2.11. Electric field intensity values on the center of dipolenano antennas

When compared to that of bowtie nano antennas, they show similar electromagnetic distribution behaviors. The resonant frequency of dipole nano antennas shift towards the larger values compared to the bowtie nano antennas with same length.

When the dissipated power values on the thin film magnetic layer structure is analyzed, the distribution in Figure 3.2.12 is obtained for the maximum dissipated power values on the layer.

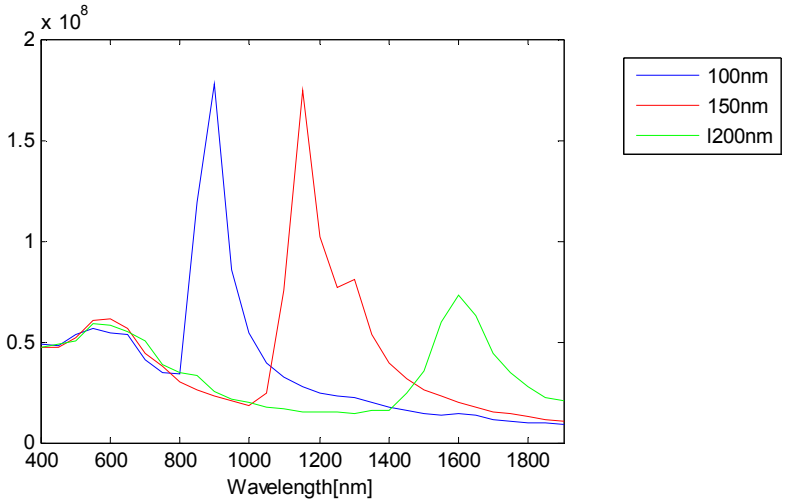

Figure 3.2.12. Maximum dissipated power values on the thin film magnetic layer of dipole nano antennas between 400nm and 1900 nm wavelength

When maximum dissipated power of dipole nano antennas are compared to that of bowtie nano antennas in Figure 3.2.3, it is seen that bowtie nano antennas create 1.5 times more power than dipole nano antennas. Besides that difference, there is not difference between two nano antennas in terms of magnetic layer power values.

The dissipated power values on the center of the magnetic layer are analyzed and the distribution is presented in Figure 3.2.13.

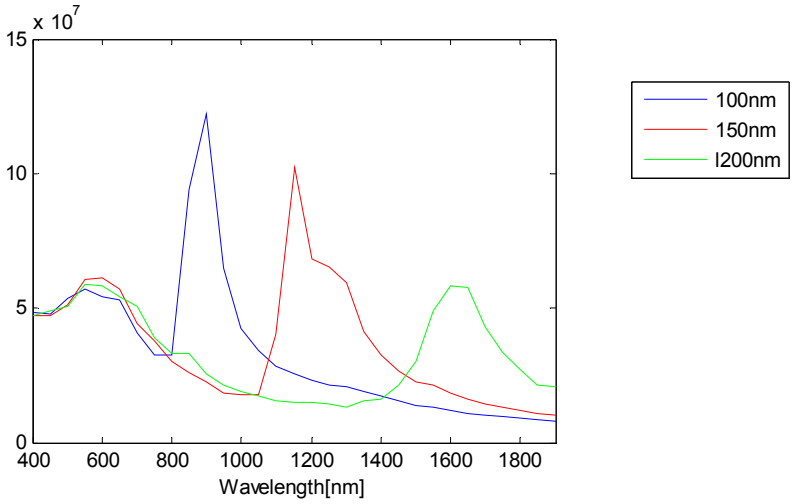

Figure 3.2.13. The dissipated power on the center of the thin film magnetic layer structure

It is seen that the center values decreases with increased length of dipole nano antennas. When compared that of bowtie nano antennas, it shows same behavior besides decreasing values with length.

In Figure 3.2.14, the square of the electric field intensity at the center of the nano antennas, maximum dissipated power value on the thin film magnetic layer and the center value on the thin film magnetic layer are presented for 175 nm long dipole nano antennas.

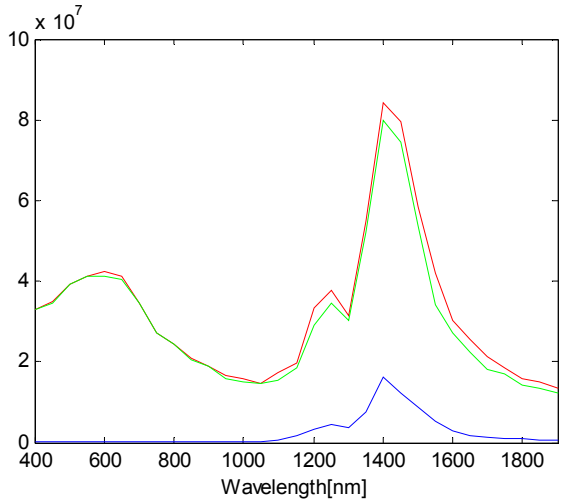

Figure 3.2.14. The electric field intensity on the center of nano antennas, dissipated power maximum and center value on the thin film magnetic layer for 175 nm dipole nano antenna.

When 175 nm bowtie and dipole nano antenna is compared, the electromagnetic performances do not show significant differences. The resonant frequency is 1100 nm for bowtie nano antenna while 1400 nm is the resonant frequency of dipole nanoantenna. The peak value does not significant difference. Therefore, in terms of electromagnetic results, these two nano antenna types do not show significant differences.

A similar analysis is conducted for 100 nm, 150 nm and, 200 nm long dipole nano antennas and they are illustrated in the following figures. As expected the single optical spots are obtained in each case with shifting wavelengths. They occur on the different wavelengths. However, the highest dissipated power values do not create the single spot in every case. The reason is that the focusing ability depend on the length of the nano antennas and the wavelength, however the dissipated power values depend on the electric field intensity and conductance values. When compared to that of bowtie nano antennas, it is seen that the dipole nano antennas generate more single optical spots than bowtie nano antennas, as seen from the number of matches between maximum

dissipated power value and the center dissipated power value of the thin film magnetic layer.

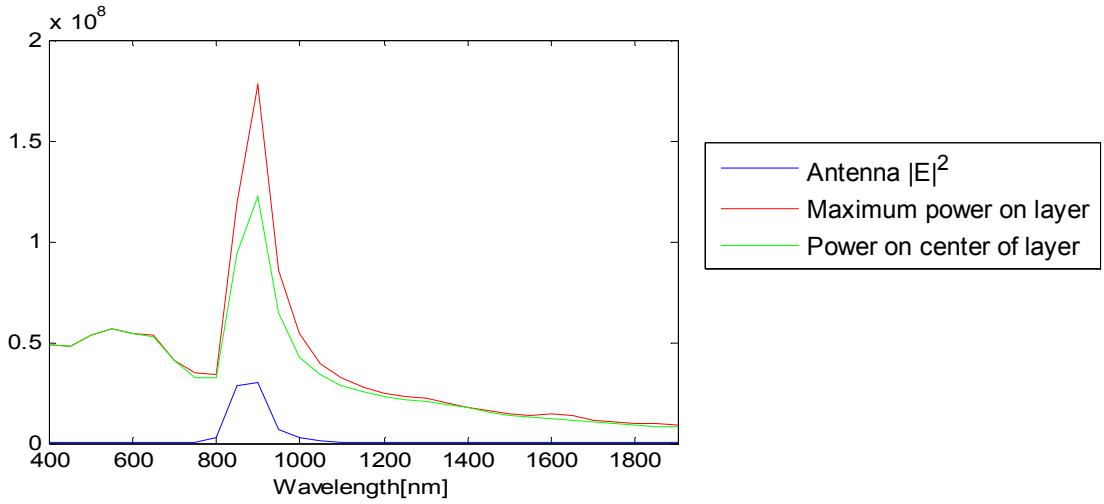

Figure 3.2.15.The electric field intensity on the center of nano antennas, dissipated power maximum and center value on the thin film magnetic layer for 100 nm dipole nano antenna.

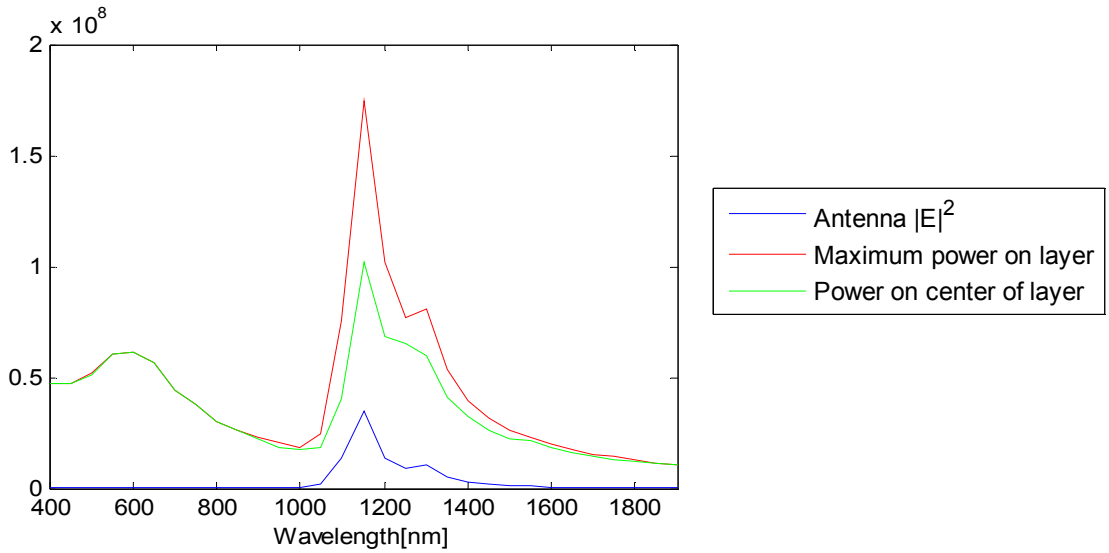

Figure 3.2.16.The electric field intensity on the center of nano antennas, dissipated power maximum and center value on the thin film magnetic layer for 150 nm dipole nano antenna.

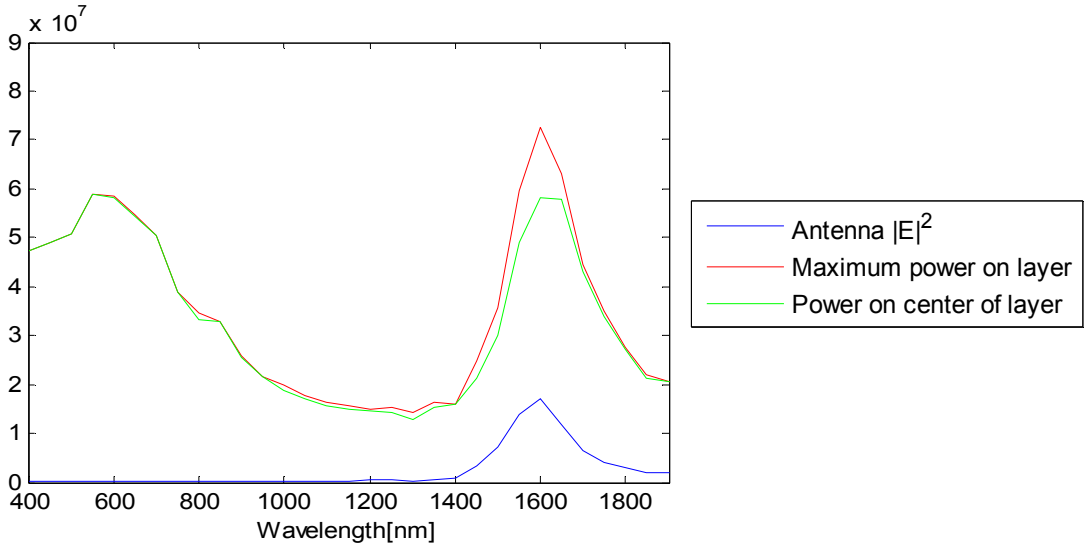

Figure 3.2.17.The electric field intensity on the center of nano antennas, dissipated power maximum and center value on the thin film magnetic layer for 200 nm dipole nano antenna.

In this section, dipole and bowtie nanoantennas are investigated for electromagnetic performances. It has been demonstrated that single spots can be obtained on the thin film magnetic layer for different lengths of the dipole and bowtie nano antennas. The dipole and the bowtie nano antennas do not show significant differences in terms of electromagnetic results. The only differences are seen in the resonant frequency points for dipole and bowtie nanoantennas and little differences on the power values.

The single optical spot points are determined by comparing the maximum value and value at the center of the magnetic layer of the dissipated power values on the thin film magnetic layer. The points where two values coincide show the single spot points. Each different nano antenna lengths show single spots on the different wavelength points. However, the single spot points for studied nano antenna lengths and types are not obtained at the resonant frequency.

3.2.2.Heat transfer results

The heat transfer analysis is conducted by utilizing commercially available ANSYS 12.1 Multiphysics problem. The problem definition and heat transfer analysis tool is discussed in detail in Section 2.

The dissipated power profiles for the nano antennas and the thin film magnetic layer structure are used as an input to the heat transfer analysis. The dissipated power profiles are obtained for nano antennas and the thin film magnetic layer structure by layer by layer to have the all dissipated power over all nano antenna and layer structure. After the analysis are conducted for electromagnetic results, they are manipulated by utilizing MATLAB to put in the input form for ANSYS.

In the heat transfer analysis, all system is same as in the case of electromangetic analysis, i.e. all geometries, all material properties, etc. As a result of the heat transfer analysis, the temperature profiles for nano antennas and the thin film magnetic layer structure are gathered for 0.7 and 1.7 nano seconds (ns). The reason of this time interval is that the thin film magnetic layer starts to reach almost 90% of steady state temperature value by 0.7 ns.

First, the temperatures at the center of the nano- antennas are illustrated for different length of bowtie nano antennas in Figure3.2.18 and 3.2.19. As seen from the graph, the peak temperature profiles are increasing for increased length of bowtie nano antenna within 100nm to 175 nm due to increasing dissipated power values as discussed in electromagnetic results section. The peak values of temperature values at the center of the nano antennas are shifting for different length of nano antennas as expected since shift occurs in the electromagnetic dissipated power values. The peak value of temperature is highest for 175 nm bowtie nano antenna due to high dissipated power value. However, in this thesis, high temperature profiles are not desired for nano antenna structure because, excessive nano antenna temperature lower efficiency of the system. Since nano antenna studied here is used repetatively in the practical writing processes such as in the heat assisted magnetic recording applications, high temperature decreases the efficiency and repeated usage causes constantly increasing temperature which causes malfunctions in the system.

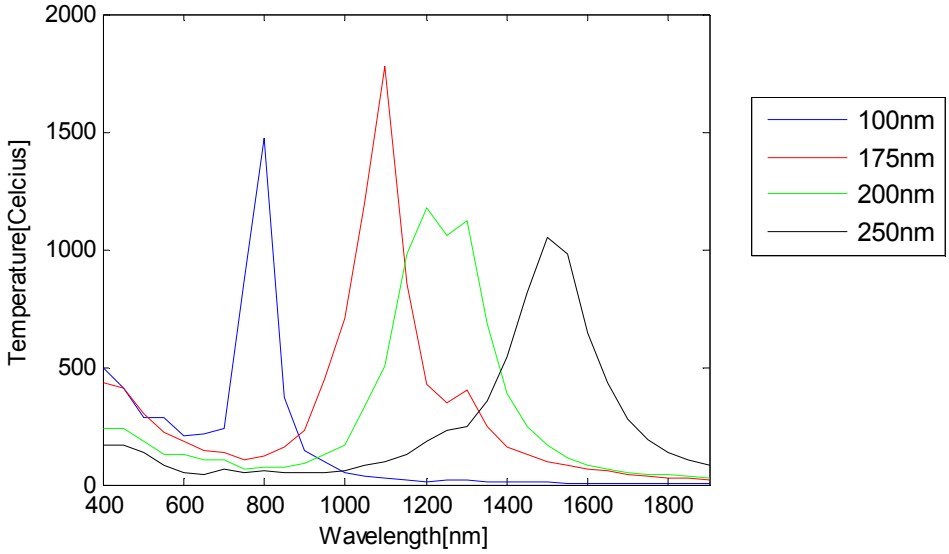

Figure 3.2.18. Temperature profiles for bowtie nano antennas at 0.7 nanoseconds

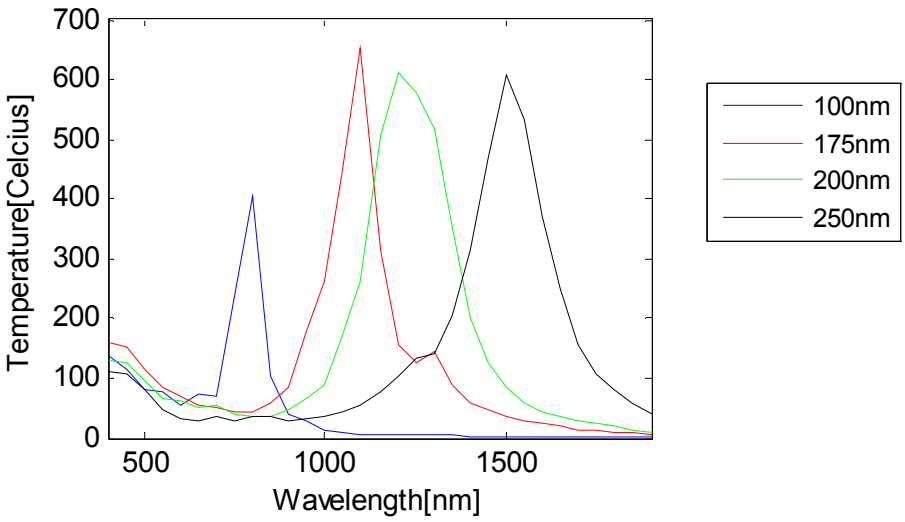

Figure 3.2.19. Temperature profiles for bowtie nano antennas at 1.7 nanoseconds

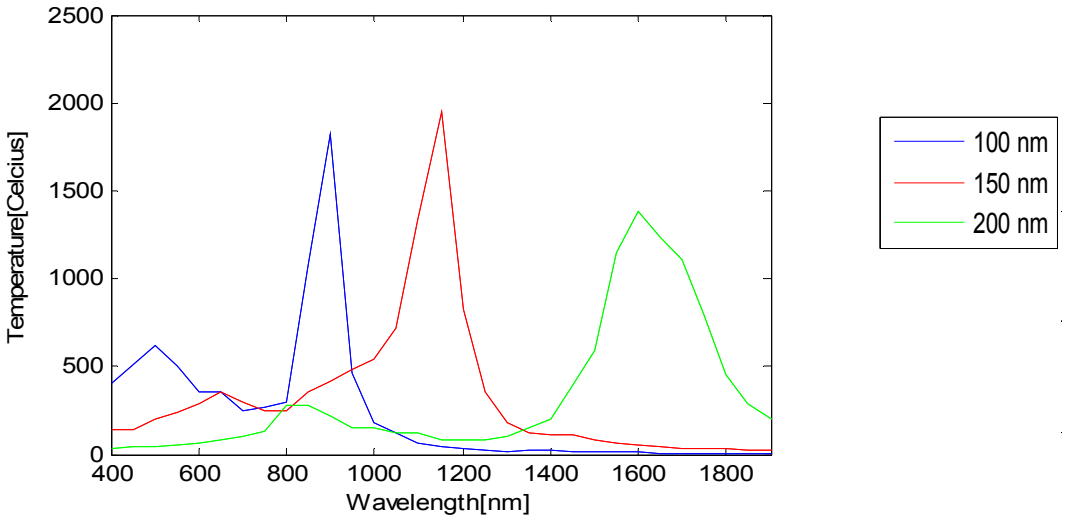

Figure 3.2.20. Temperature profiles for dipole nano antennas at 0.7 nanoseconds

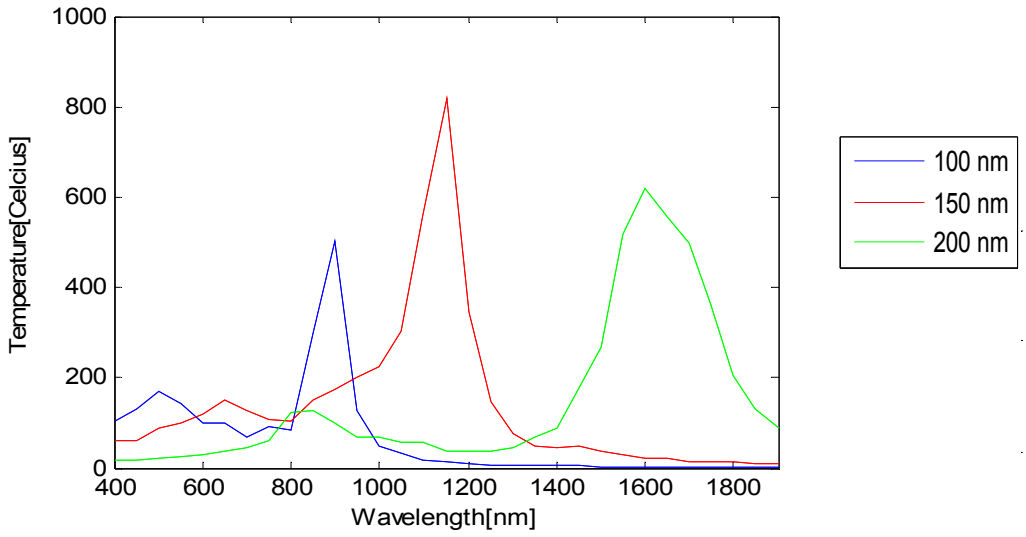

Figure 3.2.21. Temperature profiles for dipole nano antennas at 1.7 nanoseconds

The time effect on the nano antenna temperature profile and the temperature profile at the center of layer of the dipole and bowtienano antennas at 0.7 ns and 1.7 ns are shown in Figure 3.2.18 - 3.2.21. When dipole and bowtie nanoantennas are compared in terms of thermal performances, it is seen that bowtie nano antennas experience lower temperature values. Since the maximum dissipated power values do not show significant difference between dipole and bowtie nanoantennas, the reason of

temperature difference is that the volume of the bowtie nano antenna is larger than that of dipole nano antennas which is very significant since the system is in nanoscale.

The power is applied to the system for 0.7 nano seconds and after that the power is cut off. As seen from the Figure 3.2.22, the rapid temperature increase is observed. However, when power is cut off temperature is rapidly decreasing until 1.7 nanoseconds. The temperature is high on the nano antennas as seen in Figure 3.2.22 b. However, the heat is dissipated to the environment which shows the high radiation effects since temperature of the environment is also higher than default temperature of the system even at 1.7 nanoseconds. The case in Figure 3.2.15 is for 100 nm long bowtie nano antenna at 700 nm wavelength.

a)

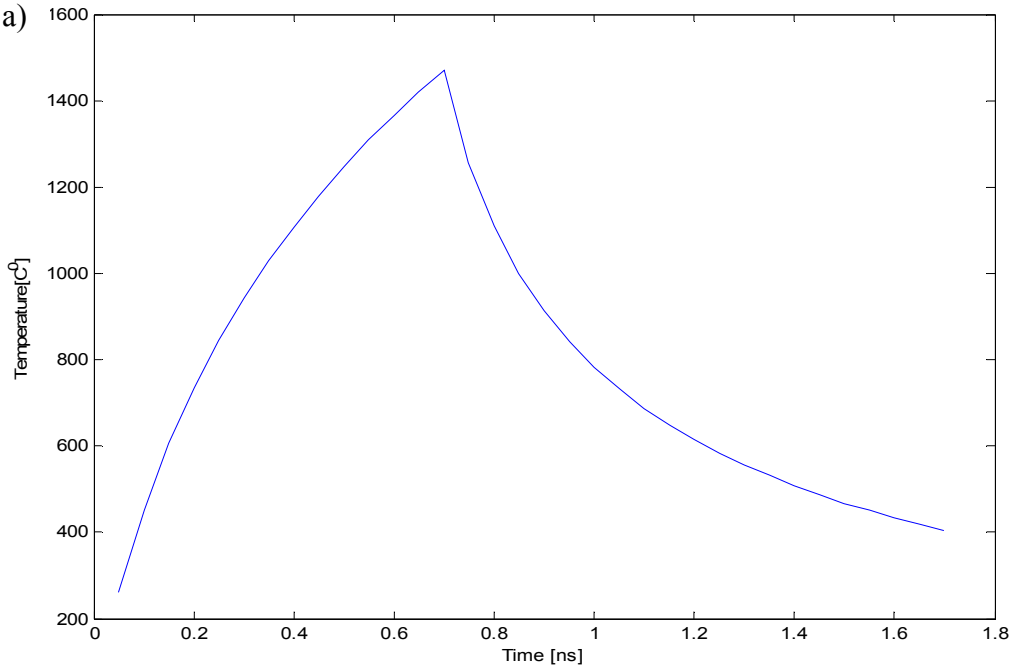

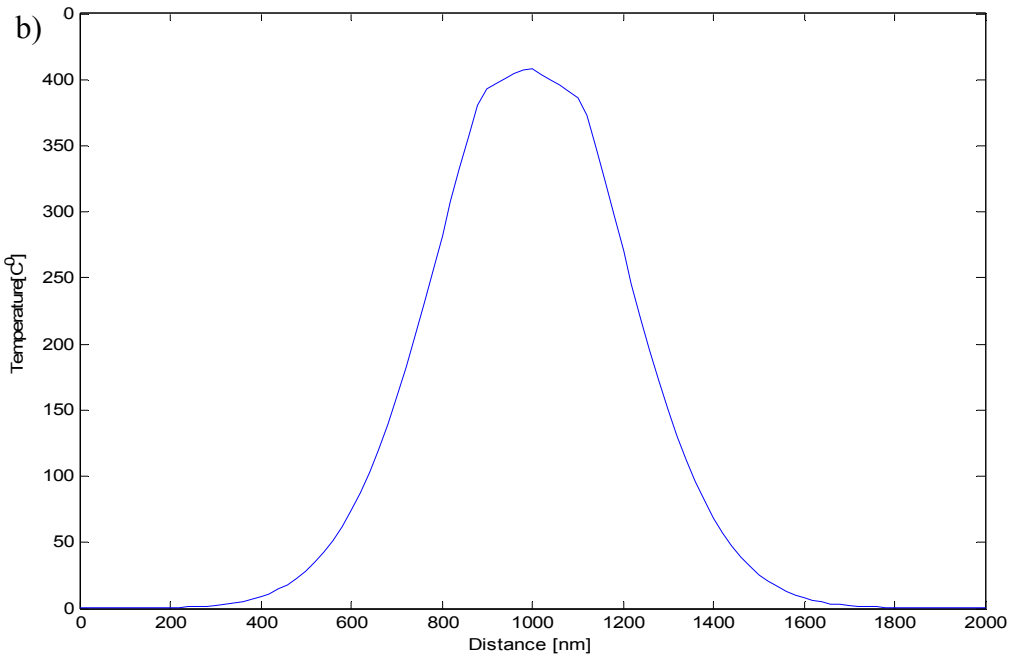

Figure 3.2.22.Temperature profile of 100 nm long bowtie nano antenna at 700 nm wavelength in terms of time (a) and distance on the center layer of the nanoantennas (b)

Similar analysis is conducted for temperature of the thin film magnetic layer corresponding different length of bowtie nano antennas in Figure 3.2.23 and for dipole nano antennas in Figure 3.2.24. As seen from the Figure 3.2.23, the peak temperature profiles are increasing for increased length of bowtie nano antenna within 100nm to 175 nm due to increasing dissipated power values as discussed in electromagnetic results section. The peak values of temperature values at the center of the nano antennas are shifting for different length of nano antennas as expected since shift occurs in the electromagnetic dissipated power values. The peak value of temperature of the thin film magnetic layer are almost same for 150 and 175 nm bowtie nano antenna due to highly focused light onto the magnetic layer. The high temperature profiles are desired to obtain hot spots on the magnetic layer because, applications in heat assisted recording, etc. requires high temperature profiles on the magnetic layer while lower nano antenna temperatures are desired for operational effectiveness. The dipole and bowtie nano antennas' magnetic layers show similar temperature profils as seen from Figure 3.2.23 and 3.2.24

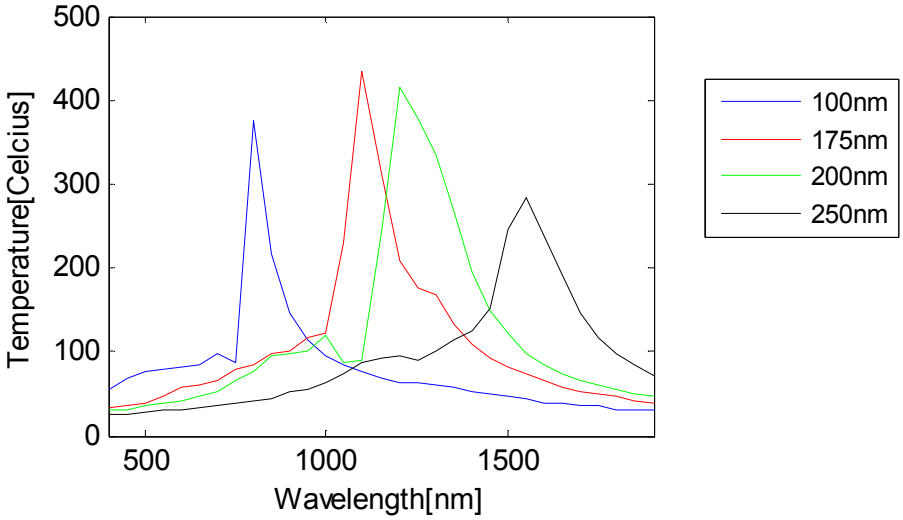

Figure 3.2.23.Temperature profiles for magnetic layer of bowtie nano antennas at 1.7 nanoseconds

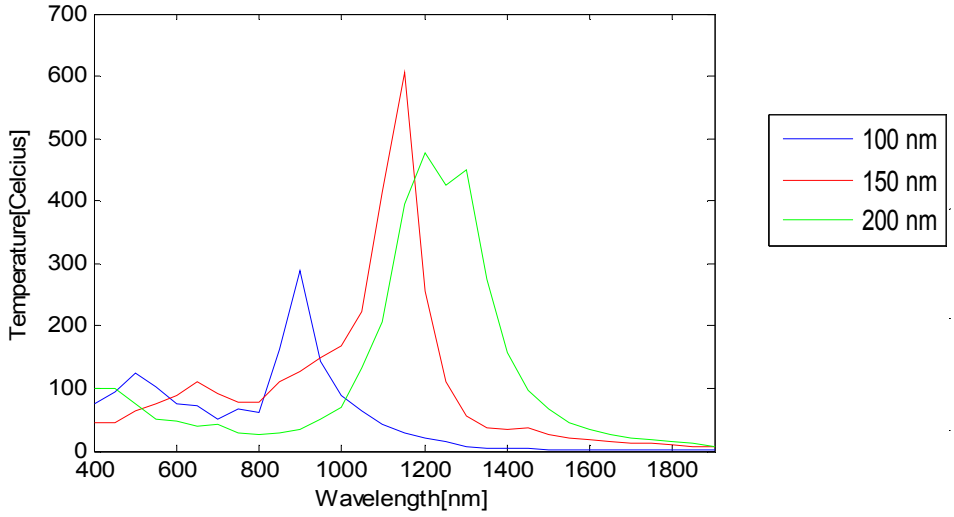

Figure 3.2.24. Temperature profiles for magnetic layer of dipolenano antennas at 1.7 nanoseconds

The time effect on the nano antenna temperature profile and the temperature profile at the mid surface of the bowtie nanoantennasat 1.7 ns are shown in Figure 3.2.25. As seen from the Figure 3.2.25a, the rapid temperature increase is observed however, the thin film magnetic layer reaches steady state value easily. When the temperature distribution

is checked on the top surface of the thin film magnetic layer structure along the center line Figure 3.2.25b is obtained. When the single hot spot is obtained the peak value is obtained at the center. The Figure 3.2.25b illustrates the case for 150nm bowtie nano antenna's magnetic layer at 1000nm where the highest temperature is obtained within the studied system

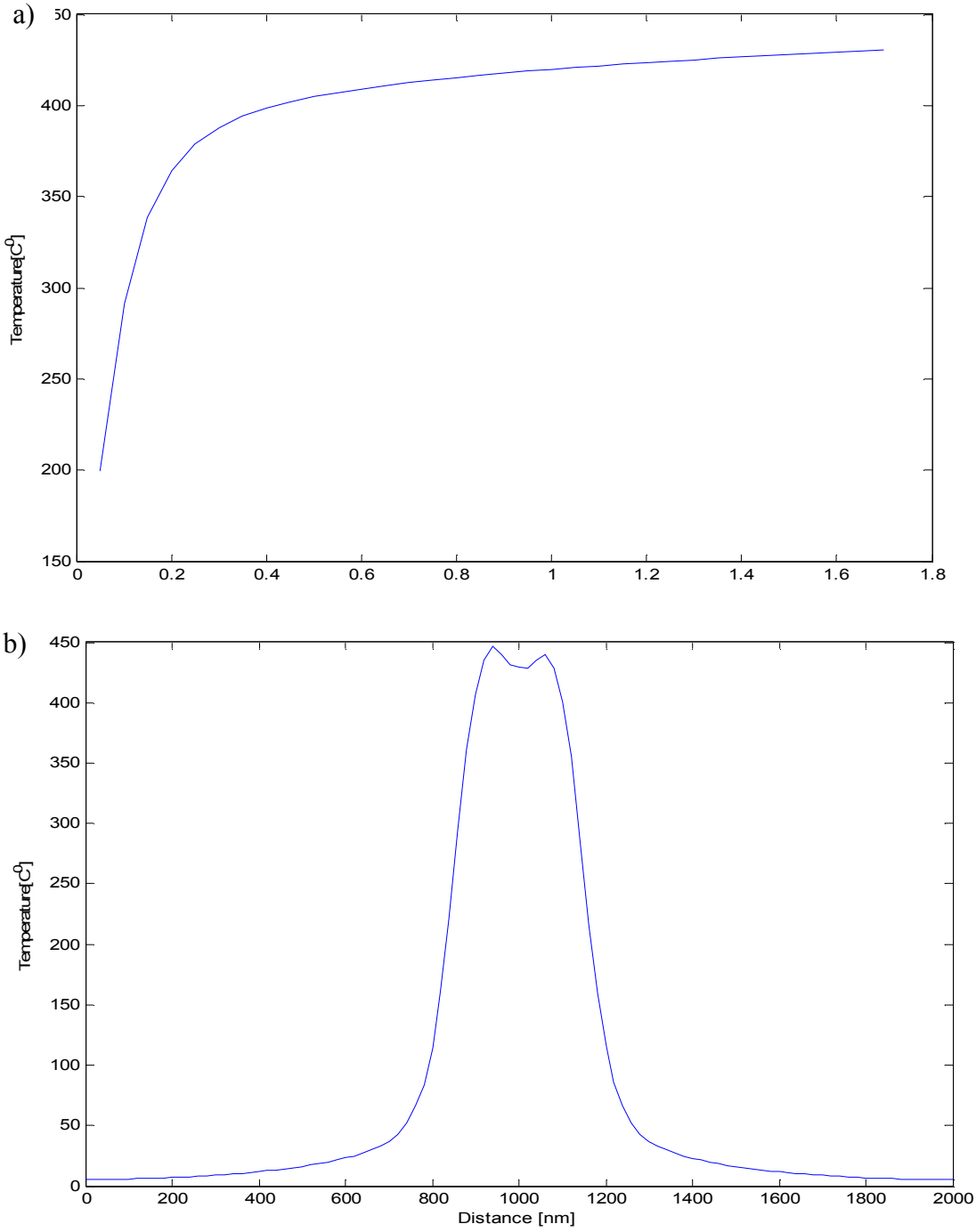

Figure 3.2.25.Temperature profile of 150 nm long bowtie nano antenna at 1000 nm wavelength in terms of time (a) and distance on the center layer of the nanoantennas (b)

To assess the magnetic layer and the nano antenna temperature profiles further, each separate antenna lengths are illustrated in Figure 3.2.26.

The peak temperature values occur at the same wavelength within each nano antenna length. However, there are wavelengths where the magnetic layer temperature exceeds the nano antenna temperatures. Especially for lower wavelength values for each antenna type, one hot spot is obtained and the temperature of the nano antenna is low compared to higher wavelengths and the temperature of the thin film magnetic layer exceeds the temperature of the nano antennas. These points give the most desired cases in which the temperature of the nano antennas are kept low while the thin film magnetic layer has higher temperature values at the center.

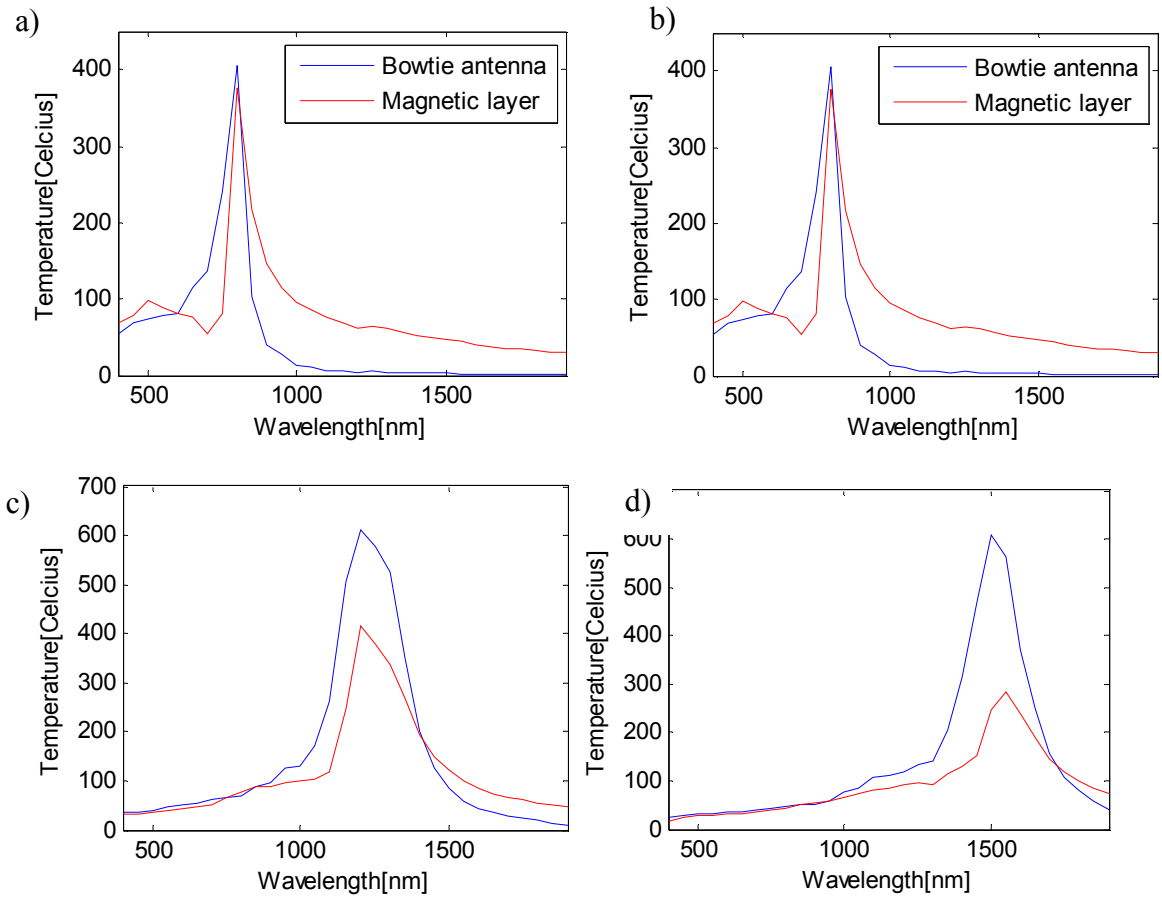

Figure 3.2.26. Temperature profiles for different lengths of bowtie nano antennas and corresponding magnetic thin film layer at 1.7 nanosecondsa) 100nm bowtie

nanoantenna b) 175nm bowtie nanoantenna c) 200nm bowtie nanoantenna and d) 250nm bowtie nanoantenna

Lastly, the heat flux from nano antennas to the thin film magnetic layer is analyzed.

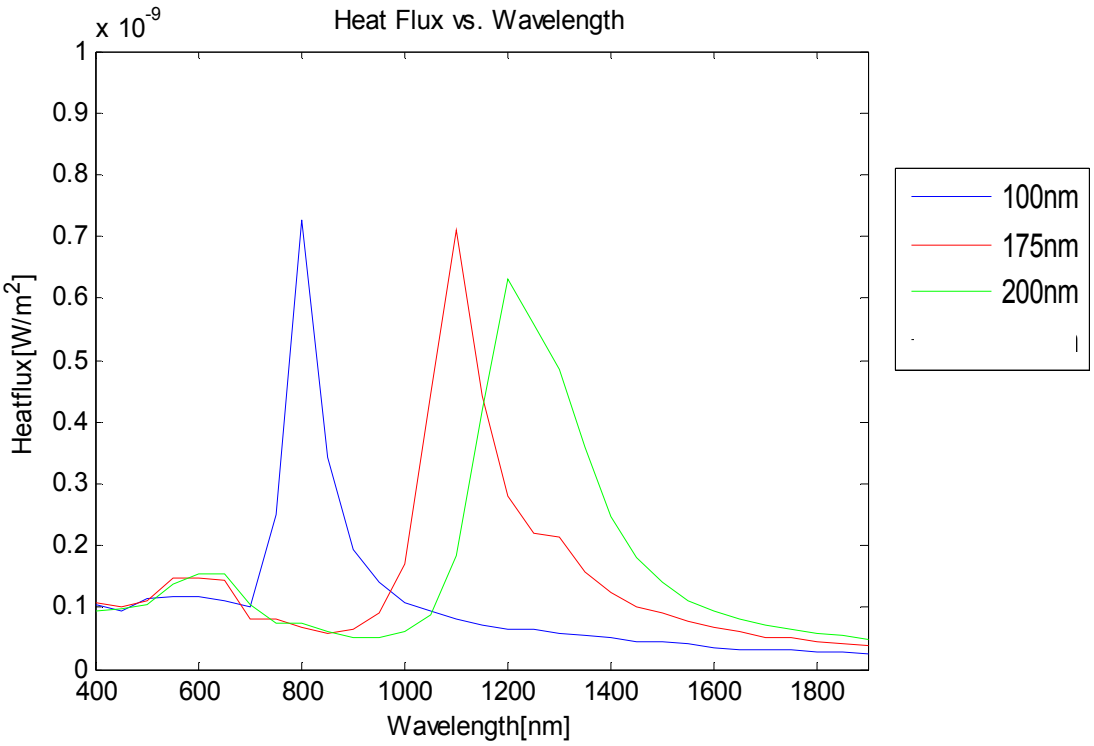

Figure. 3.2.27. Heat flux for different bowtie nano antenna lengths in terms of wavelength

As seen from the figures 3.2.27 and 28, the maximum heat flux values from nano antennas to the top surface of the thin fil magnetic layer show similar profiles for two different nano antenna types. The values reach peak values at the different wavelengths which coincide with the electromagnetic resonant frequencies for each of nano antenna length.

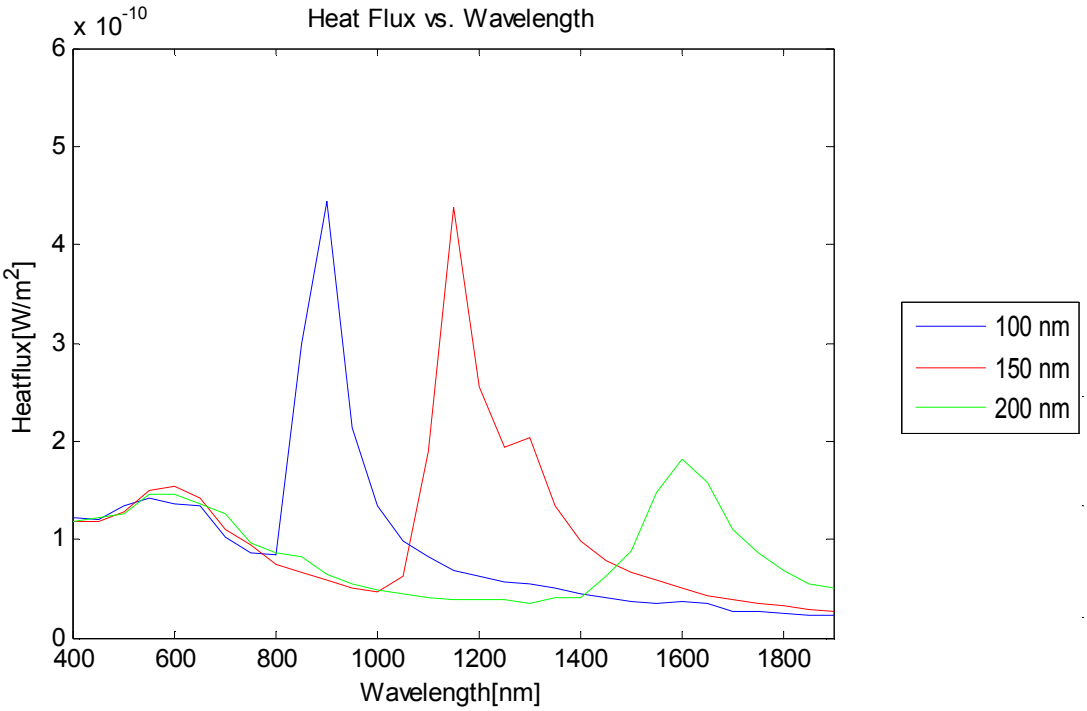

Figure 3.2.28. Heat flux for different dipole nano antenna lengths in terms of wavelength

In this section, the thermal performances of bowtie nanoantennas with different lengths and of the corresponding thin film magnetic layer are investigated. The thermal performances are determined by power input that is applied for 0.7 nanoseconds. Significant increase in the temperature of the nano antenna is observed however, when the power is cut at 0.7 nanoseconds, the temperature decreases rapidly. However, excessive temperature values are observed which is not desired. Therefore, temperature control and proposed solutions to keep temperature at the desired level are discussed in Section 4.

3.2.3. Comparison between electromagnetic & heat transfer results

In this section, the electromagnetic results and the heat transfer results will be compared to check the relation between the electromagnetic and heat transfer aspects of the system studied. When the dissipated power on nano antennas and temperature profiles on nano antennas are visited, it is seen that the temperature distribution within given wavelength range shows significant similarity. The dissipated power on the nano antennas and the temperature values at the center of the nano antennas is illustrated in Figure 3.2.27.The difference occurs for 250 nm long bowtie nano antenna where the maximum value of dissipated power on the nano antenna has lower peak than 175 nm and 200 nm bowtie nano antennas, the temperature of it is almost same with that of 200 nm bowtie nano antenna. The lower wavelength regions create single optical spots for each cases with almost same dissipated power values and same nano antenna temperatures which are generally around 100 celcius degree that are efficient for practical applications.

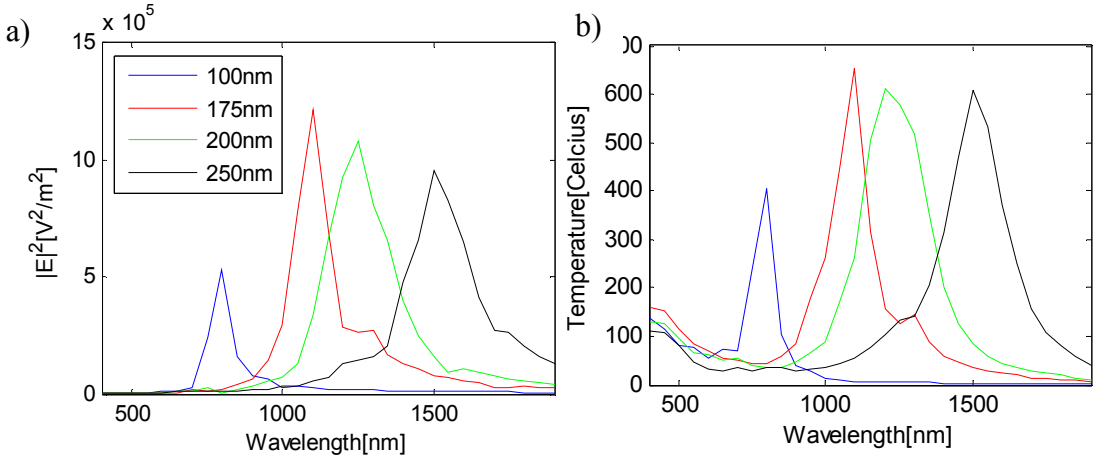

Figure 3.2.29.(a) Electric field value at the center of the nanoantenna and (b) temperature distribution profilesfor different bowtie antenna lengths

When the magnetic layer dissipated power at the center and the temperature profile at the center of the magnetic layer is investigated, it is seen that the peak values coincides in terms of wavelengths for each case. However, slight differences occur at the lower wavelength range between 400 nm and 700 nm range. When compared to the antenna temperature profiles, the single hot spots occur at the lower wavelengths as optical spots and the temperature of the thin film magnetic layer is around 100 celcius degree. The highest temperature values are reached where the highest dissipated power value reached however, these wavelength points do not generate the desired the single optical and hot spots.

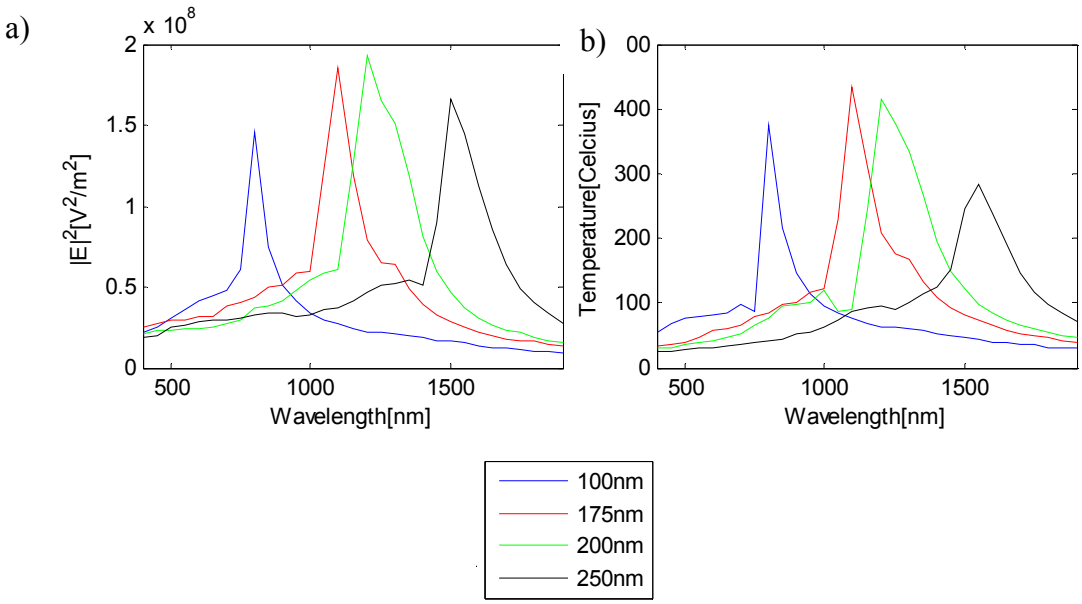

Figure 3.2.30. (a) Dissipated power distribution and (b) temperature distribution profilesfor different bowtie antenna's magnetic layer

4. DIFFERENT NANO ANTENNA STRUCTURES TEMPERATURE PROFILES AND PROPOSED SOLUTIONS FOR EFFECTIVE TEMPERATURE CONTROL

4.1. Electromagnetic and heat transfer analysis of arrow shaped nanoantenna structure

The nano antennas in the system studied are used to focus the incident beam to the magnetic layer beyond the diffraction limit to obtain hot spots that have smaller diameters than the dominant wavelength. In the applications of this system, the nano antennas are used successively. Therefore, keeping the temperature of the nano antennas low is essential for efficiency and reliability of the system. Due to scale of the system and highly focused incident beam, the temperature of nano antennas are increasing excessively which prevent successive usage of the nanoantennas for real world applicationssuch as nearfieldheat-assistedmagneticrecording. In this section the proposed solutions to keep the temperature of the nano antennas within the desired temperature limits are presented.

Since the temperature depends on the heat flux and the capacity, to be able to optimize the temperature of the nano antennas are bound to volume of the nano antennas and the material properties. The third option to affect temperature is external effects. However, in this case external effects are hard touseto optimize the temperature since the near

field radiative heat transfer dominates the heat flux compared to conduction and convection. And the assigned material for nano antennas are gold therefore, there only remains the geometry effects on the system to optimize temperature of the nano antennas.

New arrow shape nano antenna is presented to assess the thermal performances. Three different cases for arrow shape nano antenna is presented here.

First case is illustrated in Figure 4.1.1. The arrow type nano antenna consists of two parts. The first part is 175 nm bowtie nano antenna. The second part is rectangular structrure attached to the bowtie nanoantenna. The rectangular shape is 150 nm long in x direction, 105 nm long in y direction and 30 nm long in z direction which is 10 nm longer than the bowtie nano antenna.

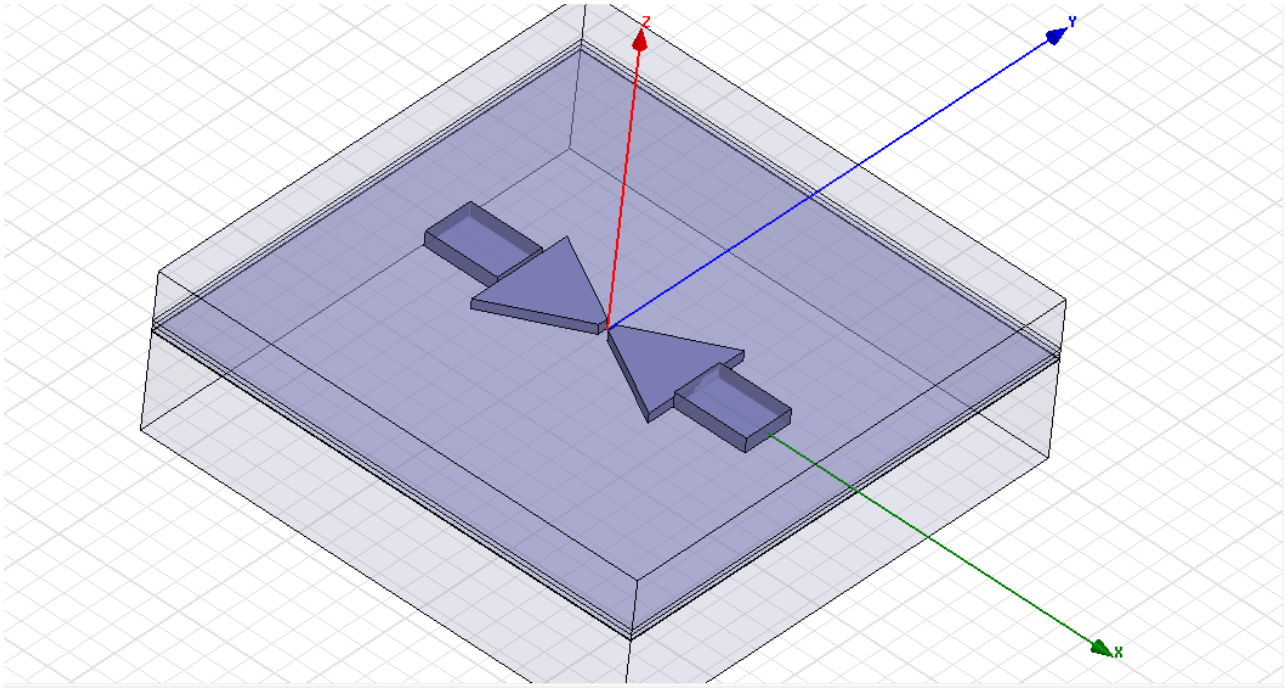

Figure 4.1.1. Geometry of the first case studied to optimize nanoantennas temperature

The geometry presented in Case 1 is assessed in terms of electromagnetic performances since the electromagnetic behavior is significant part of the performance of the system. It is seen that the single optical spot is obtained on the thin film structure via utilizing arrow shaped nano antenna in Case 1 at the 800 nm wavelength. The dissipated power is illustrated in Figure 4.1.2.

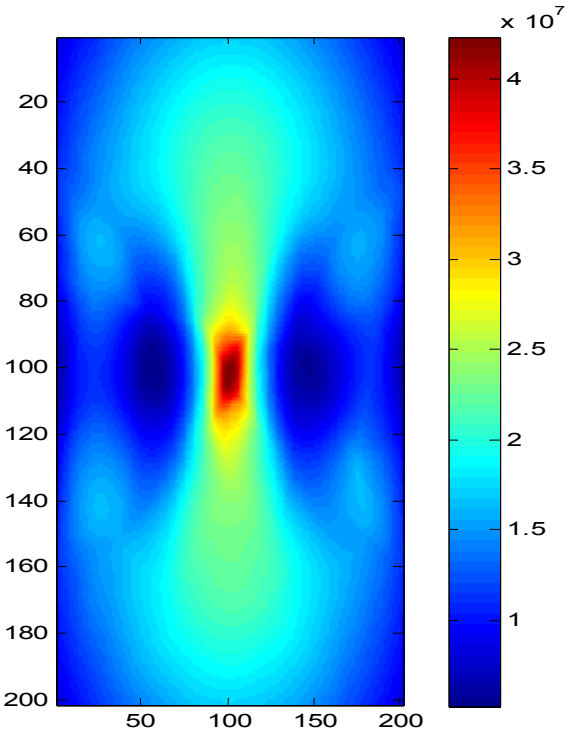

Figure 4.1.2. Dissipated power profile onthe thin film magnetic layer structure corresponding to the Case 1.

Electromagnetic behavior of nano antenna in Case 1 is compared to the bowtie nano antenna that is 175 nm long, 20 nm thick, 20nm wide bowtie nanoantennas are used with a gap of 20 nm between two nano antennas. Nano antenna in Case 1 meets desired requirements for electromagnetic results and does not show significant difference when compared to bowtie nano antenna of which dissipated power profile is presented in Figure 4.1.3. Therefore, as a second step, the thermal performance of the nano antenna in Case 1 is assessed.

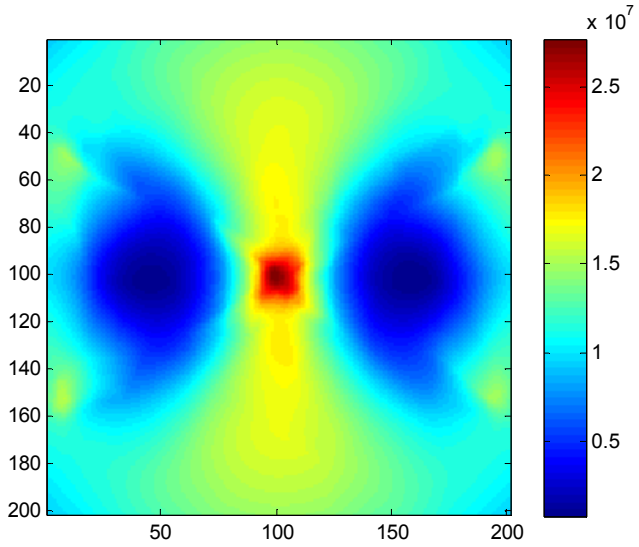

Figure 4.1.3. Dissipated power on the thin film magnetic layer for 175nm long bowtie nanoantenna at 800nm wavelength separated by 10 nm air gap from thin film magnetic layer (-100 nm to 100 nm in x-y plane at the z = 0 nm)

When the temperature profile on the nano antenna of Case 1 is analyzed, the temperature distribution in Figure 4.1.4 is obtained. The temperature profile of the 175 nm bowtie nano antenna is presented in Figure 4.1.5 for comparison with Case 1. It is seen that the temperature is 70 Celcius degree lower than that of bowtie nanoantenas at the 0.7 nanoseconds and 25 Celcius degree lower at 1.7 nanoseconds.

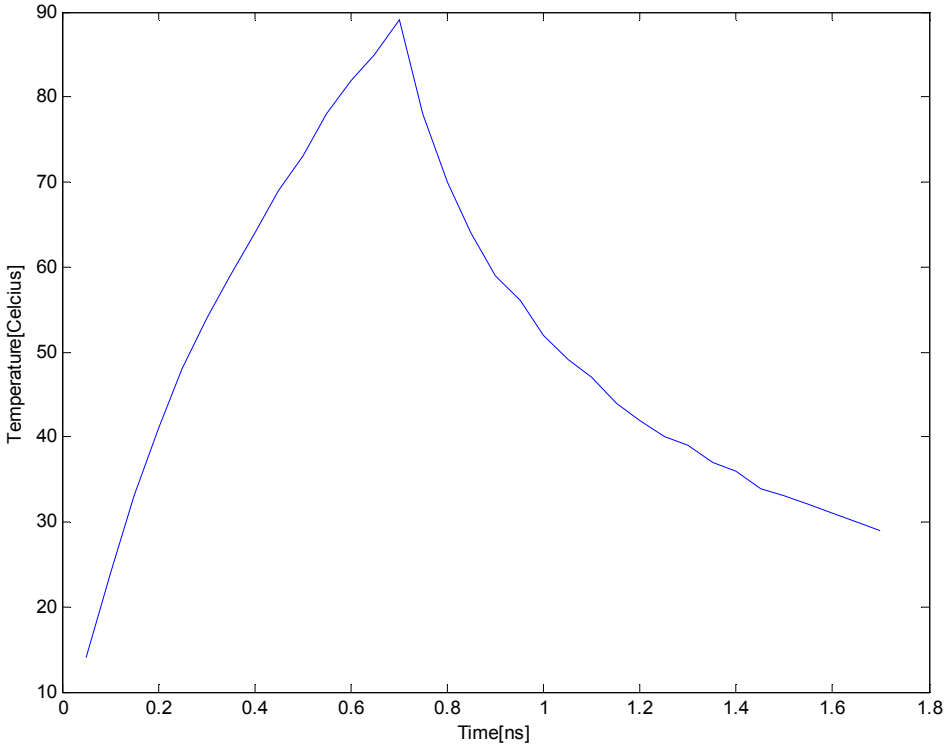

Figure 4.1.4. Temperature profile at the center of the nanoantennasof Case 1 for 1.7 nanoseconds

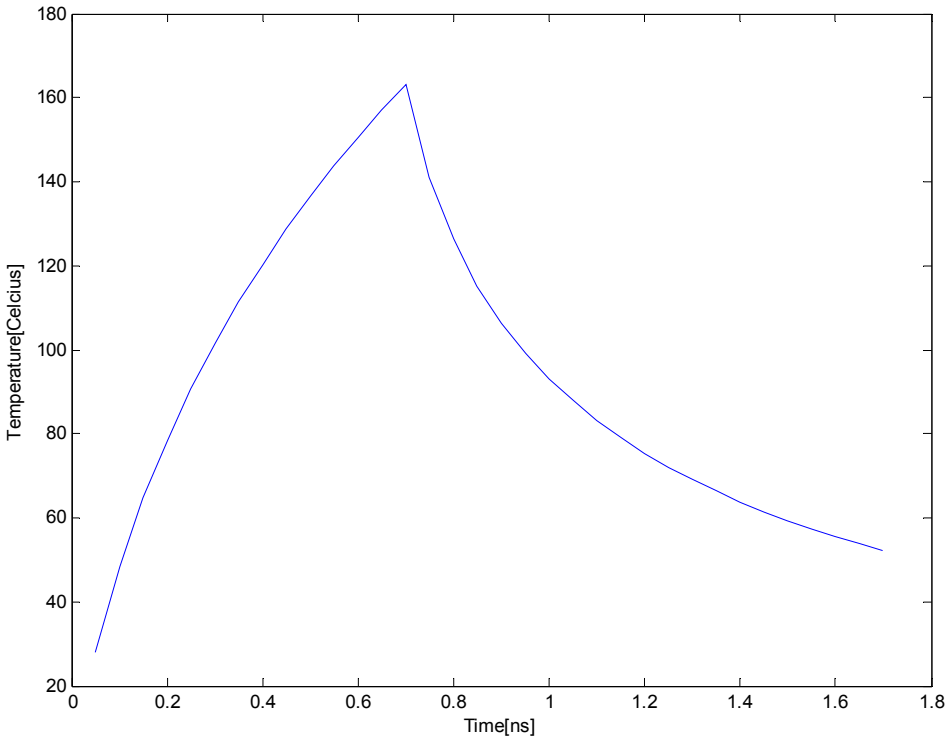

Figure 4.1.5. Temperatureprofile at thecenter of the 175 nm bowtienanoantennas.

To further analyze possible temperature control applications, the arrow shaped nano antenna in Figure 4.1.6 is investigated. The nano antenna consists of 175 nm bowtie nano antenna and the rectangular shape attached to the bowtie nano antenna. The rectangular structure is 250 nm long in x direction, 105 nm long in y direction and 30 nm long in z direction which is 10 nm longer than the bowtie nano antenna. The difference between Case 1 and Case 2 nano antenna types are length in x direction which is 100 nm long in Case 2.

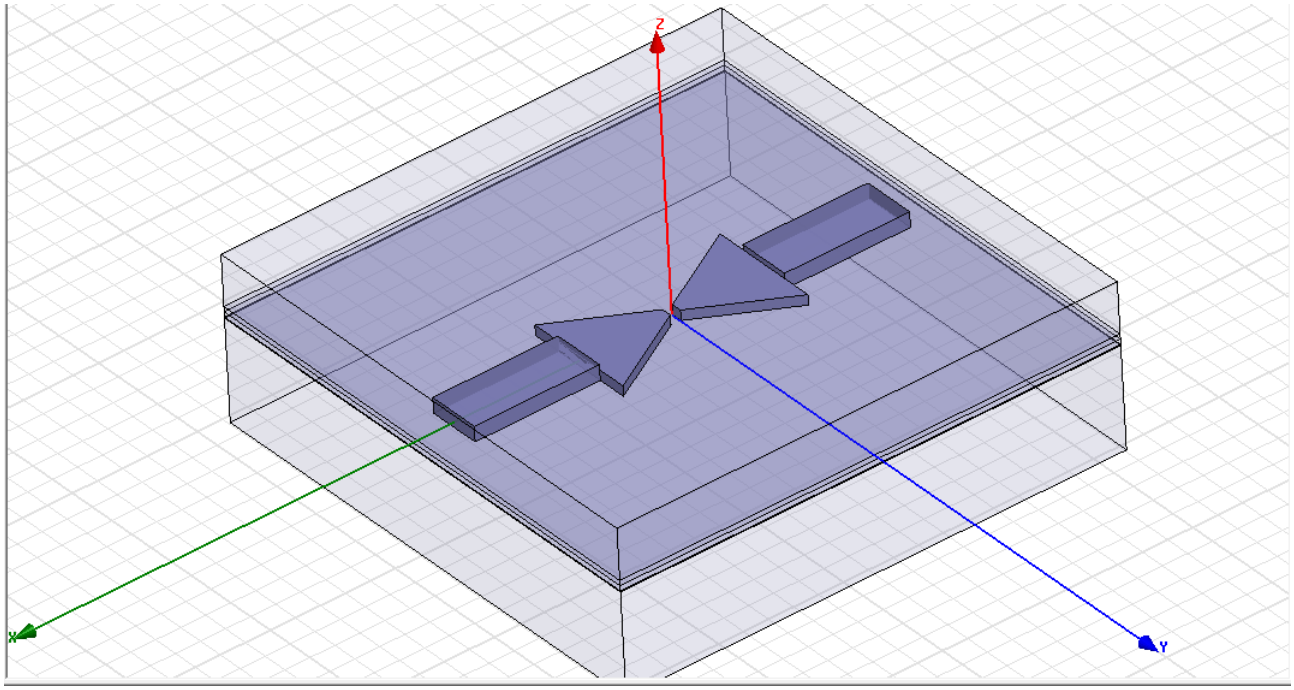

Figure 4.1.6. Geometry of the second case arrow type nanoantenna

The dissipated power distribution on the thin film magnetic layer structure for Case 2 at 800 nm wavelength is illustrated in Figure 4.1.7. As seen from the figure, the single spot is obtained in this case also. There is not significant difference betweeen Case 1 and Case 2 and when compared to the 175 nm bowtie nanoantenna there is not significant difference observed besides the maximum value of dissipated power changes from 2.5 to $4x10^{7}$Watt.

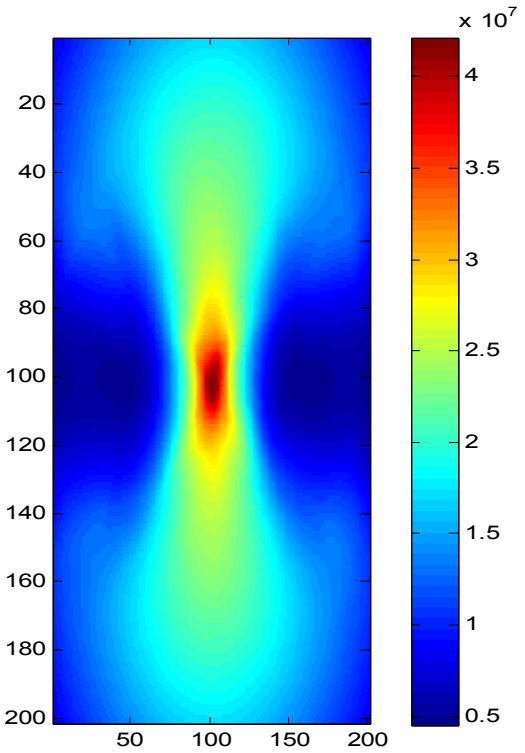

Figure 4.1.7. Dissipated power profile on the nanoantenas and the thin film magnetic layer for second case

Since the electromagnetic analysis yield similar results and single spots are obtained, the thermal analysis of the nano antenna in Case 2 is conducted. The temperature profile distribution on the center of nano antennas of Case 2 is illustrated in Figure 4.1.8. When compared to 175 nm bowtie nano antenna and the nano antenna in Case 1, Case 2 shows better thermal performance. The maximum temperature reached at 0.7 nanoseconds is 60 Celcius degree which is 30^0C lower than Case 1 and 100^0C lower than 175 nm bowtie nano antenna. Therefore, increasing length of rectangular structure in x direction does not affect electromagnetic results significantly, while increasing temperature control significantly.

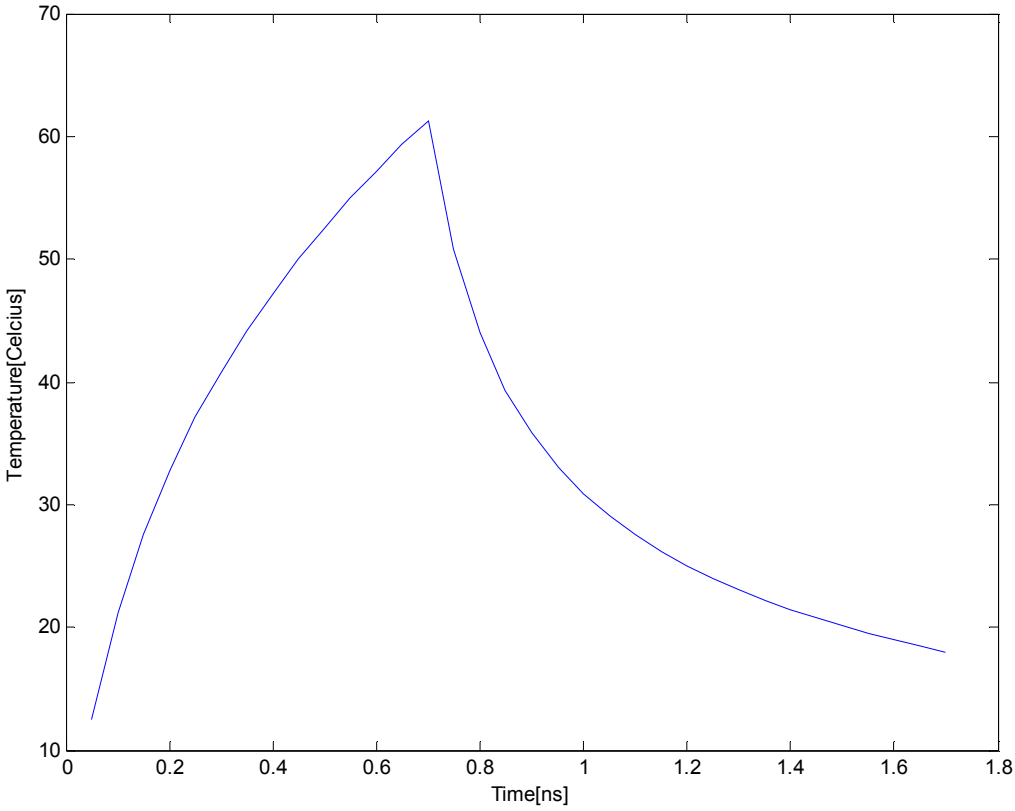

Figure 4.1.8. Temperature profile on the center of the nanoantennas for Case 2.

As a last case, the nano antenna structure in Figure 4.1.9 is investigated. In Case 3, the nano antenna consists of 175 nm bowtie nano antenna and rectangular shape which is 250 nm long in x direction, 200 nm long in y direction and 30 nm long in z direction which is 10 nm longer than the bowtie nano antenna. The reason of choosing these parameters is that in Case 1 and Case 2, the effects of length of x direction is assessed and now the length through y direction will be assessed and compared to the Case 1 and Case 2. The electromagnetic analysis is conducted for Case 3 nano antenna and dissipated power on the thin film magnetic layer is illustrated in Figure 4.1.10. As seen from the Figure 4.1.10, the single optical spot is obtained. When compared to Case 1 and Case 2, in Case 3, the power at the center of the magnetic layer increases by $0.5x10^{7}$.

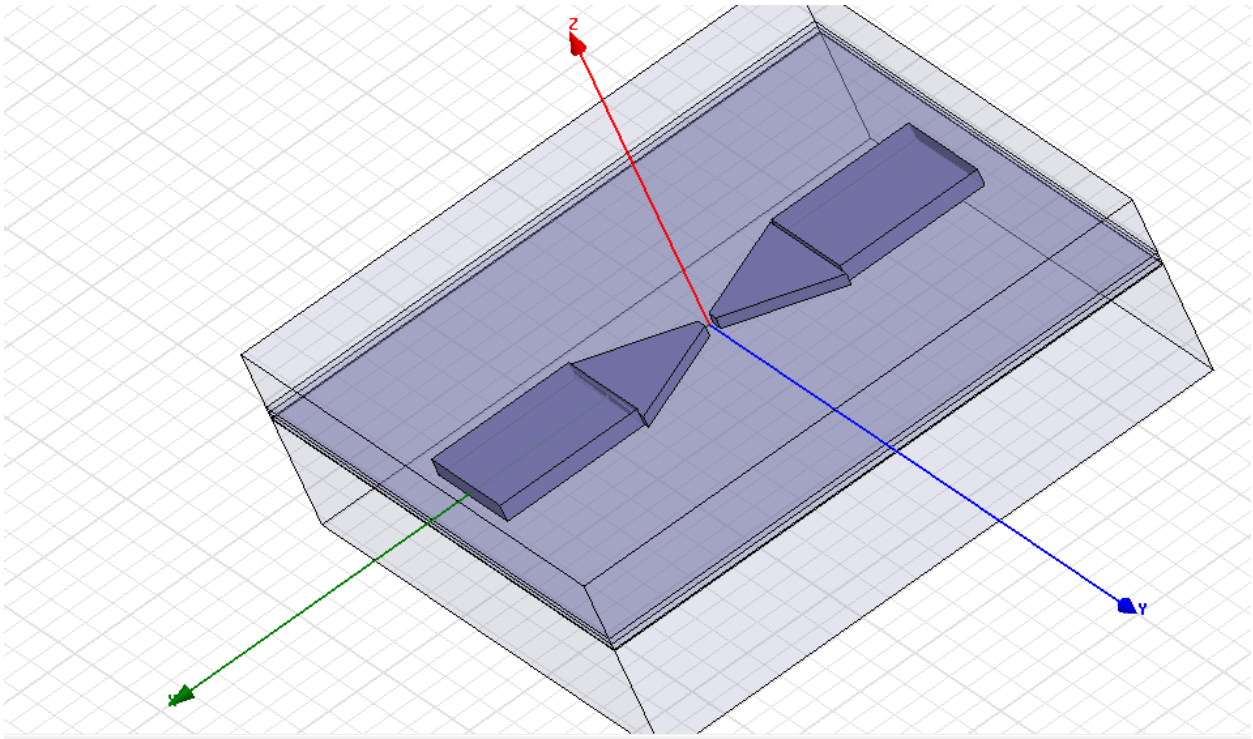

Figure 4.1.9. Geometry of thethirdcasestudiedto optimize nanoantennastemperature

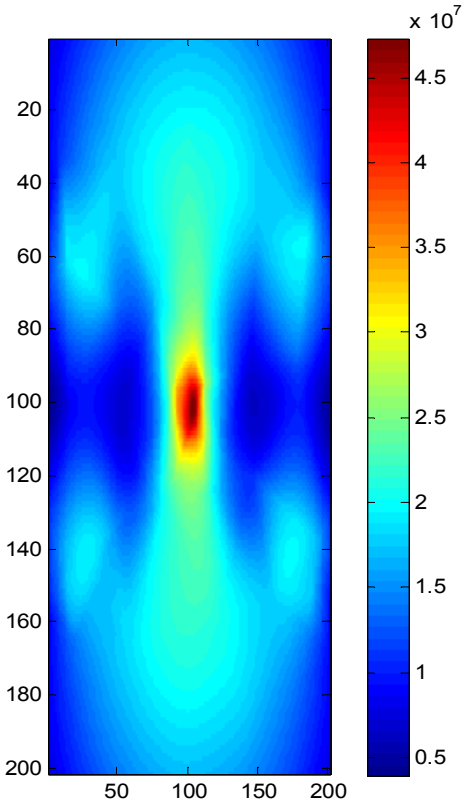

Figure 4.1.10. Dissipatedpower profile on thethin film magneticlayerstructurefor Case 3.

Since the electromagnetic dissipated power distribution yields single optical spot for Case 3, the thermal analysis for this antenna type is conducted. The temperature profile distribution at the center of the nano antennas is illustrated in Figure 4.1.11.

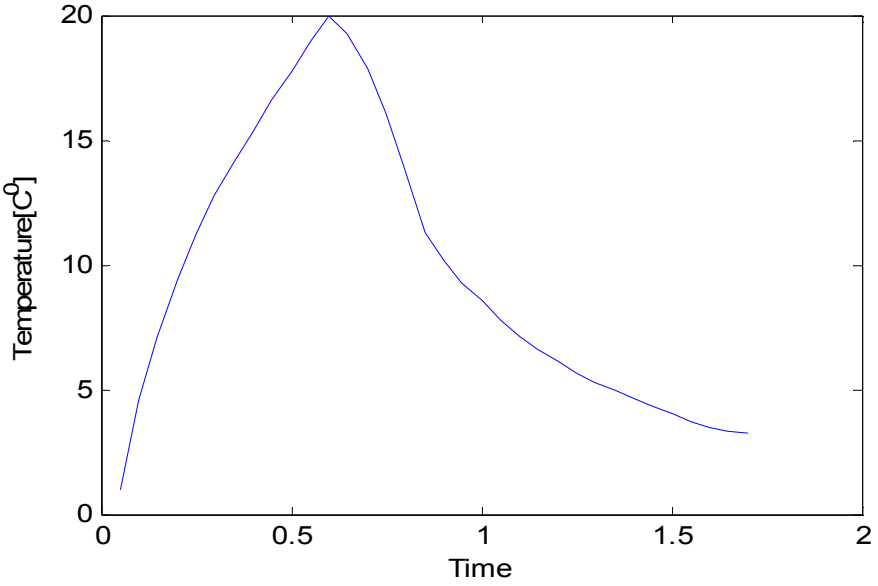

Figure 4.1.11. Temperatureprofile on thecenter of thenanoantennasfor Case 3.

As seen from temperature distribution, the temperature at the peak value reaches only 20^0C. Therefore, Case 3 shows the best thermal performance among 175 nm bowtie, Case 1 and Case 2 nano antennas.

The findings in this section show that it is possible to change the temperature of the nanoantennas without changing the electromagnetic distribution on the thin film magnetic layer. Since nanoantennas are utilized consecutively, it is significant to control their temperature. For each application the nano antennas are used, the different geometrical optimized conditions could be found as Case 1, 2 & 3 for bowtie nanoantennas studied here. For these applications, it is possible to change temperature of the nanoantennas. While temperature of the nanoantennas are important for efficiency and reliability reasons, it is also important to increase optimized temperature of the thin film magnetic layer which will be discussed in the following section.

4.2. Comparison of electromagnetic performances and the temperature profiles of dipole, bowtie and arrow shaped nanoantennas

In this thesis, so far three different nanoantenna structures are studied in various applications with different lengths and wavelengths. Since the control of nanoantenna temperature is significant in near field applications, in this section, the temperature efficiency of these three different nanoantenna structure is assessed. First of all, to understand the efficiency of these three different nanoantenna types, electromagnetic results are compared in terms of dissipated power values and single spot generation. This analysis is conducted for 175nm long dipole and bowtie nanoantennas and the arrow antenna in Case 2 which is defined in the Section 4.1.

Each of the three nanoantenna configuration shows different electromagnetic and temperature distribution. As seen from figure 4.2.1, the dissipated power on the thin film magnetic layer for each of the corresponding antenna types shows significant difference in terms of power and resonant frequency. Therefore, it is important to check their electromagnetic distribution profiles for different applications. It is seen that the bowtie nano antenna is superior as a electromagnetic power intensity generation compared to dipole and the arrow nanoantennas and arrow nanoantenna is better than the dipole nanoantenna.

In terms of heat transfer analysis, the performances of these three antenna geometry are assessed. The temperature distribution at the center of the nanoantennas at 1.7 nanoseconds is presented in figure 4.2.2.

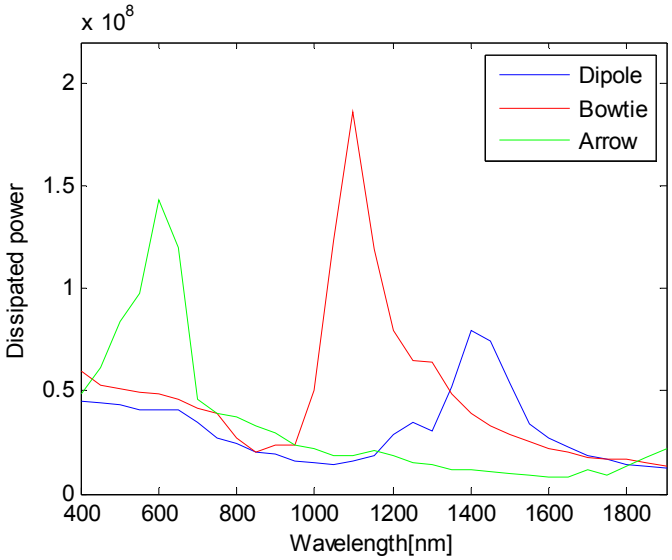

Figure 4.2.1. Dissipated power profiles on the thin film magnetic layer for dipole, bowtie and arrow type nano antennas

As seen from the figure 4.2.2, the material volume is significant for temperature distribution. Therefore, the arrow type gives the best option, which is the lowest temperature, and decreases temperature significantly. While the bowtie nanoantenna shows better performances in terms of temperature compared to the dipole antenna, at the resonant frequency it reaches significantly higher values. Since the dissipated power on the thin film magnetic layer does not show significant power reduction in these three cases, it is optimal to use arrow shaped nanoantennas in which cases temperature control is crucial.

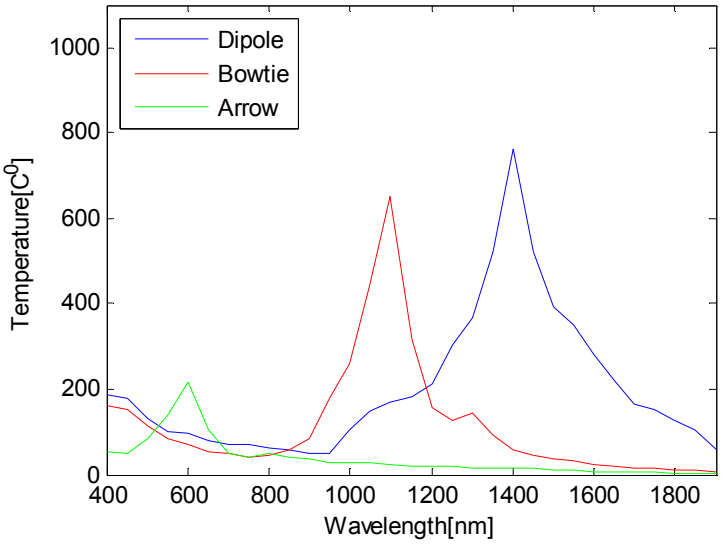

Figure 4.2.2. Temperature profiles at the center of the dipole, bowtie and arrow type nano antennas at 1.7 nanoseconds

4.3. The effects of the nanoantenna temperature to the thin film magnetic layer

Radiant energy exchanges between closely spaced bodies can exceed by several orders of magnitude the values predicted for blackbodies due to near-field effects. Bodies at temperature greater than 0 K induce oscillating dipoles emitting far- and near-field components. Far-field components are propagating waves taken into account in the classical theory of thermal radiation; near-field components are evanescent (non-propagating) waves decaying exponentially (over a distance of about a wavelength) normal to the surface of an emitting body. When bodies exchanging thermal radiation are spaced in such a way that their surfaces lay in the evanescent field of their opposite bodies, radiative heat transfer due to evanescent waves occur (radiation tunneling).

To observe the near field effects on the temperature of the magnetic layer, following steps are conducted. Firstly electromagnetic dissipated power is obtained on the nanoantennas and the magnetic thin film layer. After that according to that power, the

temperature of the nano antenna is obtained. Nano antenna temperature has effects on the temperature of the thin film magnetic layer due to small gap between the nanoantenna and the thin film magnetic layer.

Since the temperature of the thin film magnetic layer is calculated via utilizing electromagnetic dissipated power as an input it includes the propagating and evanescent waves contributions. However, the temperature of the nanoantennas which is higher than that of the magnetic layer is also contributing additional temperature increase. However, it is expected to have lower temperature effect compared to effects of the dissipated power since the geometry of nanoantennas are relatively small compared to the thin film magnetic layer structure. The effects of the temperature of the nano antennas on the temperature of the magnetic thin film layer are discussed further below.

Since the radiative heat flux increases significantly with decreasing gap distance, it is important to assess the effects of the temperature of the nano antennas on the temperature thin film magnetic layer. The significant increase in the radiative heat flux is observed. However, there is no study related to the nanoantennasradiative heat flux and the temperature profiles. In this thesis, the effects of the nearfield radiative heat transfer on the temperature will be discussed below.

For a 175nm long bowtie nano antenna at 800nm wavelength is studied at first. When the electromagnetic dissipated power on the thin film magnetic layer is observed, the distribution in Figure 4.3.1 is obtained.

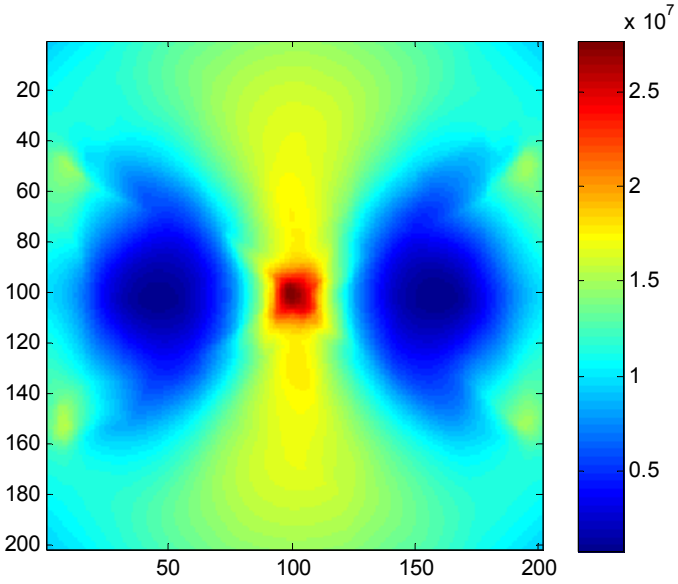

Figure 4.3.1. Dissipated electromagnetic power on the thin film magnetic layer for 175nm bowtie nanoantenna at 800nm wavelength

This dissipated power distribution is used to determine the temperature profile on the thin film magnetic layer that is caused by the focused light beam coming from the aplanatic lens and from utilizing bowtie nano antennas. This temperature profile distribution has shown both the propagating and evanescent waves effects. Therefore, it accounts the near field radiative heat transfer effects. Besides, the addition of the temperature effects of the nanoantenna's temperature will complete the temperature analysis in the system by taking account to near field contribution of nanoantenna temperature.

After the initial heat transfer analysis is conducted according to the distribution in Figure 4.3.1, the temperature of the nanoantennas are included in the analysis to see the effects. The figure 4.3.2. shows the initial temperature distribution and the temperature distribution with fluctuating current effects.

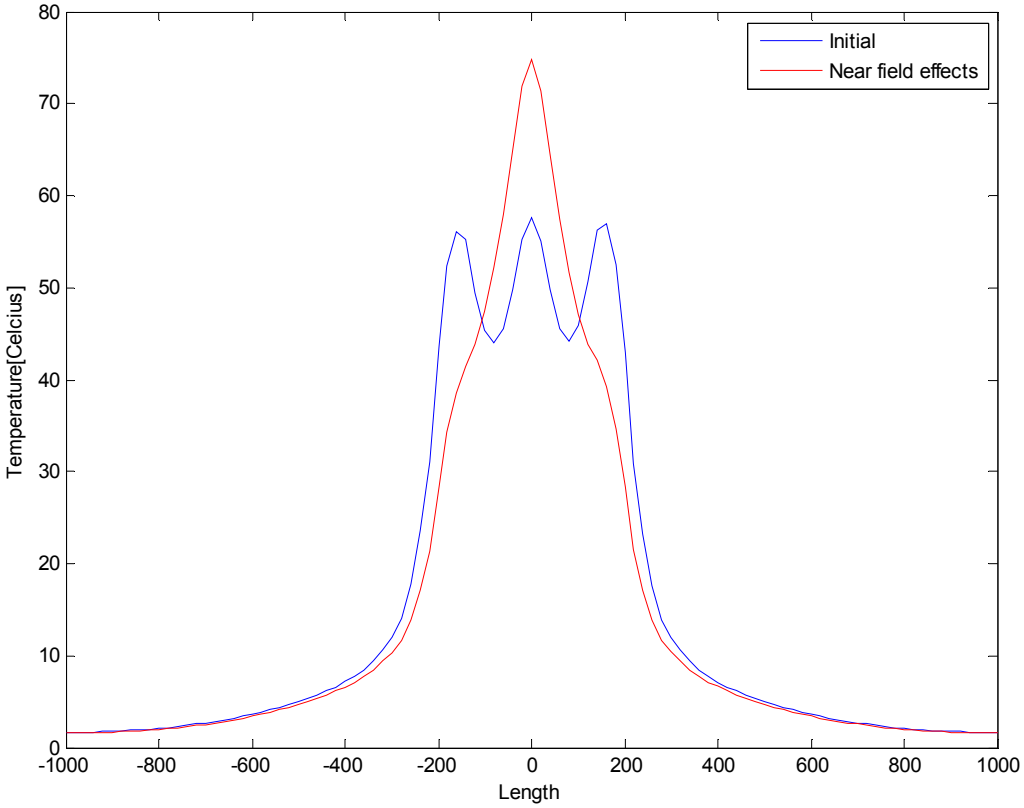

Figure 4.3.2. Temperature profile on the thin film magnetic layer corresponding to 175nm bowtie nanoantenna at 700nm wavelength. Red line corresponds to the final temperature profile that takes into account the fluctuating current on the nano antenna and the thin film magnetic layer.

As seen from the Figure 4.3.2. the temperature of the magnetic layer is increased by almost 15 Celcius degree. In the initial case the fluctuating temperature behavior is caused by the peak points at the center of the magnetic layer and the two peaks caused by the ends of the bowtie nanoantennas.In the last case, the effects of the end points of the bowtie nano antennas are decreased due to the increased temperature effect towards the center of the nanoantennas at the thin film magnetic layer. The near field temperature effects are important and cause profile distribution changes as seen from Figure 4.3.2. The further analysis are conducted for different nanoantenna lengths and wavelengths based on promising results of 175nm bowtie antenna at 800nm wavelength.

Below as a first case 175nm bowtie nano antenna system is studied in terms of heat transfer analysis. First of all, the temperatures for each wavelength between 400 to 1900nm are calculated for without nanoantenna effects and with nanoantenna effects. In Figure 4.3.3. the temperature values at the center of the thin film magnetic layer at 1.7 nanoseconds for different wavelength are presented.

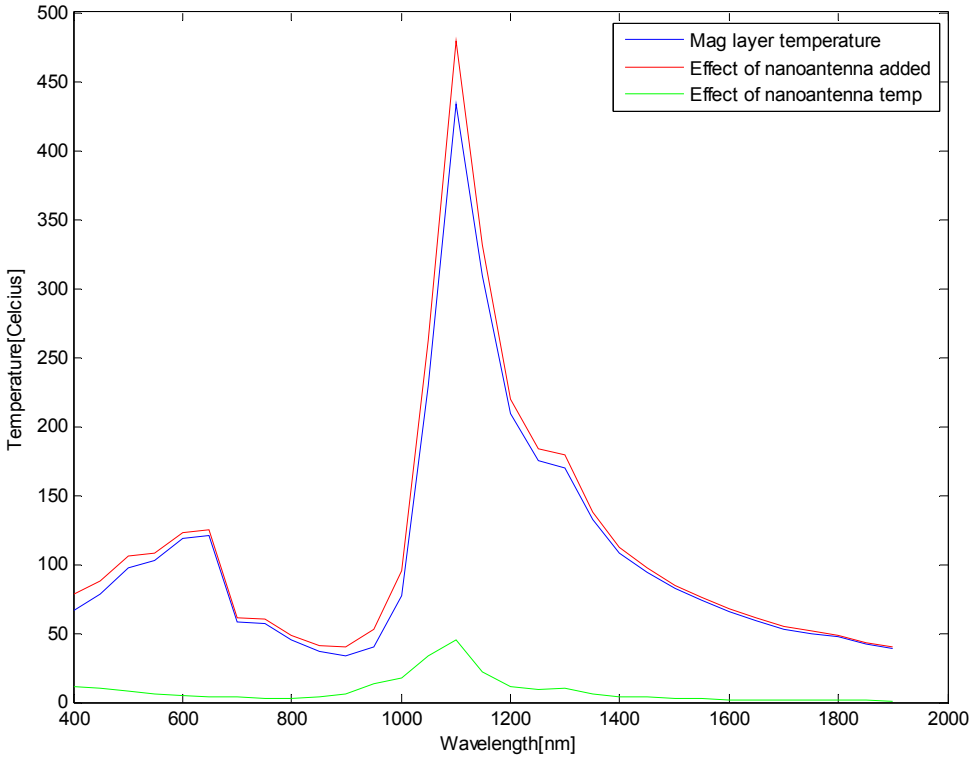

Figure 4.3.3. Temperature values at 1.7 nanoseconds at the center of the magnetic layer for dissipated power and with the effects of nanoantennatemperature for 175 nm bowtie nanoantenna

The nanoantennas temperature rise the temperature of the thin film magnetic layer as seen from Figure 4.3.3. Since wavelength increases, the effects of the current density decreased by square of the wavelength. Therefore it is expected to get higher temperature effects on the low wavelengths than higher wavelength values. Therefore, nanoantennas heat effects are almost 15% of the total temperature value at 400nm

wavelength while it remains around 3% for higher wavelengths such as 1900nm which shows the theoretical and simulation results coincide.

The temperature profile for the thin film magnetic layer in 175nm bowtie nanoantenna case shows the most of the temperature increase of the magnetic thin film layer comes from the initial focused beam of light intensity which creates dissipated power that includes also near field radiative heat transfer effects. Due to the narrow time period which is 1.7 nanoseconds, dominance of the dissipated power effects and the low surface area of nanoantennas compared to the thin film magnetic layer, the contribution of the nanoantennas heat to the rise of the temperature of the thin film magnetic layer stays around 10%.

Effects of the nanoantenna heat generation to the temperature of the thin film magnetic layer are further discussed for different lengths of the bowtie nanoantennas between 400nm and 1900nm wavelength.

In Figure 4.3.4 and 4.3.5 the temperature distribution profiles are illustrated for 100 nm and 150 nm bowtie nanoantenna respectively. As expected, the highest contribution occurs when the nanoantenna temperature reaches peak values and total contribution of the nanoantenna temperature on the temperature of the thin film magnetic layer is between 20 % and 30 % of the combined temperature values.

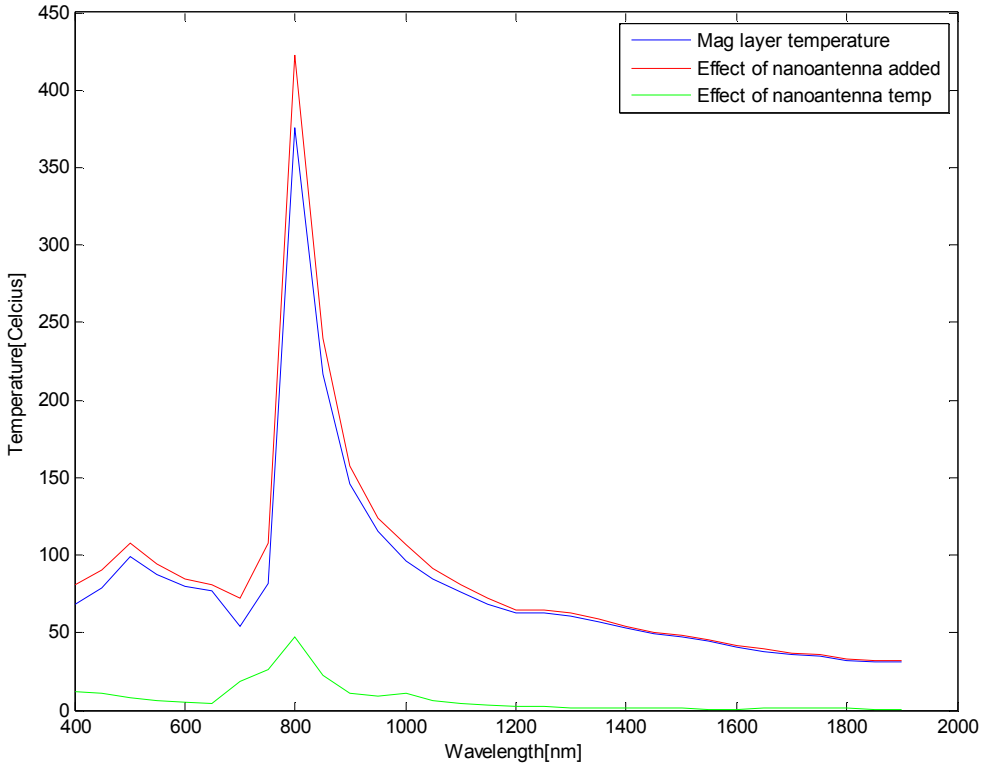

Figure 4.3.4. 100nm bowtie nanoantenna temperature effect on the temperature of magnetic layer

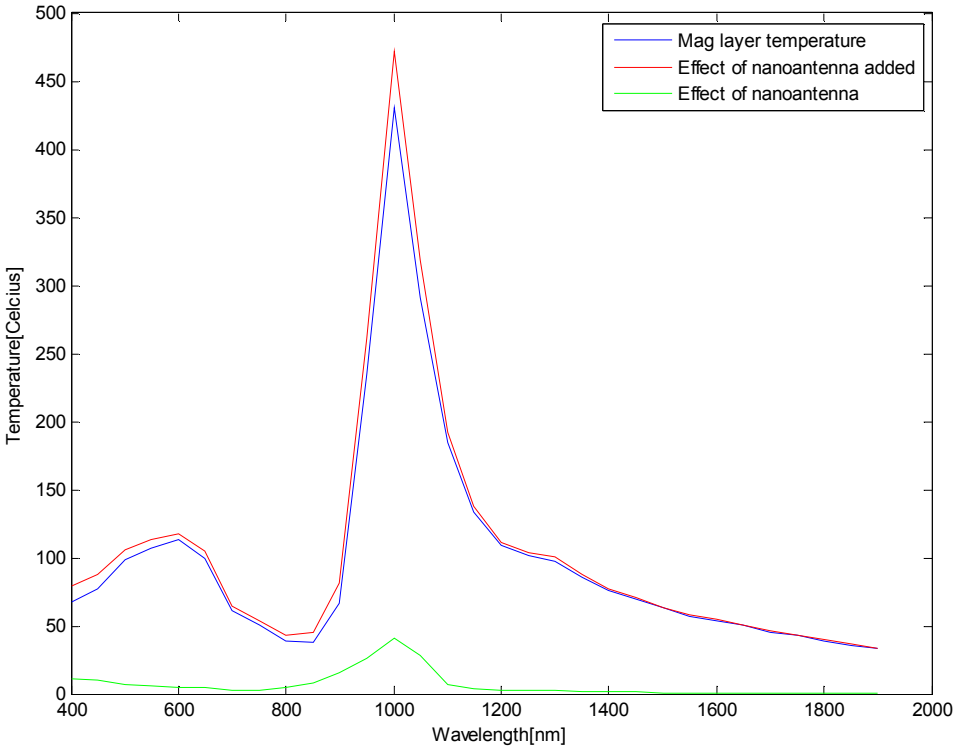

Figure 4.3.5. 150nm bowtie nanoantenna temperature effect on the temperature of magnetic layer

When the relative contribution of the temperature of the nanoantennas to the thin film magnetic layers combined temperature which is total of initial layer temperature caused by electromagnetic dissipated power and the nanoantenna temperature effects on the layer, the percentages presented in Figure 4.3.6 are obtained. The total contribution of nanoantenna temperature can reach up to 35% for 100nm long bowtie nanoantenna which is significant. However, at the peak values of temperatures for both nanoantennas and the thin film magnetic layer where the resonant frequency occurs, the contribution remains low when compared to total due to higher initial temperature values.

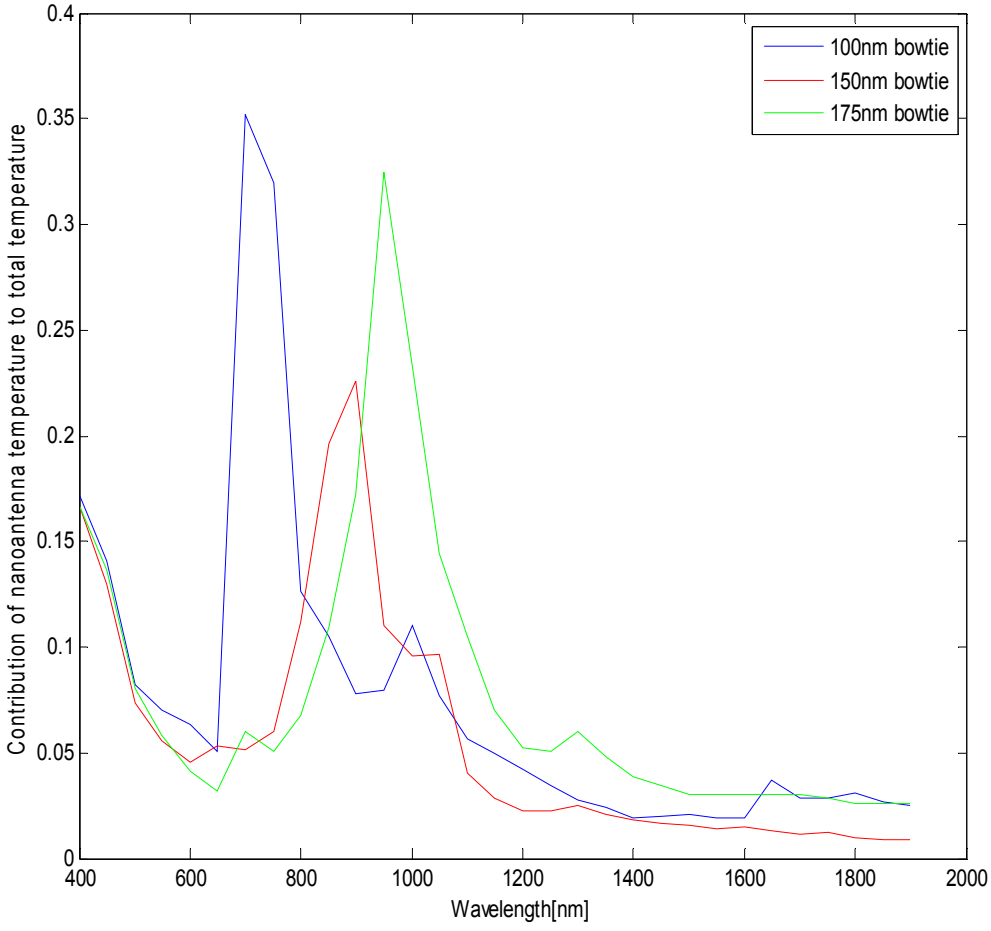

Figure 4.3.6. Percentages of nanoantenna temperature contribution to the total temperature of the thin film magnetic layer for different length of nanoantennas

5. CONCLUSIONS

In this thesis, tightly focused beam of light is defined by using Richards-Wolf theory. The electromagnetic dissipated power profiles of the dipole and bowtie nanoantennasand the corresponding thin film magnetic layers are investigated. The power absorption efficiency of the dipole and bowtie nanoantennas are compared and it is seen that dipole nanoantennas are better than bowtie nanoantennas however, bowtie nanoantennas have lower temperatures that dipole nano antennas.

The conditions where single optical and hot spots are obtained on the thin film magnetic layer structure are determined for different lengths of the bowtie nanoantennas. The dissipated power values at the center of the thin film magnetic layer and the maximum dissipated power values on the thin film magnetic layer are determined and plotted on the same graph to show the wavelengths where single optical hot spots are obtained.

The MATLAB codes for ANSYS HFSS 12 program which is used for electromagnetic analysis and for ANSYS Multiphysics program which is used for thermal analyis are written to generate scripts for those programs. Therefore, all optical, electromagnetic and thermal modeling tools are combined in one process which does not require any manual program usage.

The nano antennas which are placed 10 nm above the thin film magnetic layer structure is illuminated by focused beam of light to investigate the electromagnetic and thermal results of the dipole, bowtie and newly proposed arrow shaped nano antennas. It has been seen that the electromagnetic behaviors of the dipole, bowtie and arrow type nano antennas do not show significant differences in terms of electromagnetic power distribution however, in terms of thermal performances, arrow shaped nano antennas show significant thermal improvements which has significantly low temperatures which is important for efficiency and reliability of nano antennas in the practical applications.

REFERENCES

1. A.I.VolokitinandB.N.J.Persson,Phys.Rev.B63,205404 (2001)

2. G.Domingues, S.Volz, K.Joulain, J.-J.Greffet, Phys.Rev. Lett.94,085901 (2005)

3. I.Dorofeyev, Phys.Lett.A372,1341-1347(2008)

4. R. S. DiMatteo, P. Greiff, S. L. Finberg, K. A. Young-Waithe, H. K. Choy, M. M. Masaki, and C. G. Fonstad, Appl. Phys. Lett. **79**, 1894 2001.

5. A. Narayanaswamy and G. Chen, Appl. Phys. Lett. **82**, 3544 2003.

6. M. Laroche, R. Carminati, and J.-J. Greffet, J. Appl. Phys. **100**, 063704 2006.

7. M. Francoeur, M. P. Mengüç, and R. Vaillon, Appl. Phys. Lett. **93**, 043109 2008.

8. Wischnath, U. F., Welker, J., Munzel, M. &Kittel, A. The near-field scanning thermal microscope. Rev. Sci. Instrum. 79, 073708 (2008).

9. A. Kittel, U. F. Wischnath, J. Welker, O. Huth, F. Rüting, and S.-A. Biehs, Appl. Phys. Lett. **93**, 193109 2008

10. Challener, W. A., C. Peng, A. V. Itagi, D. Karns, W. Peng, Y. Peng, X. Yang, X. Zhu, N. J.Gokemeijer, Y.-T. Hsia, G. Ju, R. E. Rottmayer, M. A. Seigler, and E. C. Gage, "Heat-assistedmagnetic recording by a near-field transducer with efficient optical energy transfer," NaturePhoton., Vol. 3, 220–224, 2009.

11. McDaniel, T., W. Challener, and K. Sendur, "Issues in heat assisted perpendicular recording,"IEEE Trans. Mag., Vol. 39, 1972–1979, 2003.

12. Sendur, K., C. Peng, and W. Challener, "Near-field radiation from a ridge waveguide transducer in the vicinity of a solid immersion lens," Phys. Rev. Lett., Vol. 94, 043901, 2005.

13. Polder D. and Van Hove M., Theory of radiative heat transfer between closely spaced bodies, *Physical Review B* **4**(10), 3303-3314, 1971.

14. Loomis J.J. and Maris H.J., Theory of heat transfer by evanescent electromagnetic
waves, *Physical Review B* **50**(24), 18517-18524, 1994.

15. Lifshitz E.M., Zh. Eksp. Teor. Fiz. 29, 94 (1955) [Sov. Phys. JETP 2, 73 (1956)].

16. Rytov S.M., Kravtsov Y.A., Tatarskii V.I., Principles of Statistical Radiophysics 3:*Elements of Random Fields*, Springer, New York, 1989.

17. Mulet J.-P., Joulain K., Carminati R. and Greffet J-J., Enhanced radiative heat transfer at nanometric distances, *Nanoscale and MicroscaleThermophysicalEngineering* **6**, 209-222, 2002.

18. Mulet J.-P., Joulain K., Carminati R. and Greffet J.-J., Nanoscaleradiative heat transfer between a small particles and a plane surface, *Applied Physics Letters* **78**(19),2931-2933, 2001.

19. Domingues G., Volz S., Joulain K. and Greffet J-J., Heat transfer between two nanoparticles through near field interaction, *Physical Review Letters* **94**(8), 085901,2005.

20. Francoeur M., Mengüç M.P. and Vaillon R., Near-field radiative heat transfer enhancement via surface phonon polaritons coupling in thin films, *Applied PhysicsLetters* **93**, 043109, 2008.

21. Soumyadipya B. and Francoeur M., Maximum near-field radiative heat transfer between thin films, *Applied Physics Letters* **98**, 243120, 2011.

22. Francoeur M. and Mengüç M.P., Control of near-field radiative heat transfer via surface phonon-polariton coupling in thin films, *Applied Physics A Materials Science & Processing* DOI 10.1007/s00339-010-6184-0, 2010.

23. Francoeur M., Mengüç M.P. and Vaillon R., Coexistence of multiple regimes for near-field thermal radiation between two layers supporting surface phonon-polaritons in the infrared, *Physical Review B* **84**, 075436, 2011.

24. Narayanaswamy A. and Chen G., Surface modes for near field thermophotovoltaics,*Applied Physics Letters* **82**(20), 3544-3546, 2003.

25. Francoeur M. and Mengüç M.P., Role of fluctuational electrodynamics in near-fieldradiative heat transfer, *Journal of Quantitative Spectroscopy and Radiative Transfer* **109**, 280-293, 2008.

26. Francoeur M., Mengüç M.P. and Vaillon R., Solution of near-field thermal radiation in one-dimensional layered media using dyadic Green's functions and thescattering matrix method, *Journal of Quantitative Spectroscopy and RadiativeTransfer***110**, 2002-2018, 2009.

27. Baffou G., Quidant R. and Girard C., Heat generation in plasmonic nanostructures: Influence of morphology, *Applied Physics Letters* **94**, 153109, 2009.

28. Baffou G., Girard C. and Quidant R., Mapping heat origin in plasmonicnanostructures, *Physical Review Letters*, **104**, 136805, 2010.

29. Baffou G., Quidant R. and Abajo F.J.G., Nanoscale control of optical heating in complex plasmonic systems, *ACS Nano*, Vol.4, No.2, 709-716, 2010

30. Rousseau E., Siria A., Jourdan G., Volz S., Comin F., Chevrier J. and Greffet J.-J.,Radiative heat transfer at the nanoscale, *Nature Photonics* **3**(9), 514-517, 2009.

31. Shen S., Narayanaswamy A. and Chen G., Surface phonon polaritons mediated energy transfer between nanoscale gaps, *Nano Letters* **9**(8), 2909-2913, 2009.

32.Ottens R.S., Quetschke V., Wise S., Alemi A.A., Lundock R., Mueller G., ReitzeD.H., Tanner D.B. and Whiting B.F., Near-field radiative heat transfer between macroscopic planar surfaces, *Physical Review Letters*, **107**, 014301, 2011.

33.Kittel A., Müller-Hirsch W., Parisi J., Bichs S., Reddig D. and Holthaus M., Near-field heat transfer in a Scanning Thermal Microscope, *Physical Review Letters*, **95**, 224301, 2005.

34.Sendur K., Kosar A. and Menguc M.P., Localized radiative energy transfer from a plasmonic bow-tie nano-antenna to a magnetic thin film stack, *Applied Physics A*, **103**, 703-707, 2011.

35. E. Wolf, "Electromagnetic diffraction in optical systems I. An integral representation of the image field," Proc. Roy.Soc. London Ser.A **253,** 349–357 (1959).

36. B. Richards and E. Wolf, "Electromagnetic diffraction in optical systems II.Structure of the image field in an aplanatic system," Proc. Roy.Soc. London Ser.A **253,** 358–379 (1959).

37. J.M. Jin, *The Finite Element Method in Electromagnetics* (Wiley, New York, 2000)

38. Palik D. E., *Handbook of Optical Constants of Solids*, Academic Press, 1991.

APPENDIX A

Antenna parameters	Wavelength	Electric field on nanoantenna center	Electric field on magnetic layer center	Maximum dissipated power on the layer	Dissipated power on the center of layer
Length=100nm	400	40,1	14,43	4,16E+07	4,10E+07
Length=100nm	450	31,75	13,4	3,80E+07	3,80E+07
Length=100nm	500	22,72	14,16	4,53E+07	4,53E+07
Length=100nm	550	56,9	14,1	4,76E+07	4,76E+07
Length=100nm	600	90	13,7	4,66E+07	4,53E+07
Length=100nm	650	104,5	13,4	4,48E+07	4,37E+07
Length=100nm	700	172,2	12,4	4,06E+07	3,74E+07
Length=100nm	750	493,7	15,7	9,97E+07	6,04E+07
Length=100nm	800	730,7	24,2	2,91E+08	1,46E+08
Length=100nm	850	399,7	17,2	1,37E+08	7,49E+07
Length=100nm	900	283,1	14,1	7,77E+07	5,13E+07
Length=100nm	950	251,2	12,6	5,58E+07	4,11E+07
Length=100nm	1000	166,7	11,38	4,35E+07	3,37E+07
Length=100nm	1050	183,5	11,93	3,75E+07	2,92E+07
Length=100nm	1100	163,7	10,1	3,24E+07	2,71E+07
Length=100nm	1150	145,7	10,2	2,80E+07	2,40E+07
Length=100nm	1200	134,7	8,95	2,57E+07	2,20E+07
Length=100nm	1250	139,4	9	2,54E+07	2,23E+07

Length=100nm	1300	131,43	8,72	2,36E+07	2,10E+07
Length=100nm	1350	108,7	8,46	2,13E+07	1,98E+07
Length=100nm	1400	100,4	8,21	1,99E+07	1,87E+07
Length=100nm	1450	111	7,78	1,82E+07	1,67E+07
Length=100nm	1500	111	7,7	1,73E+07	1,63E+07
Length=100nm	1550	102,14	7,5	1,59E+07	1,54E+07
Length=100nm	1600	92,8	7,02	1,44E+07	1,34E+07
Length=100nm	1650	8,73E+01	6,85	1,32E+07	1,27E+07
Length=100nm	1700	86,5	6,68	1,24E+07	1,19E+07
Length=100nm	1750	87,3	6,62	1,22E+07	1,17E+07
Length=100nm	1800	81,55	6,27	1,08E+07	1,04E+07
Length=100nm	1850	79	6,36	1,09E+07	1,06E+07
Length=100nm	1900	74,5	5,94	9,44E+06	9,21E+06
Length=175nm	400	35,2125	14,3173	4,27E+07	3,99E+07
Length=175nm	450	31,0708	13,5664	4,07E+07	3,90E+07
Length=175nm	500	21,4892	13,9461	4,49E+07	4,39E+07
Length=175nm	550	48,9041	15,7718	5,98E+07	5,94E+07
Length=175nm	600	49,781	15,5139	5,87E+07	5,85E+07
Length=175nm	650	51,4335	14,4728	5,77E+07	5,10E+07
Length=175nm	700	135,0627	11,452	3,30E+07	3,20E+07
Length=175nm	750	91,5466	11,3647	3,24E+07	3,17E+07
Length=175nm	800	138,7528	10,4237	2,77E+07	2,71E+07
Length=175nm	850	197,3078	8,8757	2,36E+07	1,99E+07

Length=175nm	900	244,8491	9,6067	2,54E+07	2,37E+07
Length=175nm	950	381,5026	9,5912	3,58E+07	2,38E+07
Length=175nm	1000	545,2367	13,8417	6,80E+07	4,99E+07
Length=175nm	1050	883,7705	21,6296	1,79E+08	1,23E+08
Length=175nm	1100	1101,3	26,4126	2,84E+08	1,86E+08
Length=175nm	1150	829	20,98	1,77E+08	1,19E+08
Length=175nm	1200	536,89	17	1,12E+08	7,95E+07
Length=175nm	1250	513	15,3	8,84E+07	6,46E+07
Length=175nm	1300	523	15,2	8,48E+07	6,38E+07
Length=175nm	1350	412	13,29	6,28E+07	4,89E+07
Length=175nm	1400	360	11,87	4,93E+07	3,91E+07
Length=175nm	1450	325	10,98	4,09E+07	3,33E+07
Length=175nm	1500	280,79	10,17	3,58E+07	2,84E+07
Length=175nm	1550	264	9,64	3,16E+07	2,54E+07
Length=175nm	1600	234,93	9	2,75E+07	2,20E+07
Length=175nm	1650	226	8,62	2,46E+07	2,01E+07
Length=175nm	1700	170,55	8,1054	2,10E+07	1,76E+07
Length=175nm	1750	167	7,99	2,00E+07	1,70E+07
Length=175nm	1800	188,9	7,87	1,85E+07	1,64E+07
Length=175nm	1850	151,59	7,49	1,61E+07	1,47E+07
Length=175nm	1900	166,492	7,2174	1,49E+07	1,36E+07
Length=200nm	400	32,98	13,84	3,73E+07	3,73E+07
Length=200nm	450	29,6	13,47	3,88E+07	3,84E+07

Length=200nm	500	24,06	13,63	4,19E+07	4,19E+07
Length=200nm	550	43,45	15,04	5,42E+07	5,40E+07
Length=200nm	600	81,13	15,6	6,13E+07	5,91E+07
Length=200nm	650	101,35	15,74	6,13E+07	6,04E+07
Length=200nm	700	112,8	10,24	4,10E+07	2,56E+07
Length=200nm	750	160	10,45	3,04E+07	2,70E+07
Length=200nm	800	84,3	10,84	2,96E+07	2,93E+07
Length=200nm	850	129,53	9,67	2,46E+07	2,37E+07
Length=200nm	900	175,7	8,58	2,08E+07	1,89E+07
Length=200nm	950	228,5	8,35	2,09E+07	1,80E+07
Length=200nm	1000	268,77	9,02	2,42E+07	2,12E+07
Length=200nm	1050	362,37	9,63	3,45E+07	2,44E+07
Length=200nm	1100	582	13,46	7,39E+07	4,83E+07
Length=200nm	1150	871,73	21,64	1,67E+08	1,27E+08
Length=200nm	1200	1,03E+03	26,54	2,52E+08	1,93E+08
Length=200nm	1250	1,04E+03	24,52	2,23E+08	1,65E+08
Length=200nm	1300	898	24,14	1,94E+08	1,61E+08
Length=200nm	1350	823,6	20,72	1,44E+08	1,19E+08
Length=200nm	1400	556,47	17,1	9,86E+07	8,10E+07
Length=200nm	1450	497,5	14,67	7,16E+07	5,94E+07
Length=200nm	1500	402,6	13,03	5,63E+07	4,66E+07
Length=200nm	1550	300,55	11,58	4,49E+07	3,67E+07
Length=200nm	1600	333	10,6	3,76E+07	3,06E+07

Length=200nm	1650	302,72	9,95	3,25E+07	2,67E+07
Length=200nm	1700	273,64	9,39	2,85E+07	2,36E+07
Length=200nm	1750	254,8	9,02	2,61E+07	2,16E+07
Length=200nm	1800	242,4	8,51	2,25E+07	1,91E+07
Length=200nm	1850	221,3	8,23	2,17E+07	1,86E+07
Length=200nm	1900	215,2	8,14	2,11E+06	1,78E+07
Length=250nm	400	31,3	13,82	3,73E+07	3,71E+07
Length=250nm	450	28,13	12,95	3,75E+07	3,55E+07
Length=250nm	500	20,96	13,47	4,13E+07	4,10E+07
Length=250nm	550	38,86	15	5,43E+07	5,38E+07
Length=250nm	600	51,24	14,46	5,11E+07	5,08E+07
Length=250nm	650	91,03	13,86	4,90E+07	4,68E+07
Length=250nm	700	93,97	14,56	5,36E+07	5,17E+07
Length=250nm	750	63,93	11,33	3,86E+07	3,15E+07
Length=250nm	800	140,1	8,52	2,15E+07	1,81E+07
Length=250nm	850	174	10,1	2,68E+07	2,57E+07
Length=250nm	900	104,87	10,27	2,72E+07	2,70E+07
Length=250nm	950	112,3	8,74	2,00E+07	1,97E+07
Length=250nm	1000	138,88	8,06	1,74E+07	1,67E+07
Length=250nm	1050	180,8	7,38	1,62E+07	1,43E+07
Length=250nm	1100	228,9	7,18	1,61E+07	1,37E+07
Length=250nm	1150	268,8	7,67	1,86E+07	1,59E+07
Length=250nm	1200	370,77	8,54	2,37E+07	1,99E+07

Length=250nm	1250	367,76	8,59	2,69E+07	2,03E+07
Length=250nm	1300	366,37	9,05	2,58E+07	2,26E+07
Length=250nm	1350	449,51	10,94	4,00E+07	3,31E+07
Length=250nm	1400	689,77	13,52	6,24E+07	5,06E+07
Length=250nm	1450	810,86	18,04	1,03E+08	8,98E+07
Length=250nm	1500	974,65	23,08	1,48E+08	1,46E+08
Length=250nm	1550	960,93	23	1,65E+08	1,45E+08
Length=250nm	1600	807,87	20,29	1,40E+08	1,12E+08
Length=250nm	1650	640	17,84	9,83E+07	8,59E+07
Length=250nm	1700	524	15,47	7,24E+07	6,41E+07
Length=250nm	1750	512,45	13,63	5,76E+07	4,94E+07
Length=250nm	1800	450,69	12,35	4,57E+07	4,03E+07
Length=250nm	1850	399,92	11,3	3,88E+07	3,35E+07
Length=250nm	1900	358,74	10,35	3,25E+07	2,79E+07
Length=350nm	400	33,57	14,24	4,05E+07	3,94E+07
Length=350nm	450	30,97	13,17	3,67E+07	3,67E+07
Length=350nm	500	20,69	13,33	4,02E+07	4,02E+07
Length=350nm	550	40,11	14,47	5,02E+07	5,02E+07
Length=350nm	600	38,62	14,17	5,13E+07	4,88E+07
Length=350nm	650	45,35	13,83	4,66E+07	4,66E+07
Length=350nm	700	77,14	12,59	3,97E+07	3,86E+07
Length=350nm	750	173,42	13,14	4,37E+07	4,37E+07
Length=350nm	800	197,13	14,79	5,59E+07	5,46E+07

Length=350nm	850	89,45	11,95	3,67E+07	3,62E+07
Length=350nm	900	39,06	10,14	2,81E+07	2,63E+07
Length=350nm	950	71,05	7,64	2,13E+07	1,51E+07
Length=350nm	1000	145,25	6,88	1,48E+07	1,23E+07
Length=350nm	1050	187,1	8,07	1,81E+07	1,72E+07
Length=350nm	1100	179,19	9,23	2,41E+07	2,27E+07
Length=350nm	1150	96,15	8,34	1,93E+07	1,88E+07
Length=350nm	1200	88,62	7,41	1,53E+07	1,50E+07
Length=350nm	1250	93,3	7,05	1,40E+07	1,37E+07
Length=350nm	1300	96,49	6,83	1,34E+07	1,29E+07
Length=350nm	1350	121,49	6,4	1,18E+07	1,13E+07
Length=350nm	1400	112,91	6,13	1,10E+07	1,04E+07
Length=350nm	1450	139,1	5,65	9,76E+06	8,80E+06
Length=350nm	1500	179,54	5,46	9,57E+06	8,20E+06
Length=350nm	1550	179,72	5,59	9,97E+06	8,54E+06
Length=350nm	1600	244,49	5,42	1,01E+07	8,00E+06
Length=350nm	1650	247,35	6,2	1,23E+07	1,04E+07
Length=350nm	1700	358,96	6,2	1,45E+07	1,03E+07
Length=350nm	1750	406,67	6,91	1,82E+07	1,27E+07
Length=350nm	1800	506,06	8,57	2,65E+07	1,94E+07
Length=350nm	1850	625,6	13,07	4,88E+07	4,49E+07
Length=350nm	1900	692,37	13,68	6,29E+07	4,88E+07